

VILNIUS UNIVERSITY  
CENTER FOR PHYSICAL SCIENCES AND TECHNOLOGY  
INSTITUTE OF CHEMISTRY

IRMA LIAŠČUKIENĖ

**LIPID FILMS ON NANOSTRUCTURED ALUMINUM SUBSTRATE:  
MECHANISM OF FORMATION, STABILITY AND  
EFFECT ON SURFACE PROPERTIES**

Doctoral dissertation  
Physical Sciences, Chemistry (03 P)

Vilnius, 2014

The scientific work has been carried out at the Center for Physical Science and Technology, Institute of Chemistry during the years 2009-2013. An important experimental part has been performed in the Laboratory of Surface Reactivity at the University of Pierre & Marie Curie (Paris 06, France).

**Scientific supervisor:**

Dr. Svajus Asadauskas (Center for Physical Science and Technology, Institute of Chemistry, Physical Sciences, Chemistry 03 P)

**Scientific consultant:**

Dr. Jessem Landoulsi (University of Pierre & Marie Curie, UPMC - Paris 06, Laboratory of Surface Reactivity, Physical Sciences, Chemistry 03 P)

VILNIAUS UNIVERSITETAS  
FIZINIŲ IR TECHNOLOGIJOS MOKSLŲ CENTRO  
CHEMIJOS INSTITUTAS

IRMA LIAŠČUKIENĖ

**LIPIDŲ SLUOKSNIAI ANT NANOSTRUKTŪRIZUOTO ALIUMINIO:  
FORMAVIMOSI MECHANIZMAS, STABILUMAS IR ĮTAKA  
PAVIRŠIAUS SAVYBĖMS**

Daktaro disertacija  
Fiziniai mokslai, chemija (03 P)

Vilnius, 2014

Disertacija rengta 2009-2013 metais Fizinių ir technologijos mokslų centro Chemijos institute. Svarbi eksperimentų dalis buvo atlikta Paviršiaus Reaktyvumo laboratorijoje (UPMC, Paris 06).

**Mokslinis vadovas:**

Dr. Svajus Asadauskas (Fizinių ir technologijos mokslų centro Chemijos institutas, fiziniai mokslai, chemija - 03 P)

**Mokslinis konsultantas:**

Dr. Jessem Landoulsi (Pierre & Marie Curie - Paris VI Universitetas, fiziniai mokslai, chemija 03 - P)

## Acknowledgements

During the last three years, I experienced many different points of view of science work and I can say that it was and still is a very exciting experience. The years to write this thesis were a challenge to me and I would not be at this point now, able to present my thesis work, if not the people and institutions around me to whom I am very grateful.

I would like to thank both my supervisors:

Dr. Svajus Joseph Asadauskas who already from the first days taught me to be self-dependent, flexible, and be able to make decisions. I am very thankful for his encouragements, for his support on my choices, for his trust and his help not only for organizing things, but also for involving me in the world of lipids.

Dr. Jessem Landoulsi, my “scientific father”, who empowered me not only as a professional being able to perform experimental parts, writing, etc. but also as a person with the adequate attitude, opinion and self-confidence. He showed me that science is more than an execution work. Involving a lot of creativity, doing science is to be able to create knowledge and share it with others. Furthermore, he did the AFM images.

The French Embassy in Lithuania (Egide #719306H and Campus France N° 785192H grants) and the Research Council of Lithuania (S VP1-3.1-ŠMM-01-V-02-001, MM-01-V-V-02-003) are gratefully acknowledged for their financial support.

I am very indebted to prof. dr. Jean-François Lambert, who answered positively to my first request to come to his laboratory. His open thinking, advices and the width of scientific approach enriched not only my articles, but also my personal skills.

Dr. Nesrine Aissaoui did not only perform ATR-IR measurements, but also taught me many technical approaches to data treatment.

Marie Steffenhagen, as a physicist, played an important role in calculations related to Wenzel roughness.

I am also very thankful to dr. Christophe Methivier for the help in PM-IRRAS measurements, to dr. Vincent Humblot for teaching me the WCA technique, to Christophe Calers for XPS measurements.

I am appreciative to dr. Karim El Kirat for the useful discussion and key suggestion in phospholipids part.

I big thank you for my colleagues from the Department of Electrochemical Material Sciences for their help and support.

To Dr. Astai Judžentienė for encouraging and stimulating me to move further despite various circumstances.

Finally, I am more than grateful to my beloved family for its universal support, understanding and patience.

## **List of abbreviations**

AFM - Atomic force microscopy

ATR-IR - Attenuated total reflection infrared spectroscopy

BA – butyric acid

CA – caprylic acid

DPPC dipalmitoylphosphatidylcholine

LA – linoleic acid

LrA – lauric acid

FA - fatty acids

OA – oleic acid

PBS – phosphate buffered saline

PEM- photo-elastic modulator

PM-IRRAS Polarization modulation infrared reflection absorption spectroscopy

SA – stearic acid

WCA - Water contact angle

XPS- X-ray photoelectron spectroscopy

## Table of contents

<b>Acknowledgements</b> .....	<b>5</b>
<b>List of abbreviations</b> .....	<b>7</b>
<b>Table of contents</b> .....	<b>8</b>
<b>Introduction</b> .....	<b>11</b>
<b>I. LITERATURE REVIEW</b> .....	<b>15</b>
1.1 Lipids: one of the main group of natural biomolecules .....	16
1.1.1 Lipids in biological systems .....	17
1.1.2 Lipids in technology .....	19
1.2 Fatty acids (FA) .....	21
1.2.1 Molecular structure.....	22
1.2.1.1 Saturated fatty acids.....	23
1.2.1.2 Unsaturated fatty acids .....	23
1.2.1.3 Conformation .....	25
1.2.2 Chemical properties.....	26
1.2.2.1 Autoxidation and photo-oxidation.....	26
1.2.2.2 Hydrolysis.....	27
1.2.2.3 Ozonolysis .....	28
1.3 Phospholipids .....	29
1.3.1 Molecular structure.....	29
1.3.1.1 Glycerophospholipids .....	30
1.3.1.2 Sphingophospholipids .....	31
1.3.2 Organization .....	31
1.4 Lipids at solid surface .....	32
1.4.1 Adsorption procedures .....	32
1.4.2 Properties of the lipid layers.....	35
1.4.3 Modification of surface properties .....	36
1.4.4 Mechanism of self-assembly of fatty acids .....	40
1.4.4.1 Influence of FA properties.....	40



1.4.4.2 Influence of solvent .....	42
1.4.4.3 Influence of adsorption procedure .....	42
1.4.4.4 Influence of surface properties .....	43
1.4.5 Stability of adsorbed FA.....	46
1.4.6 Particularity of aluminum substrates.....	48
1.4.7 Mechanism of self-assembly of phospholipids .....	49
<b>II. MATERIALS AND METHODS .....</b>	<b>52</b>
2.1 Materials.....	53
2.2 Procedures .....	54
2.2.1 Hydroxylation of aluminum .....	54
2.2.2 Adsorption of FA, MO .....	55
2.2.3 Conditioning .....	55
2.2.4 UV/O <sub>3</sub> treatment.....	55
2.2.5 Adsorption of DPPC.....	56
2.3 Techniques .....	56
2.3.1 Polarization modulation infrared reflection absorption spectroscopy .....	56
2.3.1.1 Principle .....	56
2.3.1.2 Experimental conditions .....	57
2.3.2 Attenuated total reflection infrared spectroscopy .....	58
2.3.2.1 Principle .....	58
2.3.2.2 Experimental conditions .....	58
2.3.3 Water contact angle .....	59
2.3.3.1 Principle .....	59
2.3.3.2 Experimental conditions .....	61
2.3.4 Atomic force microscopy .....	61
2.3.4.1 Principle .....	61
2.3.4.2 Experimental conditions .....	63
2.3.5 X-ray photoelectron spectroscopy .....	63
2.3.5.1 Principle .....	63
2.3.5.2 Experimental conditions .....	65

<b>III. RESULTS AND DISCUSSIONS .....</b>	<b>66</b>
3.1 Self-assembly of FA and ester on hydroxylated Al substrate.....	67
3.1.1 Formation of the Al Oxy-hydroxide Layer .....	67
3.1.2 Adsorption of FA, Ester .....	69
3.1.3 Mechanism of FA adsorption.....	80
3.2 Effects of FA film stability formation on the wettability and nanoscale roughness of Al substrate .....	86
3.2.1 Effect of UV/O <sub>3</sub> treatment.....	86
3.2.2 Effect of conditioning.....	93
3.2.3 “Chemistry” vs “Roughness” .....	96
3.3. Mechanism of adsorption of DPPC on nanostructured Al substrate: Influence of surface hydrophobicity .....	101
3.3.1 Adsorption of DPPC.....	101
3.3.2 Effect of hydration.....	106
3.3.3 Discussion .....	110
<b>Conclusions and perspectives .....</b>	<b>113</b>
<b>List of publications.....</b>	<b>116</b>
<b>References.....</b>	<b>119</b>

## Introduction

Lipids interact with metallic materials in various fields of applied sciences and technologies. For instance, vegetable oils are extensively used in food industries and more recently as environmentally friendly lubricants [1], fatty acid methyl esters as biodiesel [2], and a variety of phospholipids for the design of biomaterials and biosensors [3, 4], for the drug delivery [5], and cosmetic products [6].

Lipids, one of the four main classes of biomolecules, constitute the molecular architecture of biomembranes and play key functional roles in biochemical processes [7]. They include a wide range of amphiphilic molecules which generally possess one or several hydrophobic alkyl chains and hydrophilic groups such as phosphate in phospholipids, carboxylate in fatty acids (FA), hydroxyl in cholesterol, and amino alcohol in sphingolipids [8]. The ability of lipids to self-assemble and self-organize at interfaces has attracted much interest, leading to the design of biomimetic materials with tailored properties and functions [9-11]. In particular, the ability to tailor both head and tail groups of lipid molecules may help to better understand relevant phenomena at the molecular level, such as wetting, adhesion, lubrication, and corrosion processes [12].

The mechanism of adsorption of lipids on solid surfaces is complex as it involves multiple interfacial processes, including self-assembly, self-organization, hydration, desorption, etc. Furthermore, the adsorbed phase is sensitive to physicochemical conditions of the medium (temperature, ionic strength, etc.) and the properties of the substrate (hydrophobicity, charge, etc.).

The adsorption of FA on solid surfaces often creates major technical hurdles, when “clean” surfaces are necessary. The propensity of FA and their derivative esters to bind chemically to metal surfaces makes them difficult to remove. Furthermore, most fatty acids are not soluble in water and are not volatile. When washed with water, detergents must be used for their removal, but this typically leads to even further surface contamination with soaps, detergents,

etc. Indeed, even a simple touch of bare hands immediately leaves a trace of human sebum and epidermal lipids, which are mainly constituted of free FA [13]. Surface contamination with FA can also occur due to the mist of lubricants, exposure to vacuum pump grease, soldering flux, incidental dust, etc. Once adsorbed on the metal surface, the removal of FA requires a chemically aggressive technique, such as treatment in  $H_2O_2$ , acid etching, or reagent-free methods such as thermal annealing or UV/ $O_3$  treatment [14].

In the present study, we focus on the adsorption behavior of two categories of lipids on Al substrate: FA and phospholipid. Indeed, the self-assembly of FA on Al oxides has attracted particular interest [15-22]. This is due to the relevance of the Al oxides/hydroxides chemistry [23], from the fundamental point of view, but also to the importance of this material in many technological applications such as lubrication, water/oil repellency and corrosion inhibition [24, 25]. Moreover, Al foil is widely used in food industry and many other packaging applications. Free oleic and linoleic acids are widespread in many types of food, because oils and fats easily hydrolyze during food storage and processing, producing free FA along with mono- or di-glycerides. Oleic acid is by far the most widespread fatty acid in foods, while linoleic acid is nearly as abundant as stearic or palmitic acids. Consequently, adsorption of oleic and linoleic acids on Al surface occurs almost inevitably when food is wrapped into Al foil. Previous reports showed significant increase of Al contents in foods, which were processed while wrapped into the aluminum foil [26], [27]. So far possible Al intake levels were reported to be far below 1 mg Al/kg bodyweight per day, established as a safe dose by WHO (World Health Organization, 1989). Nevertheless, bearing in mind the magnitude of FA exposure to Al foil, possibilities of chemical transformations of oleic and linoleic acids, when adsorbed on Al, deserve much more significant attention.

#### **The main objectives of the thesis:**

- Describe the mechanism of interaction of fatty acids and their esters on Al substrate at the molecular level.

- Investigate the impact of the stability of self-assembled FA on the structural and wetting properties of the Al surface.
- Evidence the origin of surface wettability: chemistry or nanoscale organization.
- Investigate the adsorption behavior of a phospholipid model molecule on nanostructured Al surface.
- Elaborate a hybrid FA/phospholipid bilayer on the nanostructured Al surface and examine the stability of the obtained “nanostructured hybrid surface” in aqueous medium.

### **Novelty of scientific investigation**

The self-assembly of fatty acids on the surfaces of inorganic materials is a relevant way to control their wetting properties. The self-assembly of FA on a superficially hydroxylated Al surface leads to the formation of a remarkable nanoscale organization which manifests with two hierarchical –levels of nanostructuration. The first is due to the hydroxylation treatment, leading to the nucleation of AlOOH compounds in the form of nanorod-like structures. The second is related to the self-assembly of FA and leads the appearance of nano-patterns aligned parallel to the rod axis, regardless of the molecular structure of FA.

Results presented in this work evidence that no correlation can be made between water contact angles ( $\theta_w$ ) and the surface roughness. By contrast,  $\theta_w$  strongly increased with the amount of  $-\text{CH}_x-$  groups exhibited by adsorbed FA. These findings suggest that the main origin of hydrophobization is the presence of self-assembled molecules and that the surface roughness has only a small contribution to the wettability.

Another relevant achievement in this work is related to the elaboration of a hybrid FA/phospholipid layer on the nanostructured Al surface, taking advantages of the findings mentioned above. The main purpose is to better control the formation and the stability of a phospholipid layer on nanostructured surface. Phospholipid-modified surfaces are, indeed, relevant

for the control of surface wettability of materials with biological interest and, as a consequence, the interaction with biomolecules.

**Statements for defense:**

1. Fatty acids interact strongly with the hydroxylated Al (AlOOH) surface through their deprotonated carboxylic acid head groups. Methyl oleate is, however, subjected to a chemical transformation (presumably a saponification reaction) at the AlOOH surface, leading to the formation of coordinative bonded carboxylate species, similarly to FA.
2. The self-assembly of FA on the nanostructured AlOOH surface leads to the formation of ordered nanopatterns with regular height and inter-distance.
3. The use of UV/O<sub>3</sub> treatments allows adsorbed FA to be removed at different rates, depending, mainly on the level of unsaturation of their alkyl chains. Stearic acid is more stable than oleic and linoleic acids, and the mechanism of degradation seems to involve ozonolysis and/or autoxidation.
4. Ageing of adsorbed FA or esters in air, UV/O<sub>3</sub> or aqueous media leads to noticeable evolution of the nanoscale organization of the surface, causing changes in surface wettability. The profound investigations, conducted in the present work, evidence that the origin of hydrophobization is “chemistry” rather than “nanoscale roughness”.
5. Phospholipids (DPPC) adsorb on both hydrophilic AlOOH and hydrophobic SA-AlOOH surfaces. However, the organization of the DPPC molecules is greatly influenced by the presence of a self-assembled FA layer. With increasing the concentration of DPPC in solution, the adsorbed phase may include multiple (bi)layers which seems to remain stable upon hydration

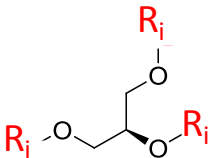
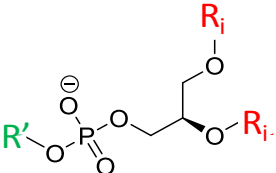
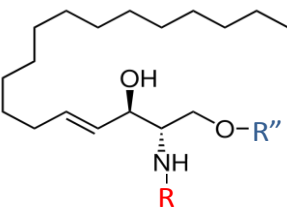
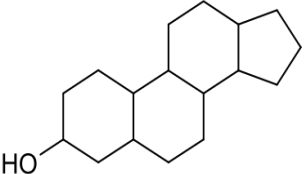
## **I. LITERATURE REVIEW**

## 1.1 Lipids: one of the main group of natural biomolecules

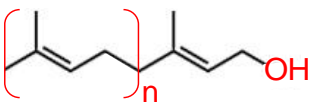
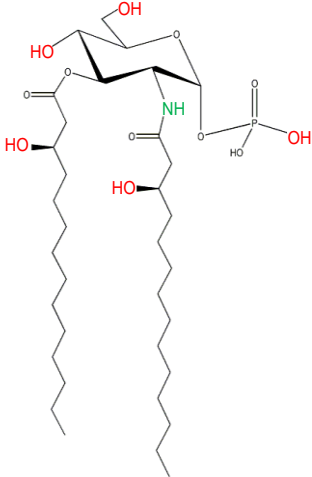
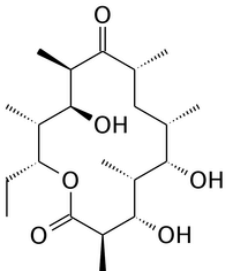
Lipids are one of the four main classes of biomolecules which constitute the molecular architecture of biomembranes over wide biological systems. They yield large amount of energy, during oxidation processes in metabolism and play key functional roles in biochemical processes [7]. This class of biomolecules includes a large number of amphiphilic molecules which generally possess one or several hydrophobic alkyl chains and hydrophilic groups. As a consequence, lipids generally exhibit a low solubility in water and high solubility in nonpolar solvents.

The classes of lipids [28] are summarized in Table 1.1.

**Table 1.1.** Classification of lipids

Classes	Subclasses*	General formula**	Examples
<b>Fatty acids</b>	Saturated Unsaturated	$R_n\text{-COOH}$	Omega-3
<b>Glycerolipids (glycerides)</b>	Mono- Di- Tri-		Vegetable oils, fats
<b>Phospholipids</b>	Glycerophospholipids Phosphosphingolipids		DPPC, Lethitin
<b>Sphingolipids</b>	Sphingoid base Ceramides Phosphosphingolipids Glycosphingolipids		Sphingomyelin (SPH)
<b>Sterol lipids</b>	Sterols Steroids Secosteroids Bile acids and derivatives Steroid conjugates Hapanoids		Cholesterol



<b>Prenol lipids</b>	Isoprenoids Quinones and hydroquinones Polyprenols		Vitamin E, Vitamin K
<b>Saccharolipids</b>	Acylaminosugars Acylmonosugar glycans Acyltrehaloses Acyltrehalose glycans		Acylated glucosamine
<b>Polyketides</b>	Macrolide polyketides Aromatic polyketides Nonribosomal peptide/ polyketide hybrids		Doxycycline, Erythromycin (antibiotics)

\*List of the subclasses is not exhaustive.

\*\*  $R_n$  – alkyl chain;  $R_i$  - fatty acid;  $R'$  - functional groups related to glicerophospholipids;  $R''$  – functional groups related to sphingolipids,  $R$  – or H atom, or fatty acid.

### 1.1.1 Lipids in biological systems

The fatty acyl group is the major entity in the lipid building block, which constitute the hydrophobic moiety of the molecule. On their own, essential fatty acids are required for the stimulation of growth (skin and hair), regulation of CH metabolism, lipotropic activity, and maintenance of reproductive performance, among other physiologic effects [29]. Glycerolipids are the major constituents of most natural fats and oils as also some of them are important intermediates in metabolism. The glycerophospholipids have a phosphate group esterefied at carbon 3 of the glycerol backbone. They are essential components of cell membranes by forming lipid bilayer, but can be also found in other parts of the cell.

Sphingolipids is another family of lipids with a complex structure. The common one is a sphingoid base (sphingosine) backbone (18-carbon amino alcohol) and can be converted into ceramides, phosphosphingolipids, glycosphingolipids and other species, including protein adducts [30, 31]. Ceramide is formed from sphingosine, which is linked through an amide bond with fatty acid. Ceramide-based lipids are important components of muscle and nerve membranes in animals. In addition, glycosphingolipids, which consist of a ceramide with one or more sugar residues, have a number of important cellular functions.

The sterols, of which cholesterol and its derivatives are the most widely studied in mammalian systems, constitute an important component of the cell membrane [32]. They all have a common structural motif of three six-membered rings and one five-membered ring all fused together. Cholesterol is a principal component of animal cell plasma membrane. The steroids, which also contain the same fused four ring core structure, have different biological roles as hormones and signaling molecules [33]. For instance, the 18 carbon atoms ( $C_{18}$ ) steroids include the family of estrogen, the  $C_{19}$  steroids constitute the androgens (testosterone and androsterone) and the secosteroids comprise various forms of vitamin D.

In spite of this fascinating diversity of lipid's molecular structures, only few classes of lipids are used by nature to build up animal cell membranes: (1) cholesterol, (2) phospholipids, and (3) cerebrosides (glycosphingolipids) (Figure 1.1), which also contain a substantial amount (of neutral lipids such as diacylglycerols (glycerol with two attached fatty acid chains and triacylglycerols (glycerol with three fatty acid chains) in addition to fatty acids and lyso-phospholipids. These types of amphiphiles are most probably involved as metabolic intermediates or transiently formed during metabolic processes where lipids play an essential role [8].

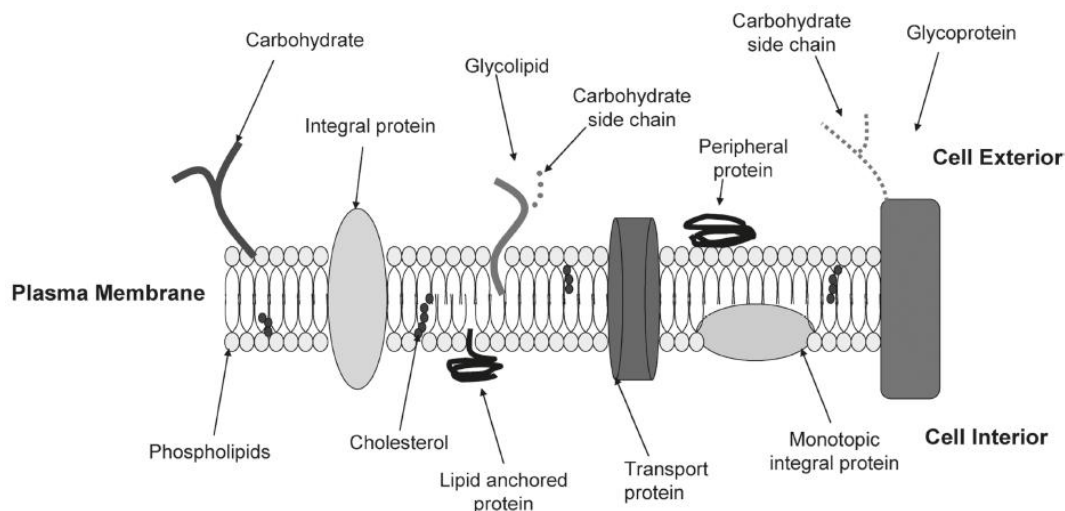


**Figure 1.1.** Cross section of generic eukaryotic cell surface (i.e., plasma membrane)[34]

The present study focuses on lipids which exhibit amphiphatic properties, containing both hydrophilic and hydrophobic parts. The interest is to investigate the abilities of these molecules to interact with inorganic materials. For this purpose, we used molecules from two classes of lipids: (i) fatty acids and derivative ester, which could be also found as fragments in the majority of more complex lipids or other bio(macro)molecules, and (ii) glycerophospholipid, containing the glycerol backbone with the fragments of two fatty acids, phosphate and choline groups, and represents more intricate system than fatty acids. Detailed presentation of the chosen molecules classes is presented below (sections 1.2 and 1.3).

### 1.1.2 Lipids in technology

For a long time, lipid had been used as food source or as oleochemical raw materials for the manufacture of surfactants, polymers, etc. During the last decade, the use of lipids in novel technological processes has attracted an increasing attention, particularly in the synthesis of biodiesel and related products. Biodiesel, usually based on fatty acid methyl (FAME), ethyl or other esters, represents an alternative diesel fuel and is made from renewable biological sources such as vegetable oils and animal fats. In these sources, the

main components are triacylglycerols (TAG). Different FA can be attached to one glycerol backbone. Because different FA have different physical and chemical properties, the FA profile is probably the most important parameter influencing the corresponding properties of vegetable oil or animal fat [2].

Advantages of biodiesel over conventional petroleum diesel fuel (petrodiesel) include derivation from renewable feedstock, displacement of imported petroleum, superior lubricity and biodegradability, lower toxicity, essentially no sulfur content, higher flash point, positive energy balance, and a reduction of most regulated exhaust emissions [35]. Usage of biodiesel will allow a balance to be sought between agriculture, economic development and the environment [36]. Recently, utilization of edible oils for production of biodiesel became highly contested in various political and social institutions. Producing biofuels requires huge amounts of both fossil energy and food resources, which will intensify conflicts among these resources, as also the use of food crops enhances major nutritional and ethical concerns, especially in developing countries [37, 38]. However, a number of non-edible oilseeds have already been found useful for biodiesel production, as well as more exotic sources, such as yeast, algae, etc. Therefore, FAME is likely to stay as a major ingredient in fuels and its studies will remain important until sufficient understanding on FAME behavior in fuel systems is achieved.

Many types of oils, with a varied composition in fatty acids, can be used for the preparation of biodiesel. For example, waste oils (such as used frying oils) and animal fats are important sources for FAME manufacture. Nevertheless, four oilseeds clearly dominate the feedstock used for world-wide biodiesel production. Soybean [39, 40], rapeseed [41, 42], palm [43] and sunflower [44, 45] oils are the most utilized for FAME production.

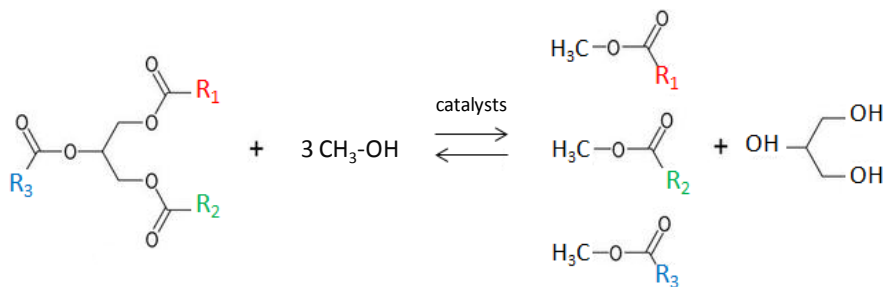


**Figure 1.2.** Simplified scheme of triglyceride transesterification reaction, where  $R_1$ ,  $R_2$ ,  $R_3$  are remaining chains of FA

FAME is produced from vegetable oils through a transesterification reaction of triglycerides with methanol in the presence of an alkaline or sometimes acidic catalyst (Figure 1.2).

Many efforts have been made to improve the rate of transesterification reaction by using different catalysts. A vast amount of literature in the subject is listed in recent reviews [46].

However, prolonged exposure of biofuels to reservoir or equipment surfaces can become problematic due to corrosion, which not only damages the container surface, but also increases metal contents in the fuel. Consequently, during combustion metal oxides are formed. Since the oxides are not volatile, they must produce solid particulates, contributing to soot formation.

## 1.2 Fatty acids (FA)

Fatty acids are aliphatic monocarboxylic acids with a common structure: an alkyl chain and a carboxylic acid head-group. Over 1000 fatty acids are known with different chain lengths, positions, configurations, types of unsaturation and range of additional substituents along the aliphatic chain, but only around 20 fatty acids occur widely in nature [47]. They can exist individually or included as fragments in other biomolecules. Each fatty acid can have its derivative ester, which would retain the same structure of the molecule (chain length, number of double bonds), except that the hydrogen atom of the

carboxylic head group (-COOH) is replaced by an appropriate alkyl group (-COOCH<sub>3</sub> for methyl ester, -COOC<sub>2</sub>H<sub>5</sub> for ethyl ester and etc.) (see section 1.1.2).

### 1.2.1 Molecular structure

Fatty acids are classified into saturated – when all carbon-carbon bonds are single bonds – and unsaturated – with one or more double bonds. They can be described by using i) *systematic name* - numbering the chain from carboxyl carbon (IUPAC-IUB,1976) with the end –anoic for saturated acids, -enoic, -adienoic, -atrienoic and etc for unsaturated ones, indicating the number of double bonds; ii) *common name* or iii) *symbol* where the first number means the amount of carbon atoms and the second one describes the amount of double bonds (Table 1.2).

**Table 1.2.** Classification of the most common fatty acids

Structure	Systematic name	Common name	Symbol
CH <sub>3</sub> (CH <sub>2</sub> ) <sub>2</sub> COOH	butanoic	butyric	4:0
CH <sub>3</sub> (CH <sub>2</sub> ) <sub>6</sub> COOH	octanoic	caprylic	8:0
CH <sub>3</sub> (CH <sub>2</sub> ) <sub>10</sub> COOH	dodecanoic	lauric	12:0
CH <sub>3</sub> (CH <sub>2</sub> ) <sub>12</sub> COOH	tetradecanoic	myristic	14:0
CH <sub>3</sub> (CH <sub>2</sub> ) <sub>14</sub> COOH	hexadecanoic	palmitic	16:0
CH <sub>3</sub> (CH <sub>2</sub> ) <sub>5</sub> CH=CH(CH <sub>2</sub> ) <sub>7</sub> COOH	9-hexadecenoic	palmitoleic	16:1
CH <sub>3</sub> (CH <sub>2</sub> ) <sub>16</sub> COOH	octadecanoic	stearic	18:0
CH <sub>3</sub> (CH <sub>2</sub> ) <sub>7</sub> CH=CH(CH <sub>2</sub> ) <sub>7</sub> COOH	9-octadecenoic	oleic	18:1
CH <sub>3</sub> (CH <sub>2</sub> ) <sub>3</sub> (CH <sub>2</sub> CH=CH) <sub>2</sub> (CH <sub>2</sub> ) <sub>7</sub> COOH	9,12-octadecadienoic	linoleic	18:2
CH <sub>3</sub> (CH <sub>2</sub> CH=CH) <sub>3</sub> (CH <sub>2</sub> ) <sub>7</sub> COOH	9,12,15-octadecatrienoic	α-linolenic	18:3
CH <sub>3</sub> (CH <sub>2</sub> ) <sub>3</sub> (CH <sub>2</sub> CH=CH) <sub>3</sub> (CH <sub>2</sub> ) <sub>4</sub> COOH	6,9,12-octadecatrienoic	γ-linolenic	18:3
CH <sub>3</sub> (CH <sub>2</sub> ) <sub>18</sub> COOH	eicosanoic	arachidic	20:0
CH <sub>3</sub> (CH <sub>2</sub> ) <sub>3</sub> (CH <sub>2</sub> CH=CH) <sub>4</sub> (CH <sub>2</sub> ) <sub>3</sub> COOH	5,8,11,14-eicosatetraenoic	arachidonic	20:4
CH <sub>3</sub> (CH <sub>2</sub> ) <sub>20</sub> COOH	docosanoic	behenic	22:0
CH <sub>3</sub> (CH <sub>2</sub> ) <sub>7</sub> CH=CH(CH <sub>2</sub> ) <sub>11</sub> COOH	13-docosenoic	erucic	22:1
CH <sub>3</sub> (CH <sub>2</sub> ) <sub>22</sub> COOH	tetracosanoic	lignoceric	24:0
CH <sub>3</sub> (CH <sub>2</sub> ) <sub>7</sub> CH=CH(CH <sub>2</sub> ) <sub>13</sub> COOH	15-tetracosenoic	nervonic	24:1

#### 1.2.1.1 Saturated fatty acids

Saturated fatty acids have only single bonds and naturally occurring even number of C atoms with chain lengths mainly between C<sub>4</sub> and C<sub>24</sub>. Fats, which are rich in saturated acids, have high melting point and they are the main characteristic of many tropical species.

Short chain acids, particularly butyric (4:0), are found in ruminant milk fats. Medium chain, such as lauric (8:0, 12:0) and others occur together in coconut and palm kernel oils. Palmitic acid (16:0) is the most abundant natural saturated acid present in plants, animals and microorganisms. Low levels of stearic acid (18:0) is found nearly everywhere, however it is abundant in cocoa butter, few tropical species, and some animal fats.

Generally, saturated acids with 10 or more carbons are solid at room temperature, and their melting points increase with increasing the chain length.

#### 1.2.1.2 Unsaturated fatty acids

Unsaturated fatty acids have one or more double bonds in their alkyl chains. Carbon-carbon double bond geometry could be described in *cis* (the hydrogen atoms are at the same side than the double bond) and *trans* (the hydrogen atoms are at the opposite side than the double bond). *Cis* configuration is dominating in nature, while *trans* configuration is most often a result of chemical processes during catalytic partial hydrogenation.

The most common unsaturated fatty acid is the oleic acid. It is found in most plant and animal lipids and is the major fatty acid in olive oil (70-75%) and several nut oils. About 75 to 80% of it is found in many genetically modified oilseeds, e.g. sunflower and safflower.

Unsaturated fatty acids with *cis* configuration with 18 or less carbons are liquids at room temperature. Moreover, double bonds positions influence the melting point.

Unsaturated fatty acids with two or more double bonds are usually called polyunsaturated fatty acids (PUFA). Plants generally insert double bonds at the Δ<sub>9</sub>, Δ<sub>12</sub> and Δ<sub>15</sub> positions in C<sub>18</sub> fatty acids, giving n-9, n-6, and n-3

compounds, respectively. “Δ” identifies at which place the double bond is, counting from the carboxyl end of fatty acid alkyl chain. The notation (n-x) shows with x the place of double bond counting from the terminal methyl carbon (designated as n or ω) toward the carbonyl carbon (Figure 1.3).

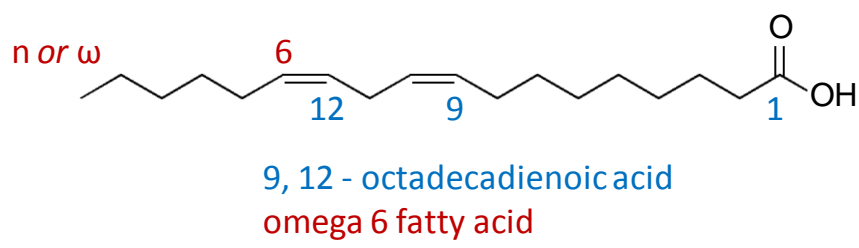


**Figure 1.3.** Nomenclature of PUFA in the basis of the positions of double bonds

Linoleic acid is present in most plant oils and is abundant (>50%) in corn, sunflower, and soybean oils, and exceeds 70% in safflower oil.

Mammalian tissues contain four families of PUFA : n-3, n-6, n-7, n-12, but only n-6 and n-3 classes are essential to the diet, as all others could be synthesized by humans from an excess of dietary energy [29]. The importance of dietary fatty acids in the evolution of the human brain has been reviewed by Crawford [48]. Brain lipids contain a very large fraction of poly-unsaturated fatty acyl chains, which mammals are unable to synthesize because they lack the enzymes to introduce double bonds at carbon bonds beyond C-9 in the fatty acid chain [49]. In humans, the poly-unsaturated lipids that seem to be of importance to the central nervous system are formed from essential fatty acids (EFA) known as linoleic (n-6) and α-linoleic (n-3) acids, which are elongated and desaturated from 18-carbon chain lengths with two or three double bonds to 20- and 22-carbon chain lengths with four and six double bonds [50].

Also exist bis- and polymethylene-interrupted acids, conjugated acids, trans acids, acetylenic and allenic acids, branched chain acids, cyclic fatty acids, fatty acids with oxygen-containing functional groups and other fatty acid structures [47]. However, in this study they are not investigated.



### 1.2.1.3 Conformation

If any of functional groups (for example, double bonds) are incorporated along the chain, it could change the chemical reactivity and the structure of the molecule. Fatty acids are flexible molecules: there is a potential rotation of the C-C bonds in the alkyl chain, and different conformations or tertiary structures are possible [47].

In a saturated fatty acids, the alkyl chain usually adopts a structure with each methylene anti to the next, resulting in a straight zigzag chain. However, functional groups more or less distort this straight chain. The distance between carbonyl carbon and the terminal carbon could help to evaluate this distortion. The double bond of unsaturated fatty acids is usually in the *cis* configuration, which enhances a bend in the chain. That is why, in the adsorbed state, unsaturated fatty acids chains do not pack closely together to form ordered arrays as do saturated ones (Figure 1.4).

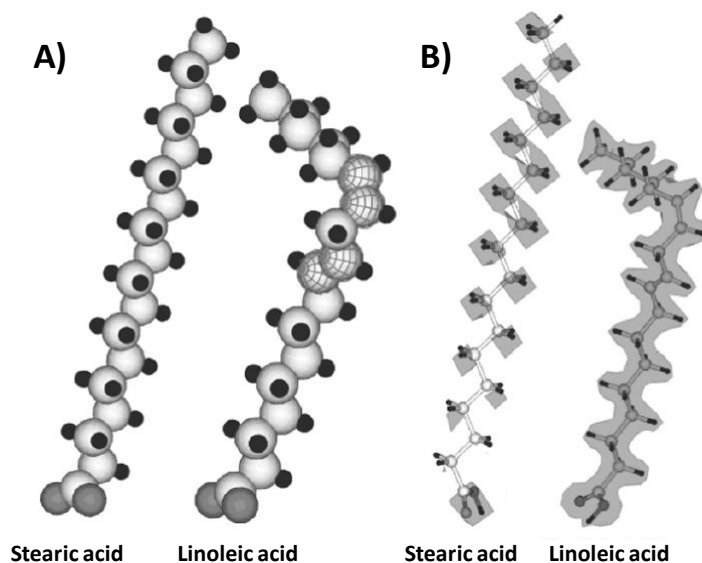


**Figure 1.4.** A) The molecular conformation and the energy minimized structures of the stearic (SA) and linoleic acid (LA). B) The calculated electron density distribution on stearic and linoleic acid [51]

## 1.2.2 Chemical properties

### 1.2.2.1 Autoxidation and photo-oxidation

Autoxidation represents a variety of chemical reactions between oils and ambient oxygen under heating or UV irradiation [52]. Typically, autoxidation is a result of free radical driven [53] peroxide formation, hydroperoxide decomposition, polymerization, scission, branching and related processes (Figure 1.5).

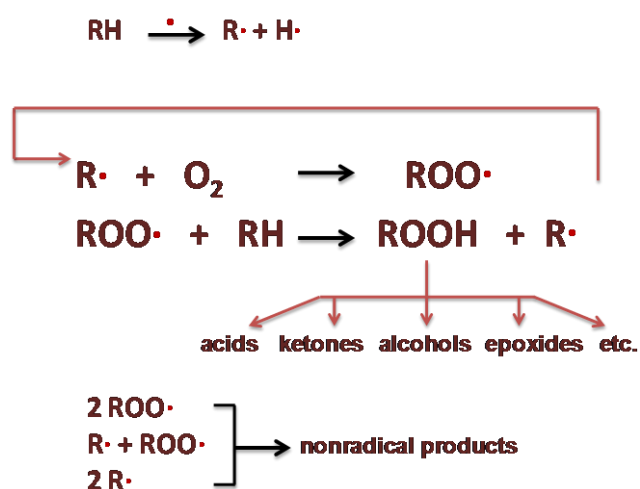


*Figure 1.5. The pathways of free radical reactions during autoxidation process*

The initial cause of oxidative degradation is free radicals, which are often generated due to the presence of metal ions. Double bonds are oxidized more easily than fully saturated hydrocarbon chains. Free radicals attack the so-called allylic hydrogen, located next to the double bond. Alkyl radicals rapidly react with the ambient oxygen, which is usually available due to its solubility in vegetable oils. Peroxy radicals are formed. A peroxy radical can attack the allylic hydrogen of another molecule as well, turning into hydroperoxide. Consequently, another alkyl radical is formed, transforming into peroxy radical, again capable of attacking another double bond. As a result, the reaction propagates and produces progressively increasing levels of hydroperoxides. During the free radical attack not only the hydroperoxide is produced, but, as the double bond usually stays intact, the remaining allylic

hydrogen atoms can be also subject to another free radical attack. Also, the double bond is delocalized during the loss of hydrogen.

Mono-unsaturated FA contain isolated double bonds, which make allylic hydrogen atoms more prone to free radical attacks compared to saturated FA (Figure 1.6a). Polyunsaturated fatty acids, however, contain two or more double bonds, which are interrupted with methylene, i.e. two unsaturated bonds around one saturated C atom with so called ‘bis-allylic hydrogens’ (Figure 1.6b). These are much more vulnerable to oxidation than regular allylic hydrogens.

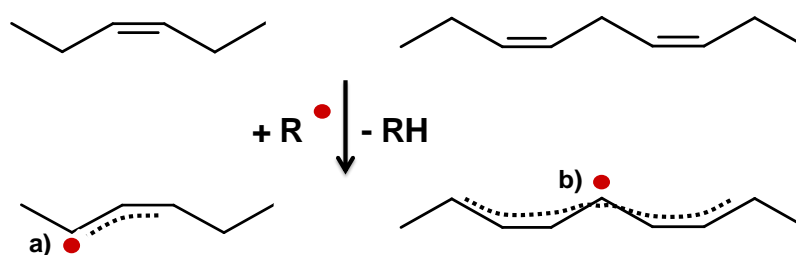


**Figure 1.6.** Free radicals attacks on a) allylic hydrogen in monosaturated acids and b) bis-allylic hydrogen in polyunsaturated acids

### 1.2.2.2 Hydrolysis

The most prevalent types of biodiesel are methyl esters of rapeseed and soy fatty acids, predominantly oleates and linoleates. Exposure to humidity, which is very likely at the metal / biofuel / air interface, leads to ester hydrolysis and free fatty acid formation, especially if the media deviates from pH 7 (Figure 1.7).



**Figure 1.7.** Formation of free fatty acid in biodiesel through hydrolysis and metal soaps

Compared to bulk oil conditions, various chemical processes are much more intensive at the interface between fuel, metal and air (Figure 1.8).

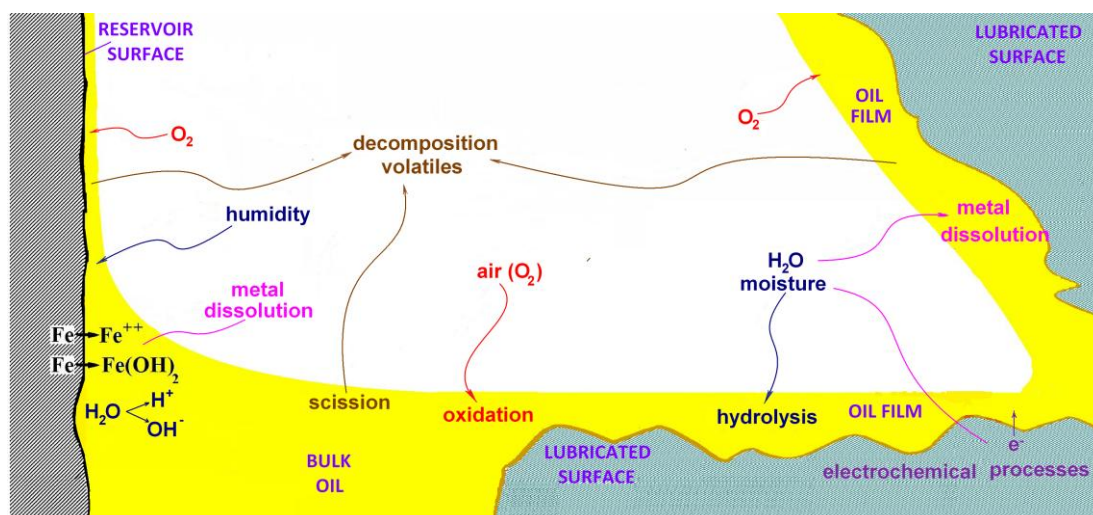


**Figure 1.8.** Occurrence of major degradation processes in thin oil films on steel surfaces, consumption of  $O_2$ ,  $H_2O$  and emission of volatile products [54]

Ambient humidity can produce condensation of water on the inside walls of a lubricant reservoir and lead to hydrolysis reactions. During hydrolysis, formation of ionic species, such as free carboxylic acids and soaps, results in increased electrical conductivity. Lower electrical resistance favours electrochemical mechanisms, leading to various processes, such as dissociation, hydroxide formation or metal dissolution in the oil film [55]. Dissolved metals are free radical precursors, consequently the oil oxidises faster, leading to even more reactive and polar, or sometimes ionic media.

### 1.2.2.3 Ozonolysis

Ozonolysis is the most versatile method for oxidative cleavage of the double bond [56], so it occurs only for unsaturated compounds through electrophilic addition [57]. In bulk, the reactivity of unsaturated FA in the presence of  $O_3$  is well described in literature [58-60]. Indeed,  $O_3$  inserts through the double bond and forms primary ozonide, which decomposes leading to the formation of two types of products: aldehydes (or ketones) and Criegee intermediates (biradicals). Criegee intermediate, depending on the place of cleavage, could form mono or dibasic acids. The schema is presented in Figure 1.9.

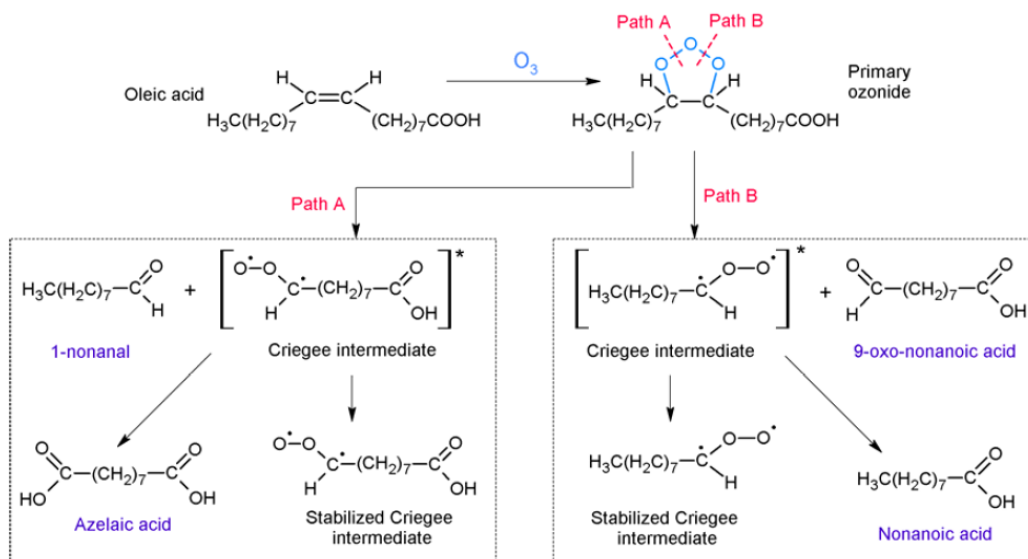


**Figure 1.9.** Reaction scheme for formation of volatile and liquid-phase products [59]

After that stabilized Criegee intermediate could react with one of the products by forming secondary ozonide or others.

### 1.3 Phospholipids

Phospholipids are amphiphatic compounds containing one or more phosphate groups.

They are divided into two main classes depending on the presence of either a glycerol or a sphingosine backbone: glycereophospholipids and sphingophospholipids, respectively.

#### 1.3.1 Molecular structure

The head group which contains phosphate and/or others functional groups is always hydrophilic. The fatty acids which are linked with the other two positions of glycerol backbone create hydrophobic character. They could vary in the level of unsaturation and the number of carbon in the alkyl chain thus creating specific character and stability to entire molecule.

### 1.3.1.1 Glycerophospholipids

This class is the most abundant class found in nature. Two fatty acids and a phosphoric acid are attached as esters in the glycerol backbone. The stereospecific nomenclature usually places the phosphate with each headgroup class at the *sn*-3 position of the glycerol backbone.

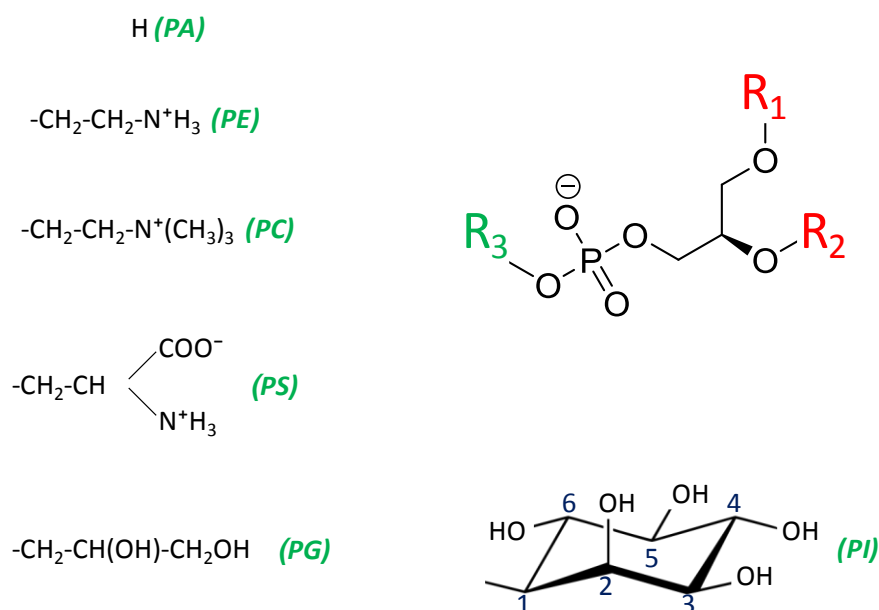


**Figure 1.10.** The structure of glycerolphospholipids

Phospholipids could be divided into 6 subclasses depending on which functional groups are linked to the phosphate group (Figure 1.10).

- i) Phosphatidic acid (PE) is negatively charged lipid. It is not an abundant lipid constituent of any living organism, but it is extremely important as an intermediate in the biosynthesis of triacylglycerols and phospholipids and as a signaling molecule (web).
- ii) Phosphatidylethanolamine (PE) is neutral or zwitterionic phospholipid. It is widespread lipid and important components in biomembranes.
- iii) Phosphatidylcholine (PC) has a neutral charge. It is the main component of biological membranes, also react as pulmonary surfactant. PC is the major component of lecithin.

- iv) Phosphatidylserine (PS) is negatively charged lipid.
- v) Phosphatidylglycerol (PG) is negatively charged lipid
- vi) Phosphoinositide is a part of membrane and participates into the metabolic processes. It is negatively charged lipid with the inositol group linked with the phosphate group (phosphatidylinositol PI), depending how many additional phosphate groups (1 to 3) are linked it is divided into: phosphatidylinositol phosphate (PIP), phosphatidylinositol bisphosphate (PIP<sub>2</sub>), phosphatidylinositol triphosphate (PIP<sub>3</sub>).

### 1.3.1.2 Sphingophospholipids

For Sphingophospholipids, the phosphate group is linked to i) sphingosine backbone ( $R=H$ ), ii) ceramide ( $R$  is an amide-linked fatty acid). From the other site phosphate group could be linked with such groups as cholines, ethanolamines, inositols ( $X$ ). (Figure 1.11)

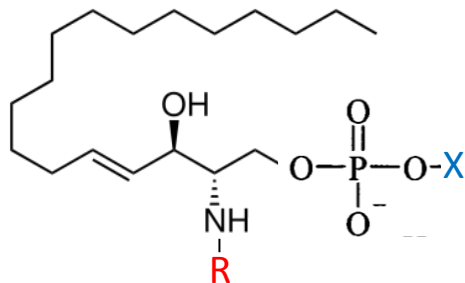


**Figure 1.11.** Simplified structure of sphingophospholipids

### 1.3.2 Organization

Phospholipids could form various structures in aqueous media, owing to the interaction of hydrophilic head groups and hydrophobic alkyl chains with water molecules. In Figure 1.12 the main organization are demonstrated.

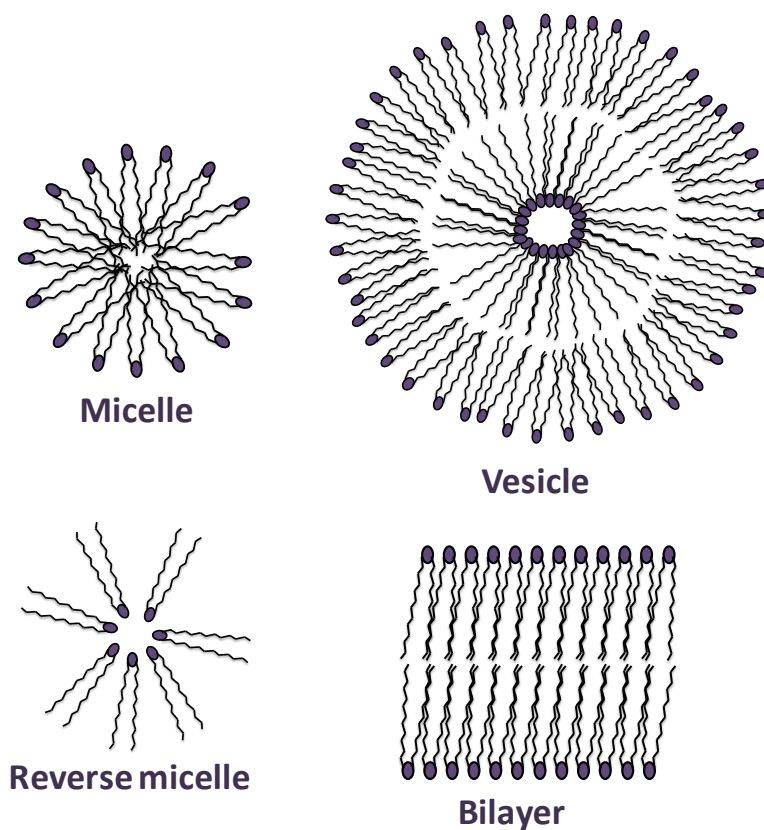


*Figure 1.12 Organization of phospholipids in aqueous media*

## 1.4 Lipids at solid surface

### 1.4.1 Adsorption procedures

Several methods could be used for the deposition of lipid films on solid surfaces. In this section three main procedures are described which are mostly used and described in literature [12, 61].

#### a) Langmuir-Blodgett

Langmuir-Blodgett monolayers or multilayers are transferred layer-by-layer from water/air interface to the solid surface (Figure 1.13.). Deposition of the first layer depends on the nature of the substrate, which could be i) hydrophilic, where lipids interact with their head group and ii) hydrophobic, where lipids interact with their tail group [62]. Usually, in order to obtain monolayer fatty acid/n-hexane [63, 64] or phospholipid/chloroform [65-67], the solution is spread on a subphase of pure water or salt  $TbCl_2$ ,  $CdCl_2$  or other salt solution



(depending on pH is needed). After solvent evaporation, the monolayer is compressed to a specified surface pressure and is transferred to the substrate by lifting it vertically out of the subphase at chosen speed.

Two thermodynamical variables, temperature and surface pressure, can be directly controlled. Furthermore, the intramonolayer and the monolayer-subphase interactions can be widely varied by changing the head or tail parts of the molecule, or by changing pH or ion content of the subphase [68].

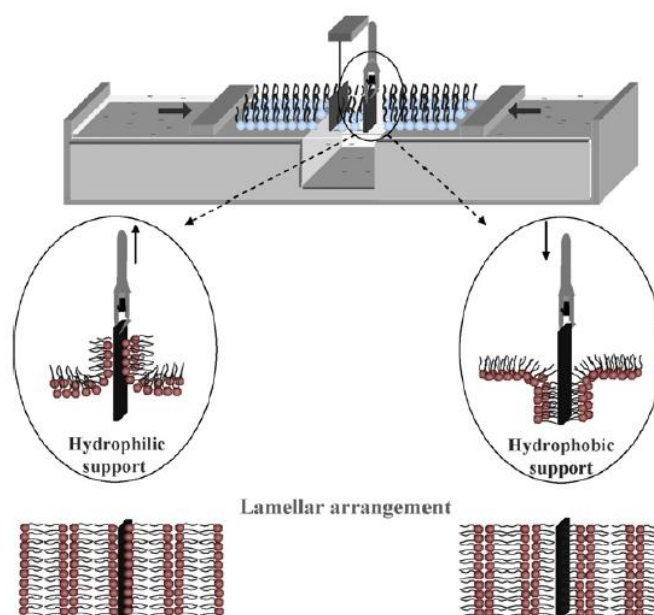


**Figure 1.13.** Principle of Langmuir-Blodgett technology [69]

#### b) Vesicles fusion

The spreading of unilamellar vesicle of phospholipid is very popular method for preparation of solid supported bilayers [11, 70, 71]. Firstly, lipids, usually phospholipids, are dissolved in the organic solvent. After solvent evaporation, the dried lipid film is resuspended in an aqueous buffer solution yielding to multilamellar or unilamellar vesicle suspensions, which are deposited on to the surface. Experimental conditions such as temperature, buffer pH, sonicating time, vacuum and etc. should be carefully controlled.

Several different surface-confined membrane models could be suggested depending on the properties of the solid support and in which form the phospholipid is expressed (Figure 1.14).

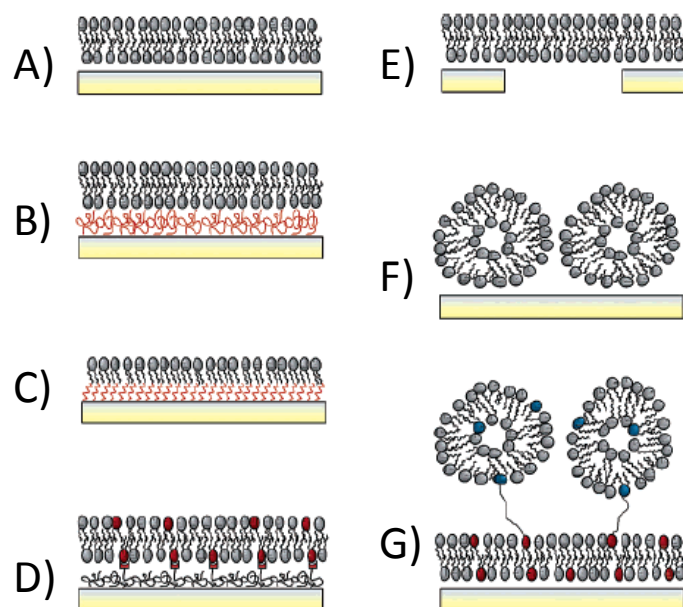


**Figure 1.14** Surface-confined membrane models: A) solid-supported lipid bilayer; B) polymer-cushioned lipid bilayer; C) hybrid bilayer, consisting of a self-assembled monolayer (e.g., thiols on Au or silanes on glass or silica) and a lipid monolayer; D) tethered lipid bilayer; E) freely suspended lipid bilayer; F)-G) supported vesicular layers [11].

### c) Adsorption from lipid solutions

The adsorption of lipids can be also carried out from diluted solutions, obtained by dissolving lipid solid in organic solvents. The main criterion for the choice of solvent is lipids solubility in it (see 1.4.4.2). The substrate is immersed in solution of solvent containing soluble fatty acid or other lipid molecules. After a an incubation time, the sample is put out of the FA solution, thoroughly rinsed, usually using the same solvent (pure) and dried under inert gas flow. When the solid substrate is immersed into a solution of the surface-active material, molecules spontaneously self-organize on the surface.

However adsorption from lipid solution, even very easy to perform, comparing with Langmuir-Blodgett technique, could not control the density of the film.

#### 1.4.2 Properties of the lipid layers

The properties of the adsorbed phase are related to its thickness and density, as both reflect the degree of self-assembly and self-organization.

The backbone generally is C-C aliphatic chain, differing on length, terminal functional groups or level of unsaturation. The angle between it and the substrate surface normal (axis z) is called tilt angle ( $\theta_t$ ) with the tilt direction ( $\chi_t$ ) and twist angle ( $\psi$ ) of the molecule (Figure 1.15A). Different backbones have different degrees of freedom to describe their conformational state.

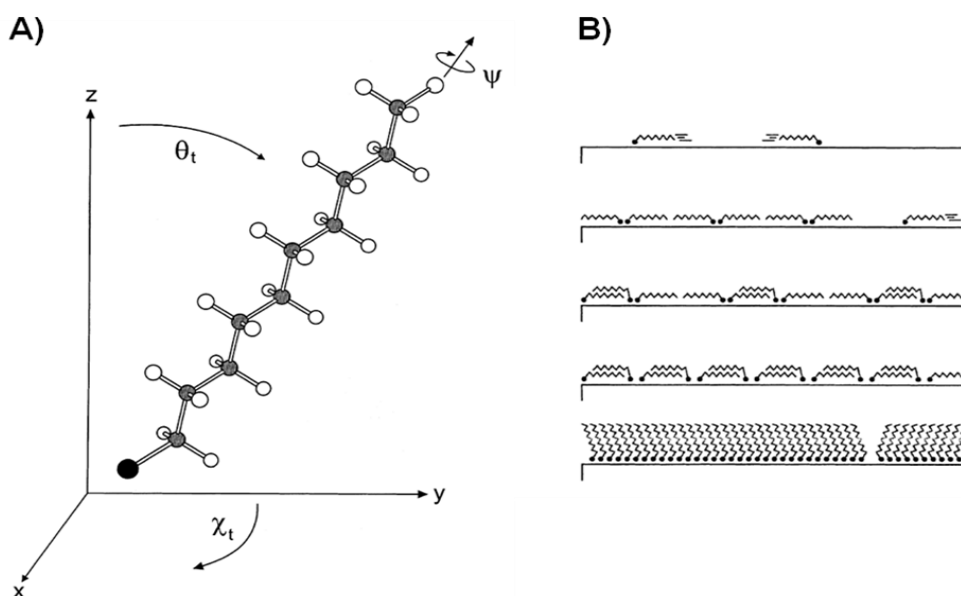


**Figure 1.15.** Decanethiol on gold schematic representation of A) angular degrees of freedom; B) evolution of structures during growing (adapted from [72])

The density of adsorbed molecules depends on the how hydrocarbon chain is tiled. The long alkyl chains may be involved in intermolecular interactions, mainly van der Waals in nature, enhancing the molecular organization of the adsorbed phase and inducing a high packing density.

Actually, the mechanism of formation of fatty acid SAMs could thus resemble the one described for alkane thiols, broadly reported in the literature [73-76]. Different stage of film formation depends on variation of the concentration or adsorption time (Figure 1.15B). When the surface is saturated, it means that molecules are in the highest possible packing. The thickness and orientation of the film depends on the origin, especially level of unsaturation, of the alkyl chain. It is in keeping with the extended zig-zag molecular length for trans saturated ones.

Orientation of the molecules could be perpendicular or parallel to the surface normal.

#### *1.4.3 Modification of surface properties*

Lipids, as amphiphilic molecules, may adsorb on a variety of solid surfaces and could organize on the surface in different ways. Ability to manipulate both head and tail groups of entire molecules let to create an excellent system for fundamental understanding of phenomena affected by competing intermolecular, molecular-substrates, molecule-solvent interactions like ordering and growth, wetting, adhesion, lubrication and corrosion [12]. Phospholipids films on solid substrate is particularly attractive for biomimetic systems, which could be used for biological membranes [77], biosensors [78].

##### a) Water repellency

Wettability is an important feature of the surface. Nowadays, superhydrophobic surfaces have attracted a big interest for the self-cleaning properties [69], which principal is known in many biological surfaces [79, 80].

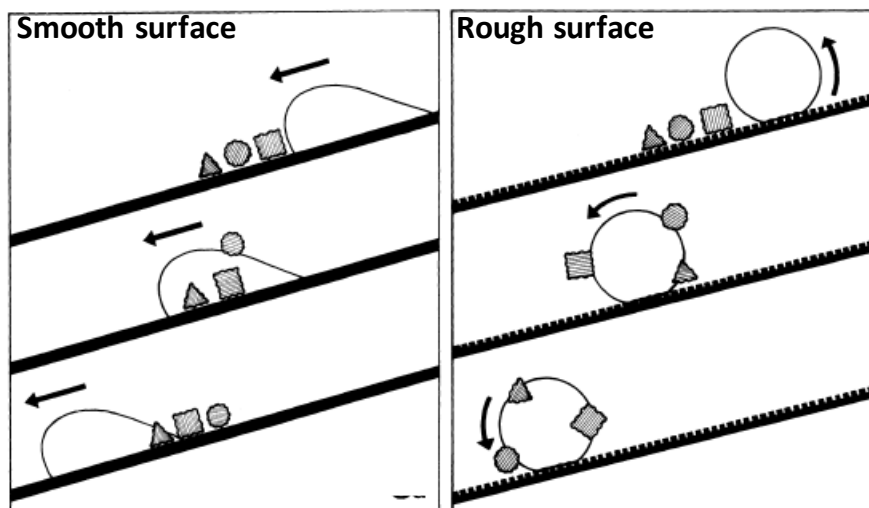


**Figure 1.16.** On smooth surfaces (left) the particles are mainly redistributed by water, they adhere to the droplets surface; and on rough surfaces (right) are removed from the leaves when the droplets roll off [79]

Wettability depends on two factors i) the surface energy (chemical composition) and ii) the roughness of the surface. The influence of rough surface is presented in Figure 1.16.

Fatty acids, especially saturated ones, have a flexible hydrocarbon chain which, if adsorbed on the surface with *trans* configuration, extend into a long zig-zag. This alkyl chain creates hydrophobic feature. So the adsorption of long fatty acids on rough surfaces such as nanorods or nanowire of ZnO, creates superhydrophobic surfaces, which are stable in environmental storage [81-83]. By combining both factors to reach repellent surface, before chemical adsorption of stearic acid, alumina was modified by creating rough boehmite surface coated with polyethyleneimine (PEI) [24, 84].

Water or other solvent contact angle with the surface is the main characteristic for evaluation of this phenomenon and it is defined by Young's equation (see chapter 2, section 2.3.5)

## b) Lubricating effect

Fatty acids are widely used as friction modifiers in fuels and lubricating oils as lubricating additives. Purified crude tall oil, which is a byproduct in paper making, is a mixture of unsaturated fatty acids among other components. These mixtures are currently used as renewable and environmentally friendly additives in diesel fuels [85]. Organized films of fatty acids on the surface reduce friction coefficients, because they, as surfactant molecules adsorb from the solution onto polar, metal surfaces by forming single monolayers or semi-ordered, viscous layers which are sufficient to limit or prevent metal-metal adhesion and thus friction and rubbing contacts [86].

Carboxylic acid systems on iron demonstrated good lubricity on the friction surfaces, whereas alcohol, amine and ester systems showed poorer lubricity [87]. Different techniques could be used to evaluate the stability and effect of boundary lubricant. Combination of the measurements of ball-on-plate type sliding friction tester and from a two-dimensional elastic modulus showed that the frictional properties of the ultrathin film depends on the film strength [88]. Scanning force microscope (SFM) probes not only surface topography, but also measures friction forces, both allow to compare tribological properties of different areas of monomolecular films [89]. Ultrathin (till 1nm and higher) film interferometry is measuring the boundary film-forming behavior of long chain carboxylic acid [86]. Friction force microscopy could measure the effects of adhesion, contact area, pressure on the lubricating properties of self-assembly monolayers on metallic substrate [90]. The frictional properties of the dry monolayers also could be recorded by atomic force microscope (lateral mode) and by nanotribometer [51].

Friction measurements on steel after adsorption of saturated and unsaturated fatty acids also showed that increasing degree of unsaturation friction coefficient and critical shear stress also increased, showing not so close-packed system as in stearic acid case [90].

Tribological behavior was different for SA and LA adsorbed on steel surface, where for LA interactions with iron surface yield a low friction carboxylate

soap film because of the high density of the double bond region of the backbone [51].

### c) Biomimetic surfaces

Phospholipids are natural amphipatic molecules which are able to self-assemble both in bulk and at interfaces, leading to the formation of wide ranges of ordered structures [91, 92]. These molecules had, indeed, been extensively used in the design of biomimetic systems in applications related to biomaterials and biosensors [4].

For example, protein adsorption on the hydrophilic head groups of these amphiphilic molecules could be used as a model to study protein membrane interactions. Surfaces with hydrophobic alkyl chains have a high significance in bioseparations and intravenous drug delivery systems in which proteins can be incorporated in micelles and liposomes [93].

There can be done various manipulations between hydrophilic and hydrophobic features depending on desired nature of substrates or final goal of applications. For example, Lazzara et al modified the surface of the anodic aluminum oxide using silanization procedure by creating hydrophobic character, then by the mean of unilamellar vesicles phospholipid monolayer was created and finally mobile lipid phase could be functionalized with mobile receptors for proteins in solution [94].

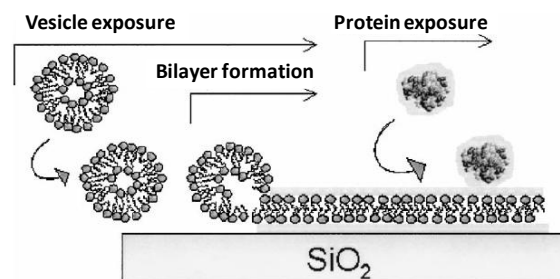


**Figure 1.17.** Possible scheme of biomimetic surface [71]

Figure 1.17 demonstrates one of the possibilities for biomimetic surfaces, where phospholipids are adsorbed on neorganic substrate by leaving hydrophilic head groups on top, for further interactions of proteins or other biomolecules.

Phospholipids, especially the ones which have zwitterionic and ionic head groups, also act as excellent capping agents for the synthesis of noble metal nanoparticles [95-97].

#### *1.4.4 Mechanism of self-assembly of fatty acids*

The mechanism of self-assembly of fatty acids on solid surfaces has been broadly described in literature. It results essentially in the contribution of the main interactions:

- i) molecule–surface binding;
- ii) intermolecular interactions between alkyl chains;

Both mechanisms are greatly influenced by the nature of substrates and the intrinsic properties of molecules. The parameters related to the adsorption procedure and the environmental conditions also highly impact the organization and stability of the film.

The behavior of adsorption of FA (varying the concentrations from 0.001 to 10mM) on the metallic surfaces can be explained by different factors, as described below.

##### *1.4.4.1 Influence of FA properties*

It appears that FA properties such as chain length and level of unsaturation influence only the interactions between alkyl chain molecules.

- a) Effect of chain length

The tendency of saturated FA to form organized monolayers on the flat substrates increases by increasing the length of aliphatic chain. A process of self-organization may occur due to the intermolecular (van der Waals) interactions between the hydrophobic aliphatic chains of the molecules, and



may contribute to their alignment. The acids with chain lengths of C<sub>12</sub> or longer are at or near bulk packing density [21, 98]. FTIR spectra intensity of C-H bands after C<sub>10</sub>, C<sub>12</sub>, C<sub>16</sub> adsorption on stainless steel increased as the number of carbons in the hydrocarbon chain increased, and for C<sub>10</sub> showed conformational disorder [99]. According to ellipsometric measurements, the thickness of the adsorbed film corresponds to the extended zig-zag molecular length increased with the length of the alkyl chain [15, 19]. This trend was also observed on nanostructured surfaces. For example, after modification of porous alumina membranes with C<sub>8</sub> and C<sub>18</sub> fatty acids, contact angle and infrared results demonstrated that long fatty acid created more hydrophobic and more ordered surface [100]. For creating superhydrophobic features of ZnO nanowire array, chemical modification by various fatty acids (C<sub>6</sub>, C<sub>8</sub>, C<sub>10</sub> and C<sub>12</sub>) were performed and they did not exhibit sufficiently low surface energy to prevent penetration by water as stearic acid (C<sub>18</sub>) [83].

b) Effect of level of unsaturation

In addition to the chain length or surface properties, it is important to evaluate the effect of unsaturation. Due to double bonds, conformational features, they would not demonstrate exactly the same behavior and stability as saturated FA. Badre et al compared saturated fatty acid (stearic) and two unsaturated fatty acids (elaidic and oleic) which were adsorbed on zinc oxide. By combining results of WCA and PM-IRRAS, the conclusions were made that aliphatic chains of the SA were packed and very well ordered whereas such structures were not so well expressed with the two unsaturated acids, by contrast oleic acid (*cis* configuration) presented less flexible alkyl chain than elaidic acid (*trans* configuration) [81]. By comparing the adsorption of three unsaturated fatty acids (oleic, linoleic and linolenic) the authors concluded that the chemisorbed amount was not influenced by the alkyl chain of the fatty acid but was dependent on the interactions between the carboxylic headgroup and the surface, however physisorbed amount increased with increasing unsaturation of fatty acids [85].

#### 1.4.4.2 Influence of solvent

The choice of solvent also affects the formation and stability of lipid layer.

Such factors as polarity, the chemical structure of the solvent, also the solubility of corresponding fatty acid in this solvent, influence the quality of the final result.

The adsorption of stearic acid on the surfaces was performed from solutions in ethanol or hexane, however the stearic acid films formed from both solutions were spectroscopically identical [101].

Taylor and Schwarts performed the adsorption octadecanoic acid in different solvents including hexadecane, hexane, ethanol, THF and acetone [20]. Hexadecane was the most suitable, as others left the surface wetted and always resulted in film dissolution.

In another study the adsorption of stearic acid on alumina was done from three different solvents, hexadecane, ethanol and toluene [102]. It appeared that in ethanol SA adsorbed weakly and required longer time of adsorption if to compare in another solvents. Water contact angle was the highest after SA adsorption from hexadecane and toluene. After exposure in air, hydrophobic species was retained on the surface from hexadecane or a contaminant, so for further experiments the authors chose toluene.

To investigate the effect of solvent in the organization of linear alkanes on solid surface, Lundgren et al. have used were n-hexadecane and its highly branched isomer viz., 2,2,4,4,6,8,8-heptamethylnonane to absorb fatty acids on steel. The authors demonstrated that there was only a slight difference [85].

#### 1.4.4.3 Influence of adsorption procedure

The most common method for the formation of FA layer on solid surfaces is “spontaneous adsorption” from solution (as described previously in section 1.4.3.c). This procedure is simple to perform and does not need many adjustments. FA layer could also be deposited from the gas-phase. As high vacuum is needed, it is a complicated and expensive procedure. But there are no residues of the solvent or other contamination.

The differences between gas-phase and solution-phase layers could arise from three major possibilities: lower surface coverage, higher cant of the head group or combination of both. That is why gas-phase was consistent with more densely packed array of alkyl chains than for the solution [103, 104].

#### 1.4.4.4 Influence of surface properties

Carboxylate ions could coordinate with metallic surfaces in several ways, depending on the nature of metal: crystalline, oxide, hydroxide, alloy and etc, by bidentate or monodentate binding (Figure 1.18).

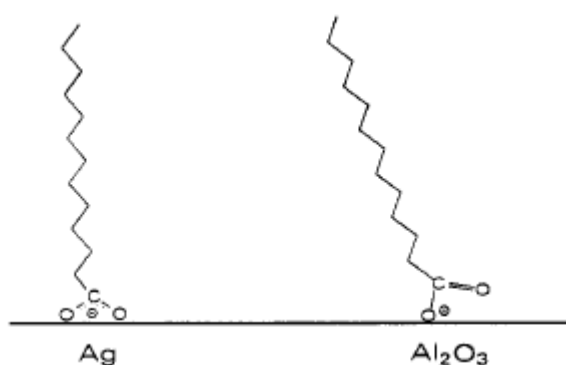


**Figure 1.18.** Scheme of adsorption of stearic acid on smooth Ag surface and Al<sub>2</sub>O<sub>3</sub> [101]

The chemical composition of the substrates seems to play a pivotal role in the formation of adsorbed films [105]. The binding strength of the FA to glass substrates is lower than those to aluminum substrates. By using IR analyses, the COO<sup>-</sup> bands were observed after adsorption on Al<sub>2</sub>O<sub>3</sub> substrate, while on glass the free acid C=O stretch band was clearly observed. This may indicate that metal ions on the surface caused deprotonation [15]. Carboxylate formation could indeed occur by reaction of the acid at surface hydroxyls with release of water and/or reaction at Al-O lattice bonds with the formation of a surface hydroxyl [22, 106].

Also the structure of adsorbed film depends on the metal substrate. Tao compared three different FA/metal systems, where in all cases FA were linked

with the surface through carboxylate ion [19]. The silver provided a unique binding in a highly ordered array, even for very short chains. On the surface of copper and aluminum, oleophobic monolayer can be formed for acids  $C_{10}$  and longer but FA/Cu system was more ordered than FA/Al system. Other authors also claimed that the carboxylic acid group dissociatively chemisorbed at Ag surface by carboxylate species with a specific orientation [103, 107, 108].

Conversely, Thompson and Pemberton claimed that on  $Al_2O_3$  stearic acid adsorbed on the surface through a single oxygen, while on Ag surface – through carboxylate, which could reduce van der Waals interactions of the alkyl chains and create less ordered film [101]. After adsorption of different length of fatty acids on silver and copper on gold (prepared by underpotential deposition), in all cases IRAS spectra showed carboxylate ion, however Au/Cu suggested less ionic characteristic than on bulk copper oxide [98].

Alkanoic acids weakly adsorb with native oxide surface of aluminum, so not only hydroxylation treatment could be done, but also the reaction with metal alkoxide, which changes the surface functionality for stronger interaction through carboxylate ions of alkencarboxylic acids [104].

The roughness of the Al6111 alloy surface (magnesium alloy) is 50-100 times larger than a typical evaporated metal oxide surface; anyway adsorption of stearic acid could change the nature of the active-passive transition of this alloy [109].

Hydrothermally prepared pseudoboehmite was utilized as a model aluminum oxide/hydroxide surface, because of the very low surface carbon concentration and the similarity of the surface chemistry to that of air-formed films after ambient storage, where fatty acids adsorbed through carboxylate ion [110].

Van den Brand et al. compared myristic acid ( $C_{14}$ ) adsorption on the differently prepared aluminum substrates: dehydroxylated, vacuum evaporated, acid pretreated, alkaline pretreated, pseudoboehmite; in all cases fatty acids interact with the surfaces through carboxylate ion [111]. However, in the other work, stearic acids bound to sapphire (single-crystal C plane aluminum oxide) surfaces via a bidentate interaction of carboxylate, while it bound to alumina

surfaces via both bidentate and monodentate interactions [18]. It is also known that aluminum oxide adsorbs contaminants from the ambient air, in parallel with other active surfaces [106].

On signal crystal sapphire ( $\alpha\text{-Al}_2\text{O}_3$ ) substrates, octadecanoic acid forms monolayer with a reactivity that strongly depended on the preparation steps of the substrates [20]. On stainless steel surfaces, the adsorption of FA led to two different scenarios: monodentate and bidentate bindings, according to the authors [51, 99]. However, in another study, only the bidentate bonding was evidenced using long-chain carboxylic acids with different terminal groups [112]. On ZnO and saturated and unsaturated acids adsorbed through carboxylate ion [81, 82].

The investigations of adsorption on FA on metallic surface are summarized in Table 1.3.

**Table 1.3.** FA adsorption on metallic surfaces

Substrate	Fatty acid	Solvents	References
Al	C <sub>6:0</sub> -C <sub>22:0</sub> , C <sub>18:1</sub>	hexadecane, ethanol, toluene, BCH	[17, 102]
Al <sub>2</sub> O <sub>3</sub>	C <sub>6:0</sub> -C <sub>22:0</sub>	hexadecane, ethanol, toluene, chloroform	[9, 15, 18-22, 101, 106, 111]
Hydroxylated Al	C <sub>8:0</sub> , C <sub>14:0</sub>	chloroform, gas	[104, 111]
Al(treated)*	C <sub>14:0</sub>	phase	[111]
Al alloy	C <sub>18:0</sub>	chloroform	[109]
Porous membranes	C <sub>8:0</sub> , C <sub>18:0</sub>	ethanol hexadecane	[100]
Cu	C <sub>4:0</sub> -C <sub>22:0</sub>	hexadecane, nitrobenzene	[19, 98, 113]
Cd	C <sub>18:2</sub>	Dodecane	[114]
Ag	C <sub>3:0</sub> -C <sub>20:0</sub> , C <sub>22:0</sub>	hexadecane hexane gas phase	[19, 98, 101, 103, 107, 108]
Zn	C <sub>6:0</sub> -C <sub>18:0</sub> ; C <sub>18:1</sub>	Ethanol	[81-83]
Steel	C <sub>18:0</sub> , C <sub>18:1</sub> , C <sub>18:2</sub> , C <sub>18:3</sub>	dodecane, hexadecane, 2,2,4,4,6,8,8- heptamethylnonane, nitrobenzene	[85, 90, 113, 114]
SS	C <sub>8:0</sub> -C <sub>14:0</sub> , C <sub>16:0</sub> , C <sub>18:0</sub> , C <sub>18:2</sub>	ACN, THF	[51, 99, 112]
Ge, ZnSe	C <sub>20:0</sub> , C <sub>22:0</sub>	bicyclohexyl	[105]
Bronze	C <sub>18:2</sub>	Dodecane	[114]

\*After polishing Al was pretreated by i) acid, ii) alkaline, iii) heated in air at 275°C for 24h.

#### 1.4.5 Stability of adsorbed FA

##### a) Stability in solvent

Usually, after the adsorption procedure and before surface characterization, samples are rinsed with pure solvent to remove the excess of non-adsorbed molecules. Accordingly it is important to examine the effect of this rinsing step and even further immersion in solvent (long time immersion) on the stability of the adsorbed phase. According Samant et al., chloroform removes self-assembled film made with C<sub>22</sub> on Ag surface after rinsing [17, 108]. On signal crystal sapphire ( $\alpha$ -Al<sub>2</sub>O<sub>3</sub>), the rinsing in different solvents led also to a significant removal of an octadecanoic acid layer [20], while the latter remain stable on native aluminum substrate upon rinsing in hexane, pentane, isooctane and ethanol [21, 22, 101]. This discrepancy in the stability of adsorbed FA layers at different aluminum oxide surfaces showed that the strength of RCOO<sup>-</sup>-Al<sup>3+</sup> bonding depended on surface preparation [20]. Furthermore, additional rinsing and sonification in THF or ethanol also did not remove adsorbed long chain carboxylic acid with different terminal groups on SS [112].

##### b) Stability in air

Air contains a variety of reactive components such as oxygen, water, which could enhance additional but not desirable reactions on the films of FA ion metallic surfaces.

However, after 1 to 7 days of exposure to ambient temperatures, no changes were noticeable on IR spectra of adsorbed C<sub>10</sub>, C<sub>12</sub>, C<sub>16</sub> on stainless steel. This may indicate that the films are stable under these conditions [99].

##### c) Stability in aqueous solutions

The stability of fatty acids modified alumina membrane was checked by immersing the sample in different modifications of phosphate buffer (pH=7.4) solutions [100]. The formed alkyl chain was unstable in aqueous solutions. The

presence of both NaCl and methanol in the solution provided the most stable condition for immobilized alkyl groups.

Differently treated aluminum surfaces with adsorbed C<sub>14</sub> after incubation in water showed similar behavior. Independently of surfaces, fatty acid was found to completely desorb, presumably chemisorbed carboxylate become replaced by water molecules [111]. Desorption of stearic acid after incubation in water during 240min reduced the surface coverage, but the alkyl chain packing order within the remaining islands was maintained [18].

The stability of stearic acid modified ZnO surface was evaluated by varying different pH from 1.8 to 12.6, in all cases the contact angle was unchanged and prepared surface remained superhydrophobic [82]. The tested long chain carboxylic acid with different terminal groups formed well-ordered monolayers on SS, as after additional rinsing in water the molecules were still strongly bound to the surface [112]

#### d) Stability under UV/O<sub>3</sub> treatment and heating

The photodecomposition process was investigated with contact angle measurements with SA-modified ZnO nanowire showing the decrease hydrophobicity of the surface by increasing time of UV radiation [83], where free radicals abstract hydrogen from alkyl chains and then produce alkyl radicals, which further react to form alkoxy radicals, which generate further reactive carbonyl through oxidation. These carbonyl groups dissociate through photodecomposition (in presence of UV) or attacking by radicals with the loss of carbon, and therefore reduce the carbon chain length of fatty acids [83]

The stability of stearic acid modified ZnO surface was checked at the elevated temperature 90-250°C for 24h, and contact angle results, which were measured at room temperature after these treatments, demonstrated that the temperature had no effect on the wettability [82].

#### 1.4.6 Particularity of aluminum substrates

The self-assembly of FA on Al substrates has attracted a particular interest due to the relevance of the Al oxides/hydroxides chemistry from a fundamental point of view, also because of the importance of this material in many technological applications.

The main techniques used for the characterization of FA layer on Al are listed in Table 1.4.

**Table 1.4.** Techniques used for the characterization of adsorbed FA films on various Al substrates

Techniques	Ref.
Infrared spectroscopy	[15, 17-22, 100, 102, 104, 106, 111]
Ellipsometry	[15, 17, 19, 21, 106]
Contact angle	[15, 18-21, 100, 102]
Atomic force microscopy	[18, 20]
Raman	[101]
XPS	[18, 21, 106]
others	[9, 18, 21, 100, 104, 109]

The most used technique is infrared spectroscopy, because it may evidence the group by which FA interact with the surface and may provide information regarding the pack density of layers and orientation of molecule. However most of investigations were carried out on flat “smooth” surfaces. As mentioned in previous section, the fatty acids adsorbed with the substrate through their carboxylate group, at around  $1580\text{ cm}^{-1}$  and  $1470\text{ cm}^{-1}$ , for asymmetric and symmetric  $\text{COO}^-$  modes. However, for the rough  $\text{AlOOH}$  surface, values were at  $1574\text{ cm}^{-1}$  and  $1411\text{ cm}^{-1}$  and for alkaline treated Al at  $1591\text{ cm}^{-1}$  and  $1417\text{ cm}^{-1}$ , respectively.

On flat surfaces, it is possible to deduce the orientation of the molecules with the respect of the surface plane. That is why, for  $\text{AlOOH}$ , the information on the orientation cannot be derived, because of its roughness, and infrared spectrum is a statistical average of the different orientation of the molecules with the respect to the metallic surface plane [111].



The band assignment of asymmetric and symmetric stretching modes of methylene groups with the values similar for bulk solutions at around  $2920\text{ cm}^{-1}$  and  $2850\text{ cm}^{-1}$ , respectively, showed the densely packed monolayers with the evidence of ellipsometry measurements.

Only several works described the changes of the flat surface morphology after adsorption of fatty acids using AFM (Table 1.4).

To conclude, it is obvious, that many investigations of the formation of FA layers were done on flat substrates. However we lack information about the interfacial process between these molecules and the rough surface with the deep analysis of not only chemical behavior, but also observations of the surface morphology and its wettability properties. For this reason, in this study fatty acid adsorption on hydroxylated Al substrate were investigated by using PM-IRRAS, AFM and WCA (section 2.3).

#### *1.4.7 Mechanism of self-assembly of phospholipids*

The adsorption of phospholipids on solid surface has been broadly reported in the literature, particularly in the context of supported bilayers. In the adsorbed state, phospholipid may form ordered layers at the nanoscale, by tuning parameters related to the substrate (surface wettability, charge, morphology, etc), the medium (temperature, ionic strength, etc) and the adsorption procedure. Regarding the latter parameter, the most common procedures used are: (i) Langmuir-Blodgett technique and (ii) the spreading of unilamellar vesicle of phospholipid (see section 1.4.1 a-b).

Hui et al. investigated the influence of different head groups of phospholipid on hydrophilic mica surface: phosphatidylcholine (DSPC) or phosphatidylethanolamine (DPPE and DLPE) and level of unsaturation of the linked fatty acids for the last two ones [66].

Adsorption and desorption of unilamellar vesicles of phospholipid containing PC head group on a Au(111) electrode surface were very profoundly analyzed by Bin et al using PM-IRRAS and electrochemical measurements [115]. They proved that adsorbed state of the film allows the maximum contact of the polar

head group and specifically the phosphate group with the metal. This transformation causes the chains to tilt and the heads to be less densely packed (Figure 1.19).

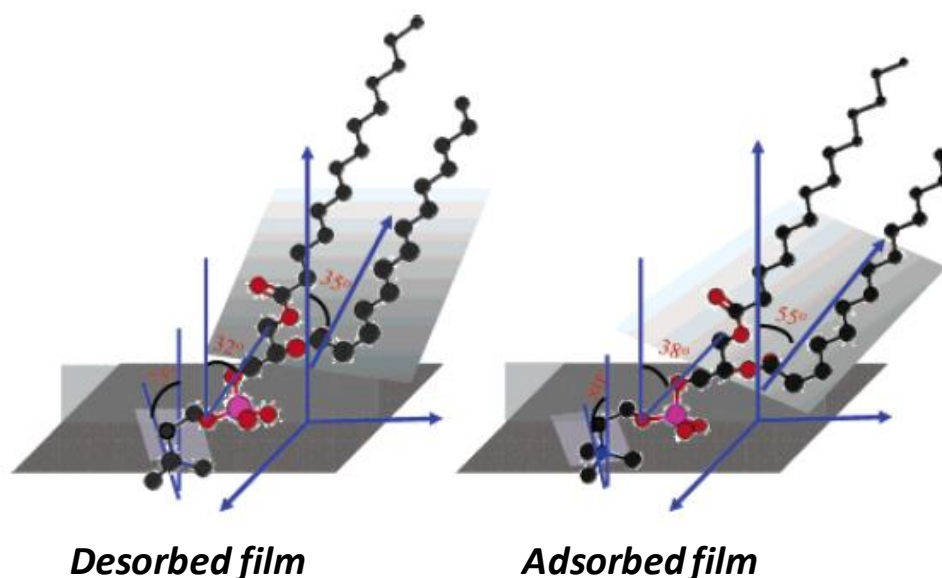


**Figure 1.19.** Scheme of orientation of the DMPC molecule in the bilayer at negative potentials (desorbed film) and positive potentials (adsorbed film) [115]

The nature of the substrate also strongly influences the properties of the phospholipid layers. In particular, hydrophobic surfaces seems to insure more stability to the system, as observed in previous studies, by means of surface modification using alkane thiols [116-119] or silanes [93, 94, 120].

Monolayers of arachidic acid and DPPC were transferred onto hydrophobic OTS (octadecyltrichlorsilane) covered silica slides, where molecules physisorbed with their tails groups [93]. They explained that the strength and rigidity of the packing in self-assembly monolayers depend mainly on van der Waals attraction between the alkyl chains together with some geometric considerations, such as the size of the polar head groups. The larger size of the DPPC head group (phosphatidylcholine) will geometrically obstruct a close packing of DPPC tails, while the zwitterionic DPPC head groups are expected to pack tightly, forming lattice network in which the head groups are

conformationally constrained due to the ionic interactions with the nearest neighbors.

Hereby using these techniques, many parameters have to be controlled, including the composition of lipid solution, concentrations of salt, pH, temperature, vesicle size, washing procedure, etc. [121].

Other procedures of adsorption have been also reported, such as spin-coating [122-125], dip-coating [126] or drop deposition/spreading of diluted lipid in organic solvent [122, 126, 127] or by other film deposition methods [128].

By combining chosen solvent, substrate and optimized concentration, desired number of layers could be formed using this simple procedure from organic solvents.

While, in the majority of studies, the adsorption of phospholipids has been performed on flat planar surfaces, investigations on nanostructured surfaces remains, however, poorly documented. Some authors have used nanoporous alumina membranes to form supported biomembranes made with phospholipids by means of vesicle fusion method [3]. Other authors have investigated the effect of surface roughness on the formation of phospholipid layer [127, 129], where one bilayer essentially smooth out the substrate.

In this study, Al surface with nanoscale roughness prior to and after modification with SA was used for adsorption of phospholipid to examining the effect of surface hydrophobicity. Adsorption, the stability of adsorbed layers and the surface wettability kinetics were analyzed with PM-IRRAS, XPS and WCA techniques (section 2.3).

## **II. MATERIALS AND METHODS**

## 2.1 Materials

All lipids were purchased from Sigma-Aldrich (France).

The chemical formula of fatty acids (FA): stearic acid (SA) ensured  $\geq 98.5\%$  minimum purity, and oleic acid (OA), linoleic acid (LA), caprylic acid (CA) and methyl oleate (MO) - 99.99%, lauric acid (LrA) -  $\geq 98\%$ , butyric acid (BA) -  $\geq 99\%$  are shown in Figure 2.1, and phospholipid, dipalmitoylphosphatidylcholine (DPPC) ( $\geq 99\%$ ), - in Figure 2.2.

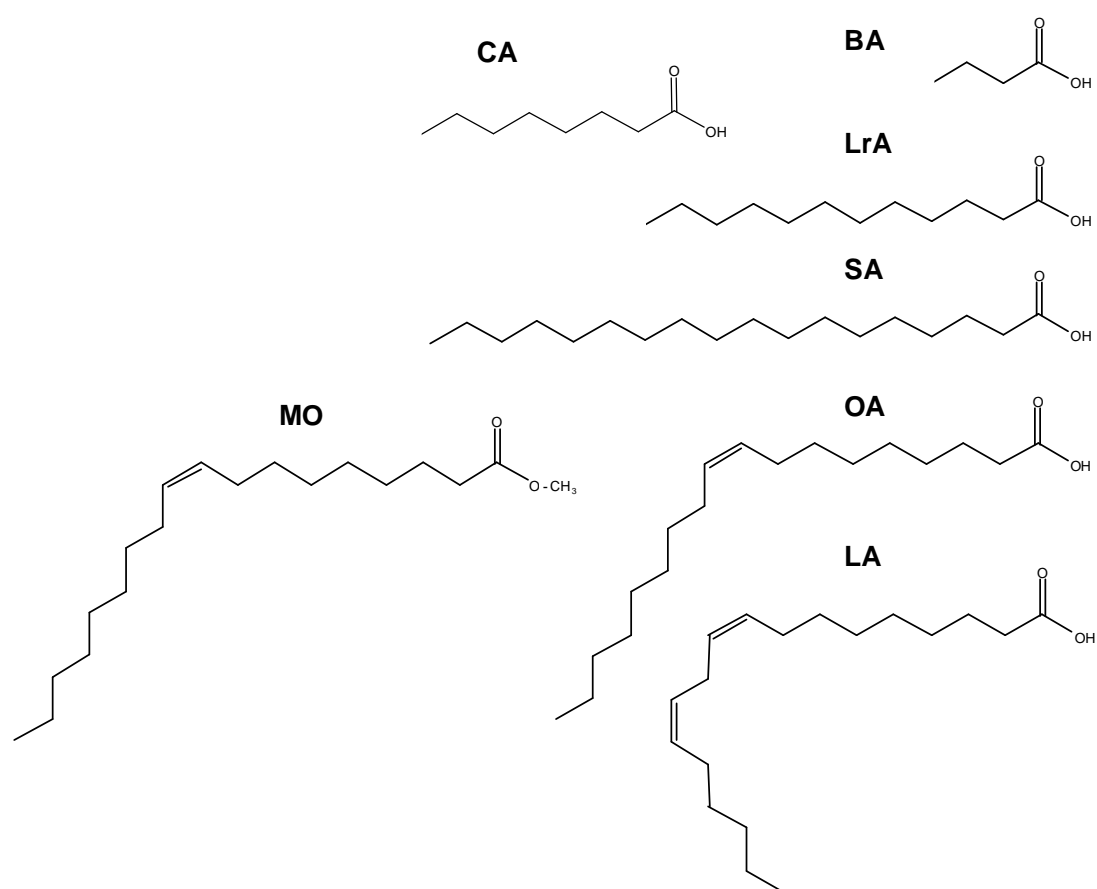


**Figure 2.1.** Molecular structure of butyric acid (BA), lauric acid (LrA), stearic acid (SA), oleic acid (OA), linoleic acid (LA) and methyl oleate (MO)

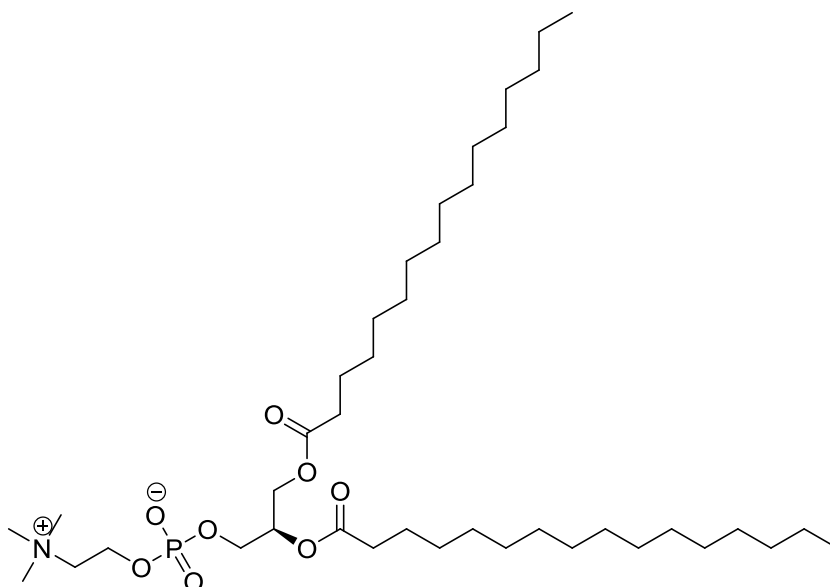


**Figure 2.2.** *The chemical structure of phospholipid dipalmitoylphosphatidylcholine (DPPC)*

Heptane (for HPLC,  $\geq 99\%$ ) and chloroform were also purchased from Sigma-Aldrich (France).

All aqueous solutions were prepared in ultra pure water. NaCl, purity 99.5 %, (concentration 0.6 mM), H<sub>2</sub>O<sub>2</sub> 30% (10 mM), phosphate buffered saline.

## 2.2 Procedures

### 2.2.1 Hydroxylation of aluminum

Polycrystalline Al (specimens of  $\sim 1 \text{ cm}^2$  surface area cut from a 2-mm thick plate, Al 99.95%; Si 0.05%, Goodfellow, France) were used for this study. The samples were mechanically polished with SiC papers of 600 and 1200 grain size (both sides) followed by fine polishing with successive 6, 3 and 1  $\mu\text{m}$  diamond suspensions (Struers, France). The samples were rinsed in binary mixtures of ultrapure water/ethanol (50%/50%) in a sonicating bath (70 W, 40 kHz, Branson, USA), and dried under nitrogen gas flow. For hydroxylation, samples were placed in boiling water for 2 min, immediately after surface preparation, then rinsed in ultrapure water and dried under nitrogen gas flow.

### *2.2.2 Adsorption of FA, MO*

Solutions of FA and MO were prepared in heptane at concentration 10 mM. The adsorption procedure consists in immersing the hydroxylated Al samples in these solutions placed on a stirring table, ensuring a reproducible process, at incubation time varying from 1 h. For rinsing, samples were immediately immersed in a solution of heptane for 5 min, keeping the same stirring procedure that to remove physisorbed molecules, and finally dried under nitrogen gas flow.

### *2.2.3 Conditioning*

To check the stability of adsorbed FA layers, the samples were placed in a Petri dish and incubated for 24 h at room temperature in the following media: air, ultrapure water (MilliQ, Millipore, France), sodium chloride (NaCl, 0.6 mM), phosphate buffer saline (pH ~ 7.4) and hydrogen peroxide solution (H<sub>2</sub>O<sub>2</sub>, 10 mM). Tris-HCl buffer solution, (pH ~ 7.4; ~ 9.4) and carbonate buffer (pH ~ 9.4).

For the stability of adsorbed DPPC layers, the samples were incubated for 2h in Tris-HCl buffer solution, (pH ~ 7.4).

### *2.2.4 UV/O<sub>3</sub> treatment*

After the adsorption of FA, Al samples were placed in the UV/O<sub>3</sub> procleaner<sup>TM</sup> (Bioforce Nanosciences, USA) and treated for a duration varying from 1 to 30 min. To operate the UV/O<sub>3</sub> treatment, a high intensity mercury vapor lamp generated emission in the UV spectrum range: the emission range includes wavelengths at 185 nm which convert atmospheric oxygen into reactive ozone, the latter being able to attack molecular fragments and create volatile organics, and at 254 nm which may lead to the cleavage of chemical bonds of organic molecules on the surface.

### 2.2.5 Adsorption of DPPC

DPPC was adsorbed on two kinds of surfaces: hydroxylated Al surface before and after modification with stearic acid. The preparation of samples and adsorption procedure for SA were described in 2.2.1 and 2.2.2.

For DPPC adsorption on the surfaces, two different procedures were done (0.007 mg/ml till 10 mg/ml):

I - 20 $\mu$ l drop of prepared lipid solution in chloroform was directly placed on the AlOOH or modified SA-AlOOH surfaces;

II - 40 $\mu$ l of solution was spread on the sample and rotated at 3000 rpm for 40 using spin-coater (Laurell technologies corporation, WS-650Mz-23NPP).

For both procedures, before further analysis, the samples with covered surfaces were left in vacuum for 2h.

## 2.3 Techniques

### 2.3.1 Polarization modulation infrared reflection absorption spectroscopy

Infrared spectroscopy is a technique for non-destructive physico-chemical analysis that allows access to molecular information, the chemical nature and even the conformational and structural organization of analyzed materials. This technique is based on the change in vibrational state of molecules subjected to infrared radiation.

#### 2.3.1.1 Principle

Polarization modulation infrared reflection absorption spectroscopy (PM-IRRAS) is often used for the characterization of floating monolayers [130] or thin films on metal substrates [44, 81, 102]. This method utilizes the differences in reflectivity of interfaces for p-polarized (parallel to surface) and s-polarized (perpendicular to the surface) light. A differential reflectance spectrum ( $\Delta R/R^0$ ) of adsorbed surface species is computed as follow (2.1):

$$\Delta R/R^0 = (R_p - R_s)/(R_p + R_s), \quad (2.1)$$



where,  $R_p$  is the intensity of p-polarized component of radiation, and  $R_s$  is the intensity of s-polarized component radiation.

Because of this polarization modulation, the disturbing atmospheric absorptions, mostly caused by water vapor and  $\text{CO}_2$ , are eliminated. The ultrathin layers on metal surfaces interact with the p-polarized fraction of light, but not with the s-polarized one, which is zero by the same film.

The principle of PM-IRRAS is widely described in the literature [131, 132]. An infrared light beam is directed to an off-axis parabolic mirror with the long focal length. The light is focused onto the sample surface at an effective incident grazing angle around  $80^\circ$ . Prior to the sample, the light beam passes through a wire grid polarizer which transmits beam at an angle  $45^\circ$  to the photo-elastic modulator. PEM is an optical device (ZnSe) which modulates the polarization state of the input light beam at a fixed frequency (usually 37 or 50 kHz). After the sample, the beam is collected with the infrared lens and focused onto the detector element (Figure 2.3).

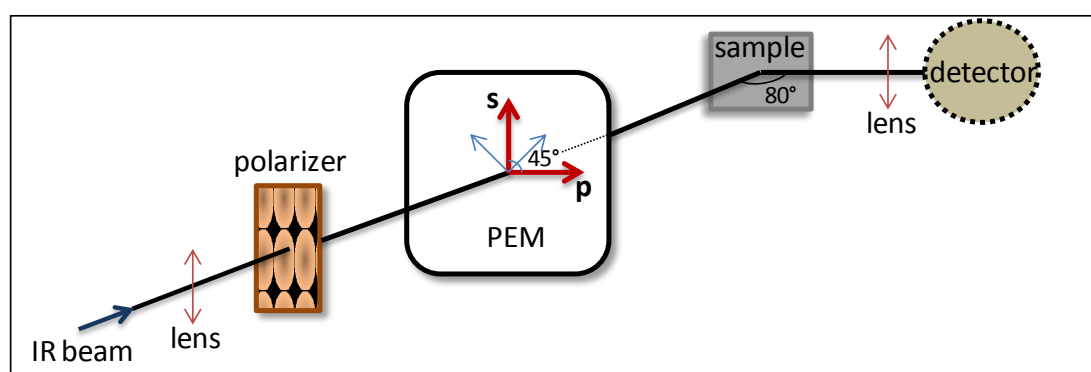


**Figure 2.3.** Scheme of PM-IRRAS

### 2.3.1.2 Experimental conditions

PM-IRRAS spectra were recorded on a commercial Thermo-Scientific (France) Nexus spectrometer. The external beam was focused on the sample with a mirror, at an optimal incident angle of  $80^\circ$ . A ZnSe grid polarizer and a ZnSe photoelastic modulator, modulating the incident beam between p- and s-

polarizations (HINDS Instruments, PEM 90, modulation frequency = 37 kHz), were placed prior to the sample. The light reflected at the sample was then focused onto a nitrogen-cooled MCT detector. All presented spectra were obtained from the sum of 128 scans recorded with  $8\text{ cm}^{-1}$  resolution.

### 2.3.2 Attenuated total reflection infrared spectroscopy

Attenuated total reflection infrared spectroscopy is often used for analysis of the surface of materials. For the bulk material no sample preparation was required.

#### 2.3.2.1 Principle

Here the infrared radiation is passed through an infrared transmitting crystal with the high refractive index, allowing the radiation to reflect within the ATR element several times and back from the crystal into the normal beam path of the spectrometer (Figure 2.4).

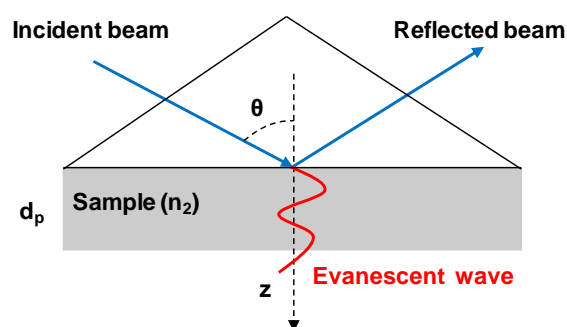


**Figure 2.4.** Scheme of the ATR principle

#### 2.3.2.2 Experimental conditions

ATR-IR analyses were performed on solution of oleic acid, linoleic acid and methyl oleate, prepared in heptanes at a concentration of 10 mM. One milliliter of each solution was deposited on the ATR ZnSe crystal, and spectra were obtained by the sum of 256 scans at  $8\text{ cm}^{-1}$  resolution using a pure solution of

heptanes as a reference. All analyses were performed with a Nicolet 5700 FT-IR spectrometer equipped with a liquid-nitrogen-cooled MCT detector.

### 2.3.3 Water contact angle

#### 2.3.3.1 Principle

Wetting refers to the study of how the liquid deposited on a solid (or liquid) substrate spreads out [133]. When two interfaces meet, the junction forms a curve known as contact line. The angle that these two interfaces make with each other is called the contact angle. According to classical Young's equation of capillarity (1805), there are three interfaces: the solid-liquid (sl), the liquid-vapor (lv) and the solid-vapor (sv), three surface tensions or energies  $\gamma_{sl}$ ,  $\gamma_{lv}$ ,  $\gamma_{sv}$  and an intrinsic contact angle  $\theta$  (2.2):

$$\cos\theta = (\gamma_{sv} - \gamma_{sl}) / \gamma_{lv} \quad (2.2)$$

Formation of a thin liquid layer (so called complete wetting) occurs when the liquid wets the surface and has strong affinity to the surface, here contact angle is zero. It also means that the surface is very hydrophilic. Partial wetting occurs when the drop does not spread completely where the surface is hydrophilic ( $\theta < 90^\circ$ ), and for hydrophobic surfaces ( $\theta > 90^\circ$ ) so called non-wetting [134] (Figure 2.5).

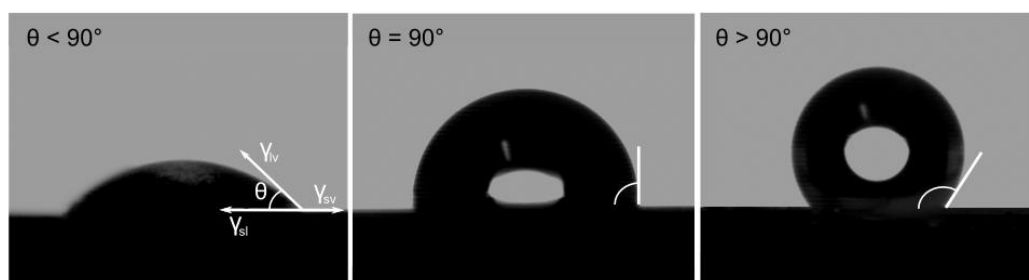


**Figure 2.5.** Demonstration of different water contact angles on smooth surface (adapted from [134])

If the surface of a substrate is rough, then the actual surface area is greater than the plan surface area and thus for a given drop volume, the total liquid–solid interaction is greater on the rough surface than on a flat surface [135]. If the smooth material gives a contact angle greater than 90°, the presence of surface roughness increases this angle still further, but if  $\theta$  is less than 90°, the surface roughness decreases the angle (Figure 2.6).

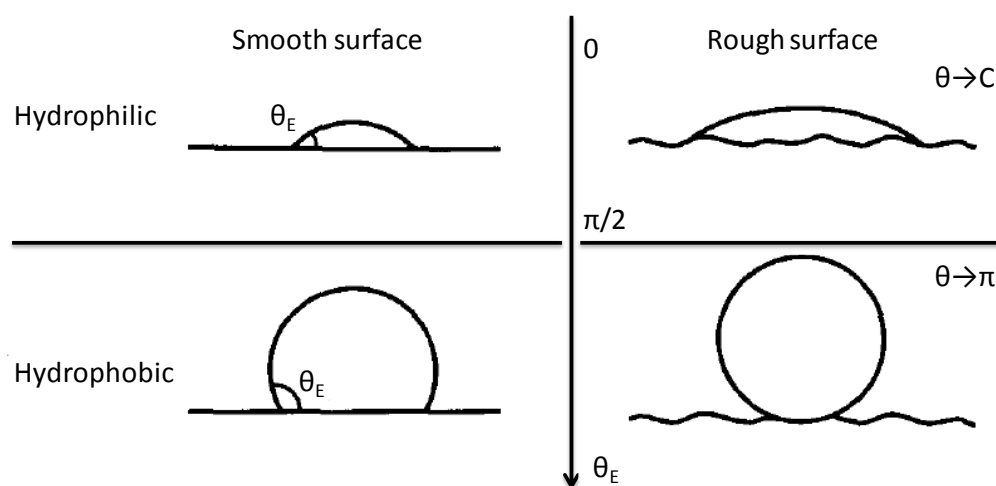


**Figure 2.6.** Controlling the wettability of the substrate through its roughness [133]

The most known models to characterize liquid contact angle with the rough surface are Wenzel and Cassie [136]. Wenzel (1936) modified Young's equation by adding roughness factor  $r$ .

$$\cos\theta' = r (\gamma_{sv} - \gamma_{sl})/\gamma_{lv} = r \cos\theta \quad (2.3)$$

Cassie (1944) evaluates area fraction  $f$  of solid surface and then this equation describes the contact angle  $\theta$  at a surface composed of solid and air.

$$\cos\theta' = f\cos\theta + (1-f)\cos 180^\circ = f \cos\theta + f - 1 \quad (2.4)$$

### 2.3.3.2 Experimental conditions

Static water contact angles were measured at room temperature using the sessile drop method and image analysis of the drop profile. The apparatus (Krüss, Germany) is equipped with CCD camera and an image analysis processor. The water (Milli-Q) droplet volume was 1  $\mu\text{L}$  and the contact angle was measured at once after the drop was deposited on the sample surface. For each sample, the reported value is the average of the results obtained with 4 droplets.

### 2.3.4 Atomic force microscopy

It has been over two decades since the invention of AFM [137], and in the last 10 years, was seen the development of AFM in probing interfaces with biological interest, including live cells [138], biomembranes [139] and adsorbed biomolecules on solid surfaces [66, 140]. This technique, originally developed for topographic imaging, now enables researchers to reveal physical and chemical properties, to manipulate individual molecules and to measure interfacial phenomena.

#### 2.3.4.1 Principle

In this technique, three-dimensional images are reconstructed by scanning a sharp tip (attaches at the end of a soft cantilever) over the sample surface while sensing the interaction force between the tip and the surface (Figure 2.7A). The sample (or the cantilever, depending of the system) is mounted on a piezoelectric scanner which ensures three-dimensional positioning with high accuracy. While the tip (or sample) is being scanned in the (x, y) directions, the force acting between tip and sample is monitored with piconewton (pN) sensitivity. This force is measured by the deflection of a flexible cantilever which is detected by a laser beam focused at the end of the cantilever and detected using a multi-segmented photodiode. The deflection signal is digitally processed to reconstruct, line by line, a topographic image of the sample. Different imaging modes are available, which differ mainly in the way the tip

is moving over the sample: non-contact mode, contact mode and tapping mode. Among them, the contact mode and the intermittent mode, commonly called tapping mode are the most widely used [141].

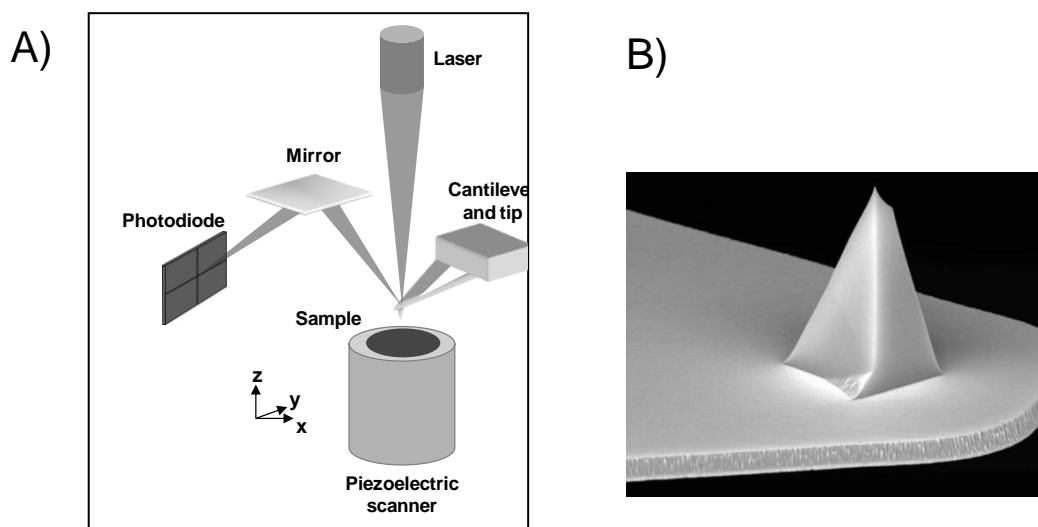


**Figure 2.7.** A) Scheme of AFM operation, B) silicon nitride tips verified with scanning electron microscopy

In this study, images were recorded using a new imaging mode called peak force tapping [142, 143]. In this mode the probe and sample surface are intermittently brought in contact for a short period, as in the tapping mode, thus eliminating lateral forces. Unlike the tapping mode, in which the feedback loop keeps the cantilever vibration amplitude constant, peak force tapping controls the maximum force (peak force) applied by the tip. Furthermore, the z-piezo, modulated far below the cantilever resonance frequency, performs very fast approach-retracting curves at each pixel of the image. The peak interaction forces obtained are used as the imaging feedback signal, allowing the applied force to be lower than in the normal tapping mode. This mode allows nanoscale details of the surface to be acquired with high resolution.

#### 2.3.4.2 Experimental conditions

AFM images were recorded using a commercial AFM (NanoScope VIII MultiMode AFM, Bruker Nano Inc- Nano Surfaces Division, Santa Barbara, CA.) equipped with a  $150 \times 150 \times 5 \mu\text{m}$  scanner (J-scanner). The substrates were fixed on a steel sample puck using a small piece of adhesive tape. Images were recorded in air at room temperature ( $\sim 22^\circ\text{C}$ ). AFM experiments were performed using Peak Force Tapping (PFT) mode, recently developed [30]. In this mode, the z-piezo is modulated far below the cantilever resonance frequency (2 kHz), with amplitude around 120 nm, to perform very fast approaching-retracting curves at each pixels of the image. Oxide-sharpened microfabricated  $\text{Si}_3\text{N}_4$  cantilevers were used (Bruker Nano Inc- Nano Surfaces Division, Santa Barbara, CA.). The spring constants of the cantilevers were measured using the thermal noise method, yielding values around 0.5 N/m. The curvature radius of silicon nitride tips was about 3 nm, as specified by the manufacturer and verified with scanning electron microscopy (Figure 2.7B). All topographic images shown in this dissertation were flattened using a third-order polynomial to correct surface tilt and eliminate bow effects.

#### 2.3.5 X-ray photoelectron spectroscopy

X-ray photoelectron spectroscopy has indeed become a technique of major importance in the field of material science, owing to the importance of interfacial phenomena such as adsorption and adhesion [144]. This includes the domain of biomaterials, and it is possible to identify the following applications headings: metallurgy (including surface engineering), corrosion, microelectronic materials and devices, polymers [145].

##### 2.3.5.1 Principle

X-ray photoelectron spectroscopy is based on the photoelectric effect, where an atom is radiated by photons of a given energy  $h\nu$  by result of excited ion and free electron with its kinetic energy ( $E_k$ ) (Figure 2.8).

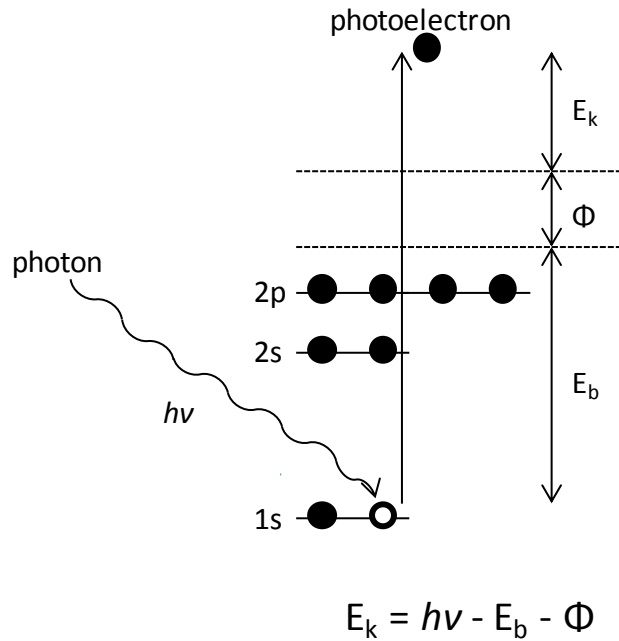


**Figure 2.8.** Schematic illustration of photoionization, where  $E_k$  - kinetic energy of ejected photoelectron,  $h\nu$  is characteristic energy of X-ray photon,  $E_b$  - binding energy of the atomic orbital from which the electron originates and  $\Phi$  is spectrometer work function.

The construction of XPS spectrometers is very complex the simplified scheme is given in Figure 2.9. The whole system is under ultra-high vacuum (UHV). X-rays are generated by bombarding an anode material with high-energy electrons and are directed at an X-ray monochromator, which purpose is to produce a narrow X-ray line by using diffraction in a crystal lattice. After that, electrons from the sample are collected by an electrostatic lens. Then they move to an energy analyzer where are sorted out according to their kinetic energy, which is detected and recorded as spectrum.



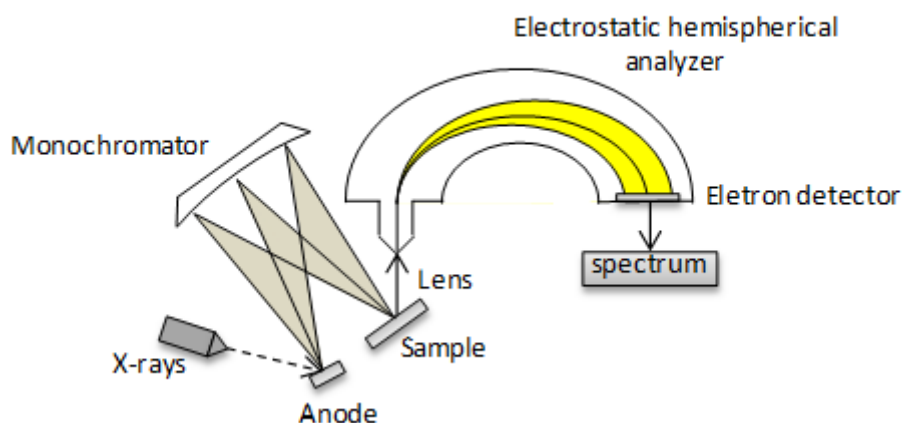


**Figure 2.9.** Schematic representation of an XPS spectrometer (adapted from [144])

### 2.3.5.2 Experimental conditions

XPS analyses were performed using a ESCA+ spectrometer (Omicron NanoTechnology), equipped with a monochromatized aluminum X-ray source (powered at 20 mA and 14 kV) and a MCD 128 channeltrons detector. Charge stabilization was used using the CN10 device with an emission current of 5.0 $\mu$ A and a beam energy of 1eV. Analyses were performed in the sweeping mode; the resulting analyzed area was 1 mm diameter. A pass energy of 20 eV was used for narrow scans. Under these conditions, the full width at half maximum (FWHM) of the Ag 3d<sub>5/2</sub> peak of clean silver reference sample was about 0.6 eV. The pressure in the analysis chamber was around 10<sup>-8</sup> Pa. The following sequence of spectra was recorded: survey spectrum, C 1s, O 1s, N 1s, Al 2p, Cl 2p, P 2p and C 1s again to check for charge stability as a function of time and the absence of sample degradation. The binding energy scale was set by fixing the C 1s component due to carbon only bound to carbon and hydrogen at 284.8 eV. The data treatment was performed with Casa XPS software (Casa Software Ltd., UK). The peaks were decomposed using a linear baseline, and a component shape defined by the product of a Gauss and Lorentz function, in the 70 : 30 ratio, respectively. Molar concentration ratios were calculated using peak areas normalized according to Scofield factors.

### **III. RESULTS AND DISCUSSIONS**

### 3.1 Self-assembly of FA and ester on hydroxylated Al substrate

This chapter is dedicated to the investigation of adsorption of fatty acids and methyl oleate on hydroxylated aluminum surface. The most important thing is to focus on such parameters, which are related to specific properties of molecules: chain length, level of unsaturation (oleic acid and linoleic acid) and the nature of head group (ester group in methyl oleate vs carboxylic group in FA). For these purpose, the adsorbed lipids layers were characterized by variety of techniques for the surface analysis, which can quite clearly describe the similarities and differences between the behavior of molecules in adsorbed state. Understanding the behavior of FA on the Al surface requires an understanding of the complexity of the interface where multiple and diverse processes take place.

#### 3.1.1 Formation of the Al Oxy-hydroxide Layer

Prior to the adsorption of lipids, the hydroxylation of the Al substrate was investigated. On the basis of previous findings, the treatment of the Al substrate in boiling water is expected to enhance the hydroxylation of the surface, leading to the formation of an AlOOH layer, presumably a “pseudo-boehmite” [146]. Figure 3.1a shows a PM-IRRAS spectrum recorded on an Al substrate after surface polishing. It exhibits a single well-defined band at about  $950\text{ cm}^{-1}$  which can be attributed to the Al–O–Al stretching vibration of the amorphous Al oxide layer [23, 147]. According to the literature, in order to create a layer of so called pseudoboehmite (AlOOH), the sample should be placed in the boiling water for 15s [111], 2min [148], 3min [149]. In this case hydroxylation treatment was checked by immersing the sample in the boiling water in different durations.

Already after 30s of hydroxylation the band due to the Al-O-Al decreased, after 40s the band at  $1095\text{ cm}^{-1}$  due to the hydroxyl bending mode  $\delta(\text{OH})$  [111, 150] starting to form, while after 1 min it was already intense and after 2 min already not so wide-already stabilized (Figure 3.1 b, c, d, e respectively). Starting 1 min other bands which characterized hydroxylated aluminum

surface appeared: the band at  $1654\text{cm}^{-1}$  and the band at  $1395\text{ cm}^{-1}$  are due to the stretching vibration of water molecules  $\delta(\text{H}_2\text{O})$  [111, 150, 151]. The large band observed in the frequency region from  $3260$  to  $3680\text{ cm}^{-1}$  is attributed to the stretching vibrations  $\nu(\text{OH})$  of hydroxyl groups and adsorbed water on the Al surface (data not shown).

Increasing the time to 5 and 10 min, no big changes happened, the band at  $1095\text{ cm}^{-1}$  also increased a little but other bands remained the same, so it was no sense to continuing experiments with these values (Figure 3.1. f, g).

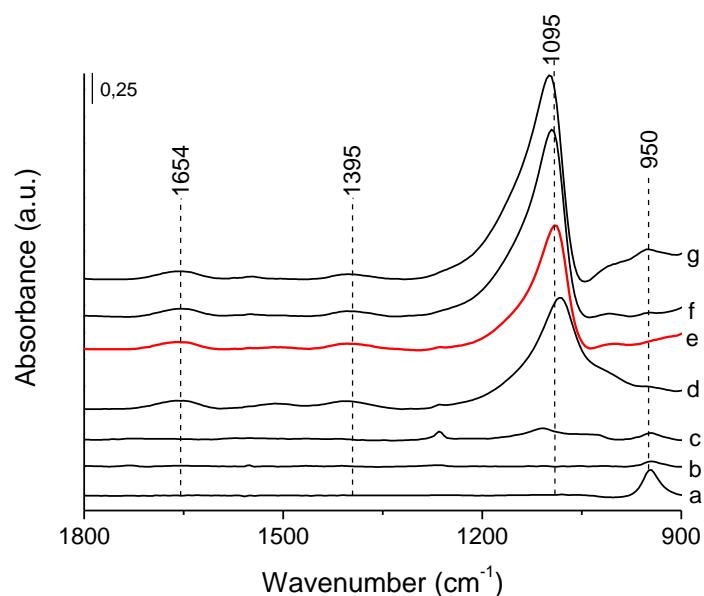


**Figure 3.1.** PM-IRRAS spectra recorded on aluminum substrate prior to (a) and after hydroxylation treatment in boiling water in different durations: (b) 30s, (c) 40s, (d) 1min, (e) 2min, (f) 5min and (g) 10min.

The presence of hydrocarbon-like compounds from adventitious contamination was not detected with PM-IRRAS on hydroxylated Al.

AFM images revealed a clear evolution of the surface morphology after treatment in boiling water (Figure 3.2).

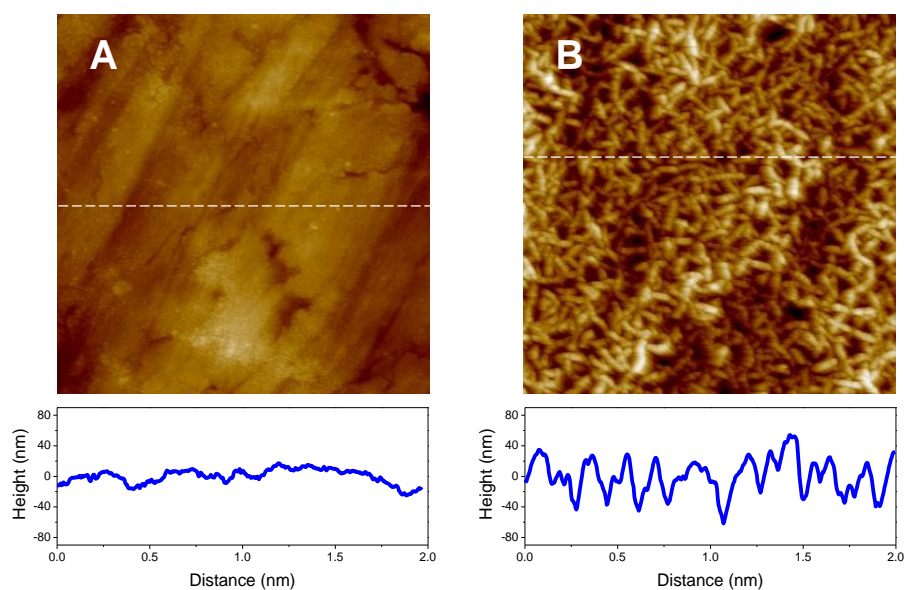


**Figure 3.2** Representative AFM height images ( $2 \times 2 \mu\text{m}^2$ , peak force tapping mode, z-scale 100 nm) recorded in air (A) prior to and (B) after hydroxylation treatment in boiling water. Cross sections were taken at the location indicated by the white broken lines on the images.

Before the hydroxylation treatment, the sample exhibited a relatively smooth surface with some stripes attributable to the polishing procedure ( $R_{\text{rms}} = 7.1$  nm, Figure 3.2A). It is obvious that the treatment applied resulted not only in surface hydroxylation but also in a deep rearrangement of the surface, with the formation of regular nanostructures appearing in the form of nanorods randomly distributed on the surface. This was accompanied by a strong increase of the roughness ( $R_{\text{rms}} = 22.1$  nm, Figure 3.2B). More quantitative evidence on the surface topography can be seen via cross sections which showed a sawtoothed profile on the hydroxylated sample, revealing that the depth created by the nanostructures is of the order of 50 nm.

### 3.1.2 Adsorption of FA, Ester

Prior to the adsorption of FA and the ester derivative on the hydroxylated Al surface, IR-ATR analyses were performed on solutions of OA, LA, and MO in heptane (10 mM) as references for the vibrational features of free molecules. Results given in Figure 3.3 show the presence of the characteristic bands of the

different lipids. The spectra of the two FA are extremely similar. MO differs from the FA mostly in having a band at  $1080\text{ cm}^{-1}$  due to  $\nu_s(\text{C-O-C})$  of the ester group, and in a shift of the  $\delta(\text{CH}_2)$  band from  $1434\text{ cm}^{-1}$  to  $1465\text{ cm}^{-1}$  (Figure 3.3). In the C-H frequency region, the bands are due to the alkyl chain of molecules.

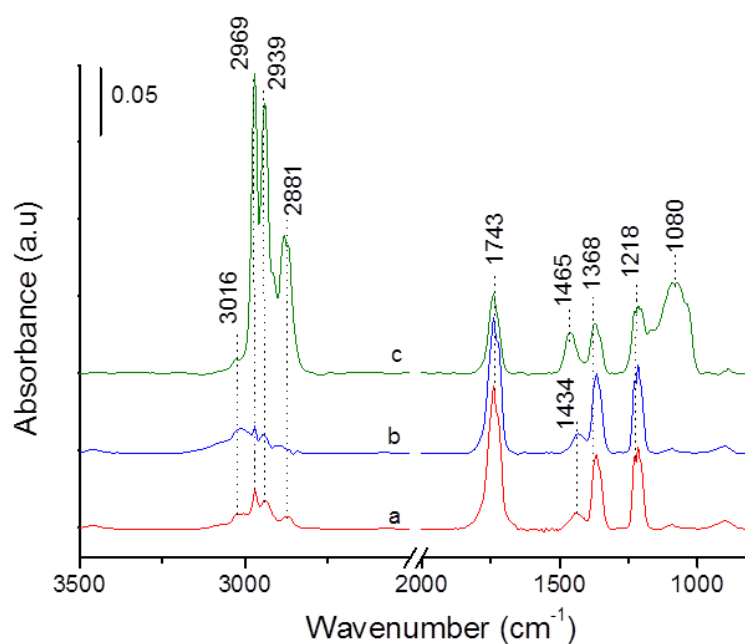


**Figure 3.3.** IR-ATR analyses of (a) oleic acid, (b) linoleic acid, and (c) methyl oleate solutions in heptane.

As detailed in chapter 1 (section 1.4.1c) the common approach used for the adsorption of (macro)molecules on substrates in liquid phase was used. This approach consists in incubating the sample in a solution containing lipids. This solution was placed on stirring table that to enhance distribution of the molecules on the surface. Samples were thus immersed in solutions with different concentrations of lipids dissolved in organic solvents. Different classes of solvents were tried: 2-propanol, xylene and heptane. They demonstrated quite similar behavior. But according literature, alkanes are the most suitable because of similar nature with fatty acids (alkyl chain) and could help organize the surface [85]. Moreover polar solvents could compete with the

polar headgroups of the molecules in the reactions with the surface and may require longer assembly time [20, 102].

At the beginning, lipids were dissolved in heptane and stirred for about 5 minutes to have a concentration from 300 mM to 10 mM. After adsorption, the values of the PM-IRRAS spectra or water contact angle were the same, so it was very important to try with the lowest concentration, in order to see the kinetics. All FA demonstrated the same behavior of adsorption. So for further optimization, OA was chosen (Figure 3.4). When the concentration was 0.01mM,  $\theta_w$  values reached the plateau. For final concentration 10mM was chosen, as this concentration was adopted in the previous studies (varying 1-10mM) for surface modification on dense alumina substrates [19, 21, 22, 100, 101].

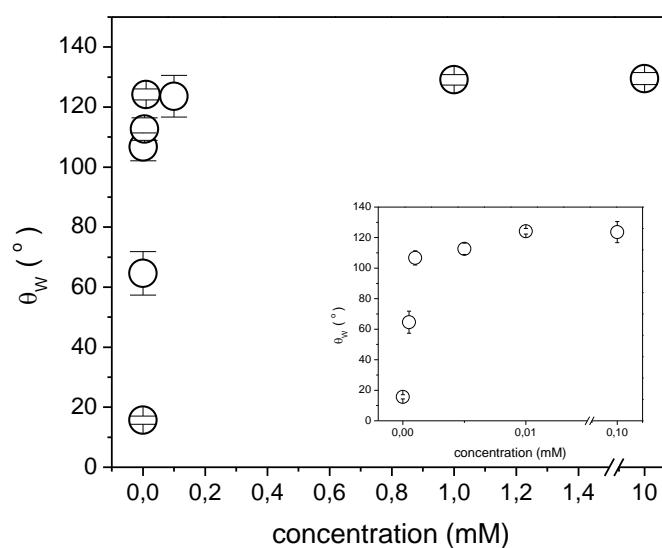


**Figure 3.4.** The evolution of water contact angle ( $\theta_w$ ) measurements as a function of different OA concentrations

Regarding the incubation time, many controversies can be found in the literature. Indeed values ranging from 1s till 165.5h were reported. For this purpose, the influence of the incubation time in OA solutions was investigated on hydroxylated Al substrate using water contact angle. Results given in Figure

3.5 showed that molecules adsorbed very quickly, already after 1min WCA was high. After 5 min the values reached a plateau which continued till 24 h. This may suggest that the surface achieve a full coverage due to the adsorption of the molecules which include hydrophobic moieties. In order to avoid big error bars, 1 h was chosen for further experiments.

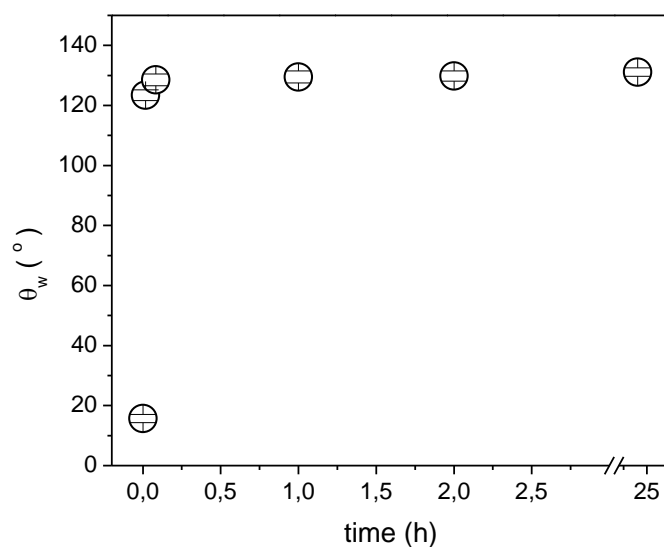


**Figure 3.5.** The evolution of OA (10mM) water contact angle ( $\theta_w$ ) measurements as a function of incubation time

PM-IRRAS analysis (data not shown) was also done in the optimization steps and was coherent for WCA results. The adsorption kinetics was rapid, in agreement with previous findings [15, 20] and no differences were noticeable in PM-IRRAS spectra recorded after adsorption times longer than 1 h.

PM-IRRAS spectra recorded on hydroxylated Al substrates after the adsorption of OA, LA, and MO are given in Figure 3.6. The vibrational features of lipid molecules in solution and in the adsorbed state are compared in Table 3.1.



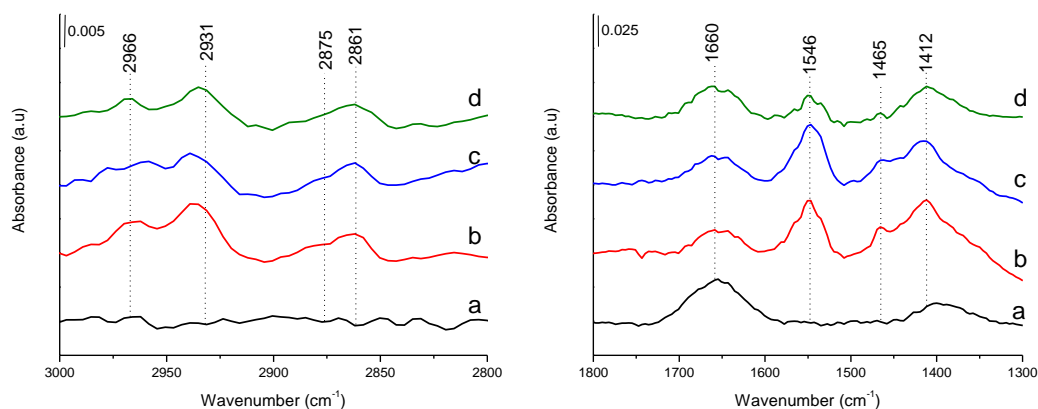


**Figure 3.6.** PM-IRRAS spectra recorded on hydroxylated aluminum substrate in the high-frequency (C-H region, left) and the low-frequency region (right): (a) prior to and after adsorption of (b) oleic acid, (c) linoleic acid, and (d) methyl oleate.

**Table 3.1.** Assignment of IR band relative to oleic acid (OA), linoleic acid (LA) and methyl oleate (MO) molecules in (a) the liquid phase, (b) the adsorbed state. Band assignments are based on the literature [81, 152-154].

Chemical group	Vibrational type	$\lambda$ (cm <sup>-1</sup> )					
		OA		LA		MO	
		(a)	(b)	(a)	(b)	(a)	(b)
=C-H	$\nu$ (C-H)	3016	–	3016	–	3016	–
CH <sub>3</sub>	$\nu_{as}$ (C-H)	2969	2966	2969	2966	2969	2966
CH <sub>2</sub>	$\nu_{as}$ (C-H)	2939	2931	2939	2931	2939	2931
-CH <sub>2</sub> -O-	$\nu$ (C-H)	2881	–	2881	–	2881	–
CH <sub>3</sub>	$\nu_s$ (C-H)	–	2875	–	2875	–	2875
CH <sub>2</sub>	$\nu_s$ (C-H)	–	2861	–	2861	–	2861
-COOH or -COOMe	$\nu$ (C=O)	1743	–	1743	–	1743	–
-COO <sup>-</sup>	$\nu_{as}$ (COO <sup>-</sup> )	–	1546	–	1546	–	1546
CH <sub>2</sub>	$\delta$ (CH <sub>2</sub> )	1434	1465	1434	1465	1465	1465
-COO <sup>-</sup>	$\nu_s$ (COO <sup>-</sup> )	–	1412	–	1412	–	1412
CH <sub>2</sub> (near olefin)	$\omega$ (CH <sub>2</sub> )	1368	–	1368	–	1368	–
COOH	$\nu$ (C-O)	1218	–	1218	–	1218	–
-C-O-CH <sub>3</sub>	$\nu_s$ (C-O-C)	–	–	–	–	1080	–

When molecules are adsorbed on the hydroxylated Al surface, the C–H stretching region is dominated by the symmetric and asymmetric stretching modes of methylene groups,  $\nu_s(\text{CH}_2)$  and  $\nu_{as}(\text{CH}_2)$ , at 2861 and 2931  $\text{cm}^{-1}$ , respectively. The asymmetric stretching mode of  $\text{CH}_3$  moieties,  $\nu_{as}(\text{CH}_3)$ , is also visible at 2966  $\text{cm}^{-1}$ , and the broadening near 2875  $\text{cm}^{-1}$  can be attributed to the corresponding symmetric mode,  $\nu_s(\text{CH}_3)$ . These vibrational features are mainly attributed to the alkyl chains of the adsorbed FA and MO molecules (when molecules are in solution, symmetric C–H stretching modes are not visible because of the random movement of free molecules). They might also be due to trapped solvent remaining from adsorption or rinsing steps, but incubating the aluminum surface in heptane did not lead to their appearance (data not shown). In the lower frequency region, the band at 1658  $\text{cm}^{-1}$  initially present on the hydroxylated aluminum surface and assigned to the bending mode of adsorbed water was still visible in all spectra. The small band at 1465  $\text{cm}^{-1}$  may be attributed to  $\delta(\text{CH}_2)$ . Vibration modes associated with the carboxylate group are clearly visible after the adsorption of OA and LA: the symmetric and antisymmetric stretching modes of the  $\text{COO}^-$  moiety are apparent at about 1412 and 1546  $\text{cm}^{-1}$ , respectively (Figure 3.6b, c). However, the band attributed to  $\nu(\text{C}=\text{O})$  of the protonated carboxylic acids of OA and LA, visible at 1743  $\text{cm}^{-1}$  in solution (Figure 3.3), disappears in the adsorbed state. These findings suggest a strong interaction of OA and LA molecules in contact with the hydroxylated Al surface, through deprotonated carboxylate head groups. Unexpectedly, MO exhibited a behavior similar to that of FA. The stretching mode of C=O in the ester group, manifest in solution as a band around 1743  $\text{cm}^{-1}$ , did not appear in the adsorbed state, while bands characteristic of  $\text{COO}^-$  moieties were present (Figure 3.6d). This may indicate that the ester end-group is subjected to a chemical transformation upon contact with the hydroxylated Al, leading to a conversion to the carboxylate group. Other fatty acids also were involved in this study (Figure 3.7). In the lower frequency region, the same bands associated with the symmetric and asymmetric stretching modes of the  $\text{COO}^-$  were seen to all FA (Figure 3.7,

right). In the C-H stretching region LrA and SA showed well defined bands with higher intensity, compared to the other FA (Figure 3.7, left), while for BA bands were barely visible in the CH stretching range (Figure 3.7, left).

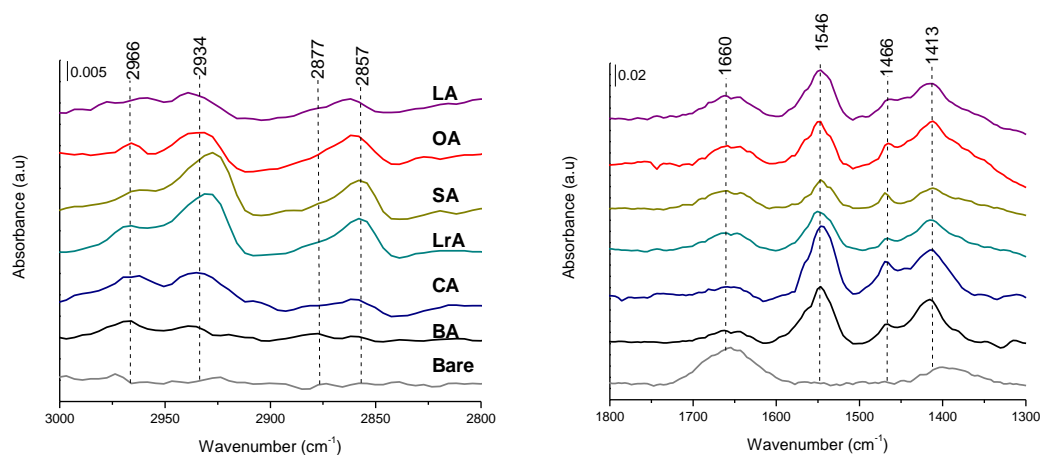


**Figure 3.7.** PM-IRRAS spectra on hydroxylated aluminum prior to (“Bare”) and after the adsorption of BA, CA, LrA, SA, OA -and LA.

The adsorption of FA was also studied by water contact angle measurements (Figure 3.8). The bare Al surface exhibited a  $\theta_w$  value of about  $15^\circ$ , which is compatible with a hydrophilic surface (oxide/hydroxide compounds and a low level of organic contamination). After adsorption of saturated fatty acids on the hydroxylated surface,  $\theta_w$  values increased markedly with increasing length of the alkyl chain of the molecules. This indicates a hydrophobic character of the surface which is due to the presence of an adsorbed FA layer on the hydroxylated Al surface. The increase of the level of unsaturation, while keeping the chain length invariable (compare SA, OA and LA, Figure 3.8, right) led to a decrease of  $\theta_w$  values. MO exhibited the lowest contact angle at about  $96^\circ$  compare with the same chain length fatty acids (data not shown).

Indeed, owing to their molecular structure, unsaturated FA may adopt conformations which do not favor a process of self-organization, and thus do not induce the formation of a highly dense packing of molecules as observed

for saturated FA [19] and generally obtained with alkane thiols on metals [155].

For comparison the same experiments were conducted on non-hydroxylated samples (presumably  $\text{Al}_2\text{O}_3$ ) which exhibit a rather flat surface. The main differences observed between “rough” (after hydroxylation) and “smooth” (before hydroxylation) surfaces was observed with the shortest FA (BA), suggesting a possible contribution of the surface roughness to the wetting properties. Furthermore,  $\theta_w$  values were slightly higher on hydroxylated Al surface for long chain FA (SA, OA and LA).

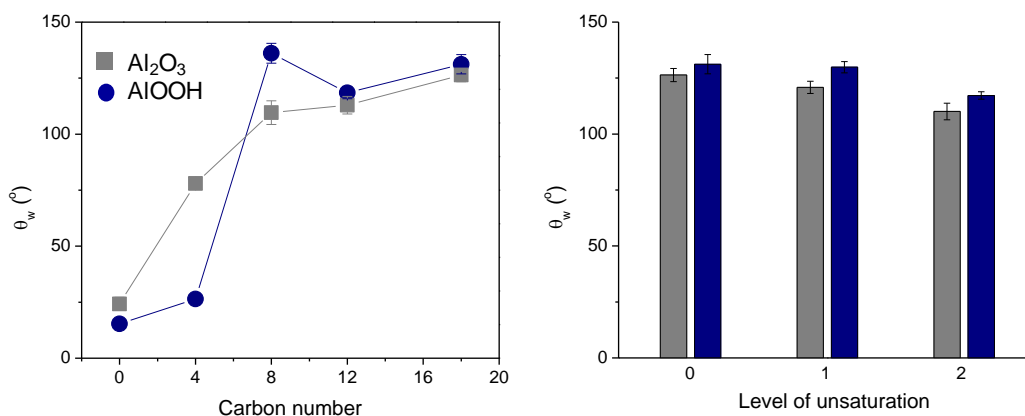


**Figure 3.8.** Evolution of water contact angle ( $\theta_w$ ) as a function of (A) chain length and (B) level of unsaturation of FA.

The evolution of the surface morphology after adsorption of different molecules was investigated by AFM. Recently, the effect of the hydroxylation treatment on Al surface nanoscale organization has been investigated in depth using this technique [140]. The treatment leads to the formation of nanorod-like structures densely and randomly distributed on the surface, resulting on the generation of nanoporous domains (Figure 3.9 A and B), which were significantly enlarged after the adsorption of FA (Figure 3.9 A–B), while this was not the case for MO adsorption (Figure 3.9 C).

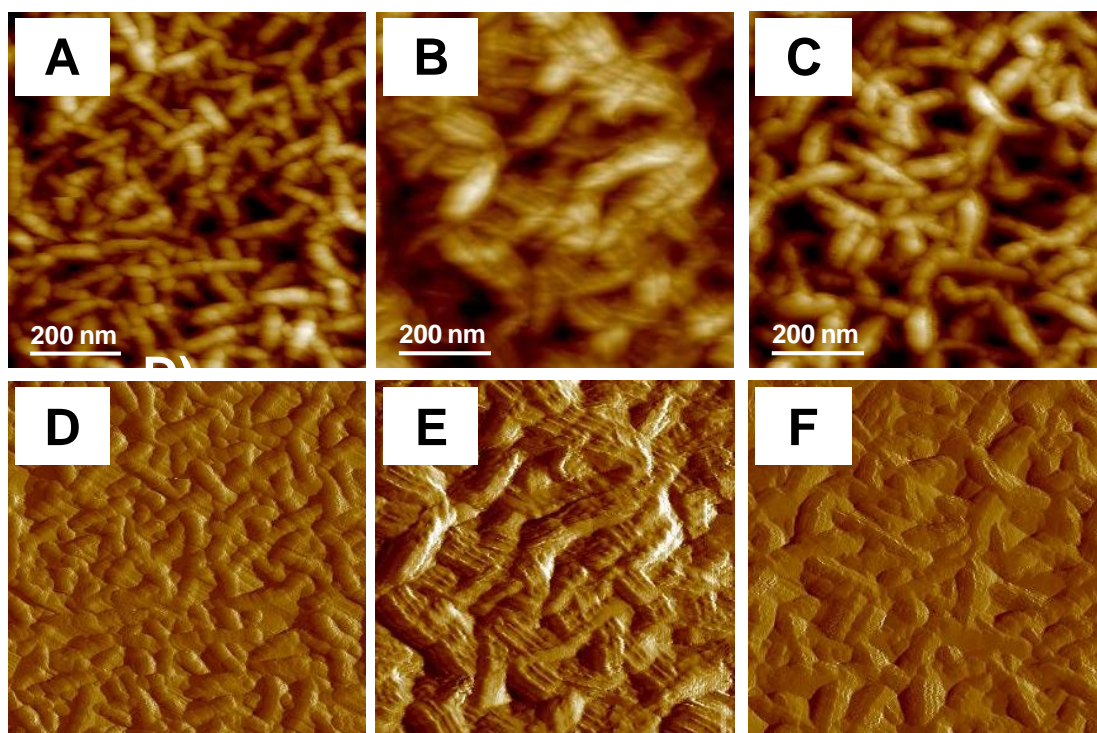


**Figure 3.9.** Representative AFM height (A, B, C) and peak force error (D, E, F) images (peak force tapping mode, in air, z-scale 150nm) recorded on hydroxylated aluminum prior to (A, D) and after the adsorption of oleic acid (B, E), and methyl oleate (C, F).

Interestingly, these high resolution AFM images revealed the appearance of lines with highly regular features after the adsorption of all FA. These regular lines are clearly apparent in the peak force error images which provide better contrast (Figure 3.9 E). On the contrary, this behavior was not observed with MO (Figure 3.9 F), and the surface morphology looked more like that of the hydroxylated Al surface (Figure 3.9A, F).

The formation of these nano-patterns was evident for long FA, i.e. LrA, SA, OA and LA, and not noticeable for BA and CA molecules (Figure 3.10, 3.11 and 3.12).

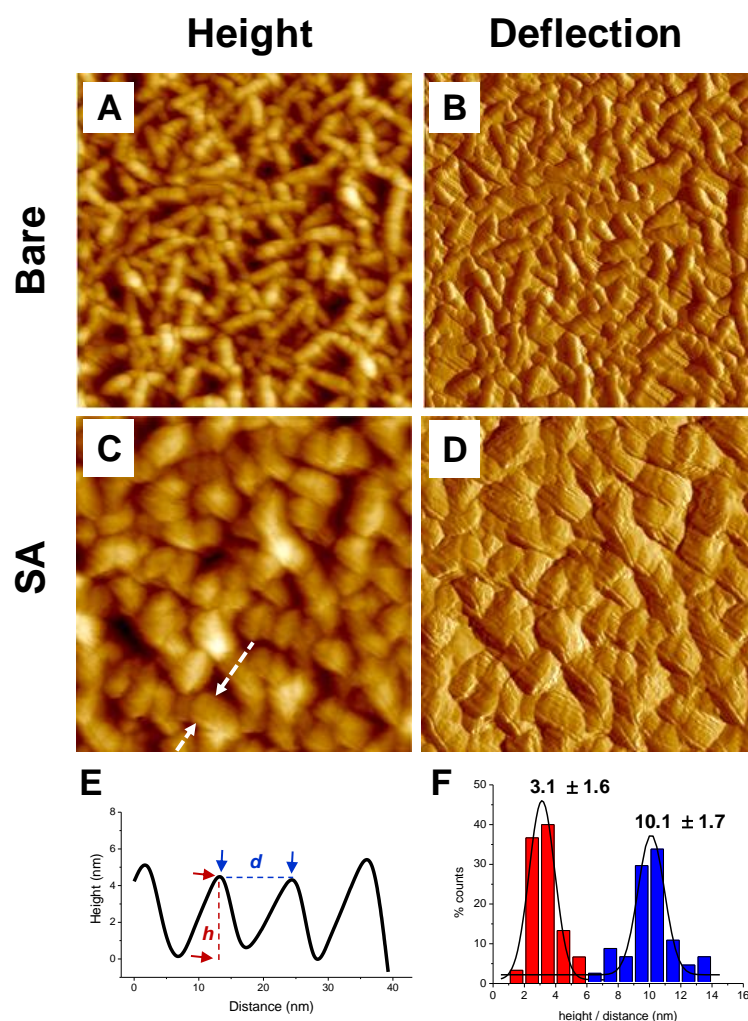


**Figure 3.10.** Representative AFM height (A, C) and deflection (B, D) images ( $1 \times 1 \mu\text{m}^2$ , Peak Force Tapping mode, in air, z-scale 180 nm) recorded on hydroxylated aluminum prior to (A, B) and after the adsorption of SA (C, D). (E) Cross sections were taken at the location indicated between the arrows in the height image (C). (F) Histograms of the nanostructure height ( $h$ ) and distance ( $d$ ) between consecutive patterns as depicted in (E).

Straightforward evidence regarding the dimensions of these nanostructures was obtained from cross sections (Figure 3.10 E) which revealed that patterns exhibited fairly regular heights,  $h$ , in the range of 3 nm. This height significantly exceeds the thickness of one fatty acid monolayer, as values ranging from about 0.9 to 1.5 nm were reported for the latter in the literature, based on quartz crystal microbalance [156] or ellipsometry measurements

[157]. Furthermore, regular distance between the patterns,  $d$ , was around 10 nm. A typical distribution obtained via several cross sections in AFM images recorded on SA-modified surface is shown in Figure 3.10F.

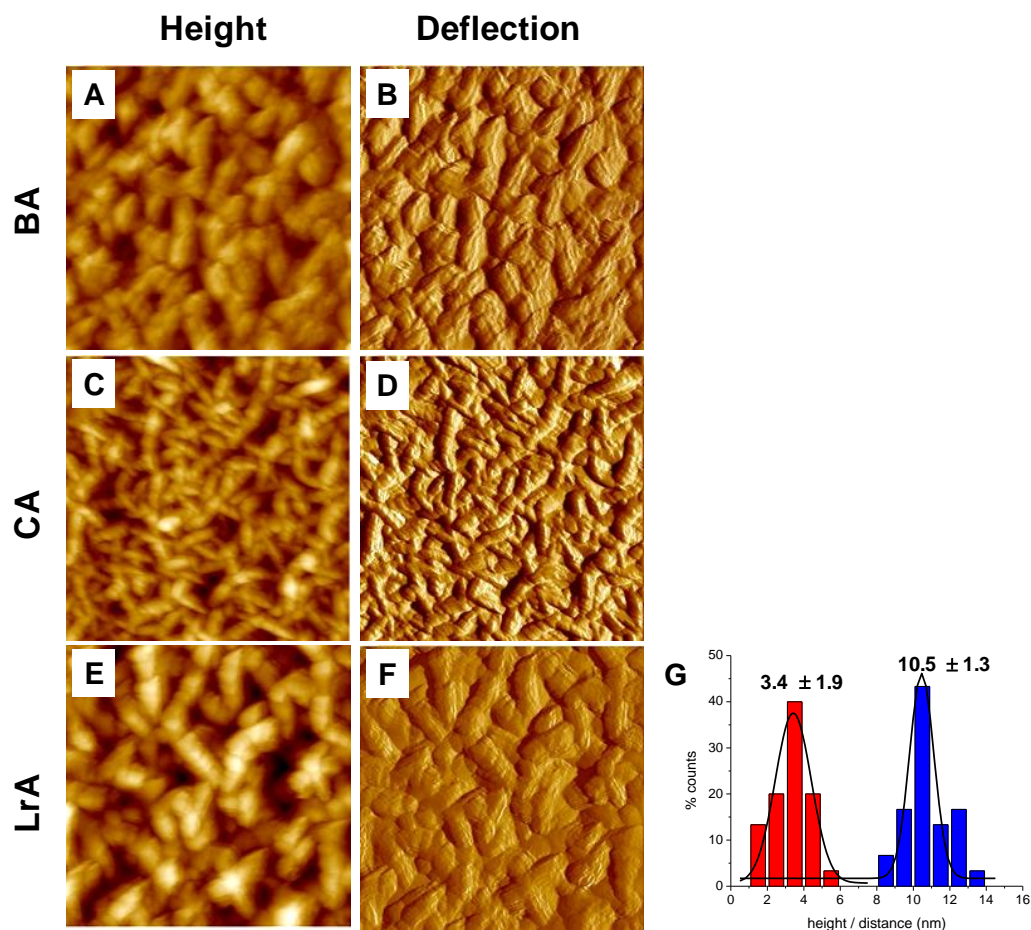


**Figure 3.11.** Representative AFM height (A, C, E) and deflection (B, D, F) images ( $1 \times 1 \mu\text{m}^2$ , Peak Force Tapping mode, in air, z-scale 180 nm) recorded on hydroxylated aluminum after the adsorption of saturated FA: BA (A, B), CA (C, D), and LrA (E, F). (G) histogram of the nanostructure height ( $h$ ) and distance ( $d$ ) between consecutive patterns (as depicted in Figure 3.10E) obtained after the adsorption of LrA (G).

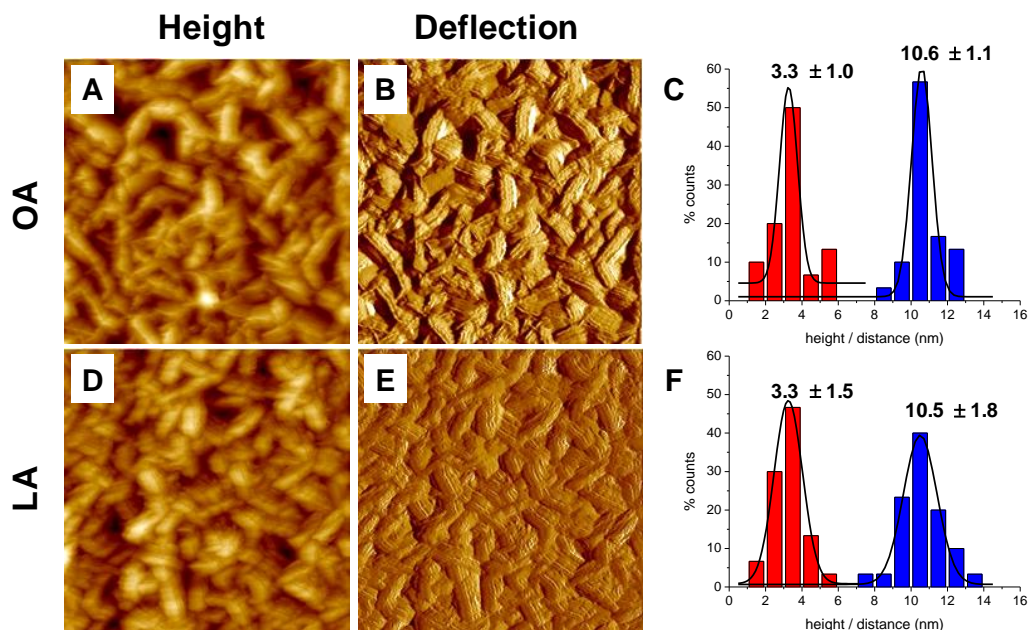


**Figure 3.12.** Representative AFM height (A, D) and deflection (B, E) images ( $1 \times 1 \mu\text{m}^2$ , Peak Force Tapping mode, in air, z-scale 180 nm) recorded on hydroxylated aluminum after the adsorption of unsaturated FA: OA (A, B), LA (D, E). (C, F) Histograms of the nanostructure height ( $h$ ) and distance ( $d$ ) between consecutive patterns (as depicted in Figure 3.10E) obtained after the adsorption of OA (C) and LA (F).

The results obtained on LrA, OA and LA were also similar (Figure 3.11 and 3.12), suggesting that the regular dimensions of these nanostructures are independent of the FA molecule. It is worth noting that the AFM tip used in the present study exhibits an average radius lower than 10 nm, as specified by the supplier and checked with scanning electron microscopy after surface imaging.

### 3.1.3 Mechanism of FA adsorption

The adsorption of FA and ester (MO) derived from OA was investigated on a superficially hydroxylated Al substrate. For this purpose, the Al sample was subjected to a treatment leading to the formation of a stable layer, presumably made of an AlOOH phase, with reproducible morphology and composition. It is worth noting that while the precipitation of aluminate solutions at temperatures near and above the boiling point of water lead to the formation of



well-crystallized boehmite, the same reaction is significantly slowed on Al oxide film and the boiling water treatment leads to the formation of gelatinous boehmite, i.e., a poorly crystallized and hydrated form [23]. Accordingly, compared to crystalline boehmite, the pseudoboehmite is structurally less well-defined and includes interlamellar water molecules [146]. The surface preparation conducted in the present study has the advantage of exhibiting a low level of carbon contamination, as shown in PM-IRRAS spectra (Figure 3.1. e) and also verified with XPS analysis (data not shown), which is also stable over time.

Vibrational spectroscopy of the adsorbed FA and MO can provide information on the adsorption mechanism. It should first be noted that the spectra observed in the present study are not superposable with those obtained by other authors on oxidized aluminum [19] or on amorphous alumina and crystalline  $\alpha$ -alumina films [18], pointing to the complexity of the phenomenon and its sensitivity to sample preparation procedures. The first thing that must be underscored is the absence for all adsorbed samples of a  $\nu(\text{C}=\text{O})$  band in the  $1700\text{--}1750\text{ cm}^{-1}$  region, indicating that the adsorbed molecules are present as carboxylates; the symmetric and antisymmetric stretches of the carboxylate function are indeed clearly present. The carboxylate functions probably form coordinative bonds to surface  $\text{Al}^{3+}$ . Several different types of carboxylate coordination could possibly exist: terminal or bridging (between two  $\text{Al}^{3+}$  centers), monodentate or bidentate, etc. A thorough comparison of the  $\nu_{\text{as}}$  and  $\nu_{\text{s}}$  positions between the complex and the free carboxylate could help choose between monodentate and bidentate coordination [158]. This work was not undertaken in our case because of the complexity of the rough surface.

Evidently, the acid–base properties of the hydroxylated Al surface play a pivotal role in the binding mechanism of FA. The quantitative transformation of carboxylic acid functions FA to the corresponding carboxylates is a Brønsted acid–base reaction, and because the solvent has no basic properties, the released protons must in some way react with the surface, i.e., the surface must have a Brønsted basic character. As regards MO adsorption, quantitative

transformation to the oleate anion upon adsorption indicates that a saponification reaction has taken place, which also indicates a basic reactivity (see below). If we accept the idea that a “pseudoboehmite” surface was obtained through the boiling water pretreatment, the latter should indeed exhibit more basic sites than alumina surfaces obtained through other procedures [146]. This is in keeping with the reactivity of the corresponding divided materials: while  $\gamma$ -alumina ( $\text{Al}_2\text{O}_3$ ) exhibits a variety of surface OH groups [159, 160] some of which are strongly acidic, boehmite ( $\text{AlOOH}$ ) has more homogeneous surface groups, with a mostly basic reactivity [161]. It is well-known in colloid chemistry that the nature of the aluminum (hydr)oxide phase has a determining effect on surface reactivity [162], and obviously the same is true for flat surfaces and films. One can probably speculate further on the adsorption mechanism of the FA. It is chemically reasonable that the approaching carboxylic acid molecules should protonate the basic terminal  $\text{OH}^-$  groups that are fixed on the surface  $\text{Al}^{3+}$ , producing terminal  $\text{H}_2\text{O}$  (aqua) ligands. The latter might then be substituted by the carboxylate groups acting as ligands, producing free  $\text{H}_2\text{O}$ : this substitution reaction should be favored by the conditions of low water activity. Regarding the organization state of the adsorbed molecules, it is difficult to compare results obtained in this study with previous reports, which focus on the growth and stability of self-assembled and self-organized monolayers.

The ability of FA to strongly interact with superficially hydroxylated Al surface and to modify markedly its morphology is clearly evident, independently on the length of their alkyl chain or their level of unsaturation, although the phenomenon is more obvious for long FA (chain length above  $\text{C}_{12}$ ). This causes an intriguing evolution of the surface morphology. AFM images showed a high level of organization at the nanoscale which manifests itself as the formation of patterns with fairly regular heights and lateral inter-distance, as revealed by cross sections (Figure 3.10). The surface exhibits, thus, two hierarchical levels of organization: the first one is due to the superficial

hydroxylation treatment (nanorods with some tens of nm length) while the second one (nano-patterns) is only revealed through the self-assembly of FA. The origin of the latter phenomenon is not completely understood but may be tentatively explained by focusing on the mechanism of FA-surface binding at the molecular level. PM-IRRAS spectra recorded on FA molecules on the hydroxylated Al surface, revealed the formation of coordinative bonds between carboxylate end groups of the fatty acids (the carboxyl moiety was deprotonated) and  $\text{Al}^{3+}$  ions on the  $\text{AlOOH}$  surface, in agreement with previous works [21, 22]. Note, however, that the average height of nanostructures is noticeably higher than the expected thickness of a monolayer ( $\sim 0.9\text{--}1.5$  nm) [156, 157] or the length of free molecules (about 1.8 nm for OA, based on theoretical calculation). If one supposes the formation of fatty acid multilayers, FA in the second and more external layers would be expected to be unbound to the surface and therefore to show the presence of free carboxylic acid groups, which is not consistent with PM-IRRAS results. Alternatively, the surface morphology change, including regular nanostructures, might be attributed to the enhancement of surface reconstruction guided by coordinated fatty acid molecules following a preferential crystallographic direction.

The fact that quite similar structures (parallel grooves with a width in the 10 nm range) were observed with different fatty acids points to a common origin in the organization of the underlying  $\text{AlOOH}$  surface. To the best of our knowledge, patterns disposed regularly on the 10 nm length scale have never been reported on hydroxylated Al, whether chemical or morphological in origin. 10-nm-scale pores have been claimed to form in anodic growth of alumina in some conditions [10], but it is unclear how they would induce the formation of the ridges and grooves we observe after FA adsorption. The nanorods observable on the oxidized Al plates consist in boehmite,  $\text{AlOOH}$ . This oxyhydroxide has a lamellar structure, with layers stacked up perpendicular to the **b** crystallographic direction. When boehmite layers are interrupted perpendicular to the **a** or **c** directions, they exhibit terminal Al-OH groups which are probably easier to substitute by other ligands, such as

carboxylates, than the  $\mu^2$  OH groups on the layers basal planes (010) - not to mention the oxide ions which are  $\mu^3$  or  $\mu^4$ . If indeed the mechanism of FA adsorption involves the formation of an inner-sphere complex by substitution of these terminal OH, the fatty acids should be adsorbed in parallel linear structures. This is indeed what we observe by AFM. This would explain the linearity of the patterns, not their size, because the spacing of the parallel ridge and grooves pattern is about 10 nm, while the repeat distance of the boehmite edges is only 1.2 nm [163]. Note that if the boehmite particles preferentially expose their edge planes, it would mean that they are formed with their layers perpendicular to the alumina surface. Thus, evidencing such structures would be an original result, and the question clearly deserves further investigation.

The properties of the alkyl chain do not influence the mechanism of binding itself but may have an effect on the density of adsorbed molecules. This may indeed explain the slight differences observed on the ordered patterns which appeared more or less obvious for the different FA molecules. The long unbranched alkyl chains are probably involved in van der Waals intermolecular interactions, resulting in the molecular organization of the self-assembled layer with a high packing density when the chains are in the all-trans conformation. By contrast, the self-assembly of OA or LA lead to the formation of more disordered layers, because the presence of one or two double bonds, respectively, influences the molecule conformation by imposing one or two kinks in the chain (Chapter 2, Figure 2.1).

Regarding the interaction of the MO, the ester derivative of OA, with the AlOOH surface, PM-IRRAS results unambiguously revealed the absence of bands characteristic of an ester and the presence of carboxylate groups in the adsorbed state (Table 3.1). This indicates that, when MO molecules are in contact with the hydroxylated Al surface, ester groups are subjected to chemical transformation, resulting in the formation of carboxylates which bind to the AlOOH surface similarly to FA. It is likely that the chemical modification of esters occurs according to a saponification reaction, generally written as follows:



Although the saponification reaction is well-known in solution and broadly used in many chemical processes, little information is available when the reaction takes place at the solid/liquid interface. In a water-deficient medium such as the heptane solvent that we used, saponification may occur through the involvement of hydroxyl groups originating from the pseudoboehmite surface, as discussed above and suggested elsewhere [146], or simply of hydration water retained between the boehmite layers. It appears that all adsorbed MO molecules were converted to soaps, as no remaining MO was detected with PM-IRRAS. Actually the term “soap” is a misnomer here, because the counterions of the carboxylates would be the surface cations to which they are coordinated, with a local structure that could be very similar to that obtained from the FA. However, the major difference between FA and ester derived systems is related to the surface nanostructure, which is not observed with MO.

### **3.2 Effects of FA film stability formation on the wettability and nanoscale roughness of Al substrate**

This chapter is dedicated to the investigation of the wettability of the hydroxylated Al surface depending on its roughness and self-assembled fatty acids. After adsorption of various fatty acids the nature of nanostructuring was checked using UV/O<sub>3</sub> treatment, conditioning in air and aqueous media. Comparison between two parameters, water contact angle ( $\theta_w$ ) and the Wenzel roughness, suggests the main origin of hydrophobisation.

#### *3.2.1 Effect of UV/O<sub>3</sub> treatment*

UV/O<sub>3</sub> irradiation is increasingly recognized as a standard technique for surface cleaning, because it is usually simple to operate, needs little or no heating and does not require handling of chemicals. It is widely used for the degradation of organic matter from surfaces of metal, oxides and semiconductors [164] which may be used in the manufacture of organic light emitting diodes and flexible panel displays [165, 166], as well as for biosensors or other biomedical devices [167]. In the present study, the main interest of performing UV/O<sub>3</sub> treatment on FA-modified Al surface is to attempt to remove self-assembled FA molecules without altering the structure of the hydroxylated Al substrate. This may clarify the role of FA self-assembly in the formation of the ordered nano-patterns on the Al surface. Long FA with different levels of unsaturation were used to this end. Accordingly, after the adsorption of SA, OA or LA, samples were treated by UV/O<sub>3</sub> during 1, 5, 10 and 30 min. PM-IRRAS analyses did not show significant changes in the high-frequency region after 1 to 10 min treatment for SA (Figure 3.13A). However, after 30 min, the intensity of the band at about 1546 cm<sup>-1</sup>, assigned to  $\nu_a(\text{COO}^-)$ , decreased appreciably, while the band at 1467 cm<sup>-1</sup>, assigned to  $\delta(\text{CH}_2)$ , disappeared totally (Figure 3.13A, right). In the high-frequency region after 1 and 5 min of UV/O<sub>3</sub> treatment, the intensities of the bands due to C-H vibration modes were almost unchanged but decreased noticeably after 10 min

treatment (Figure 3.13A, left). These bands completely disappeared when the samples were subjected to a 30 min UV/O<sub>3</sub> treatment (Figure 3.13A, left).

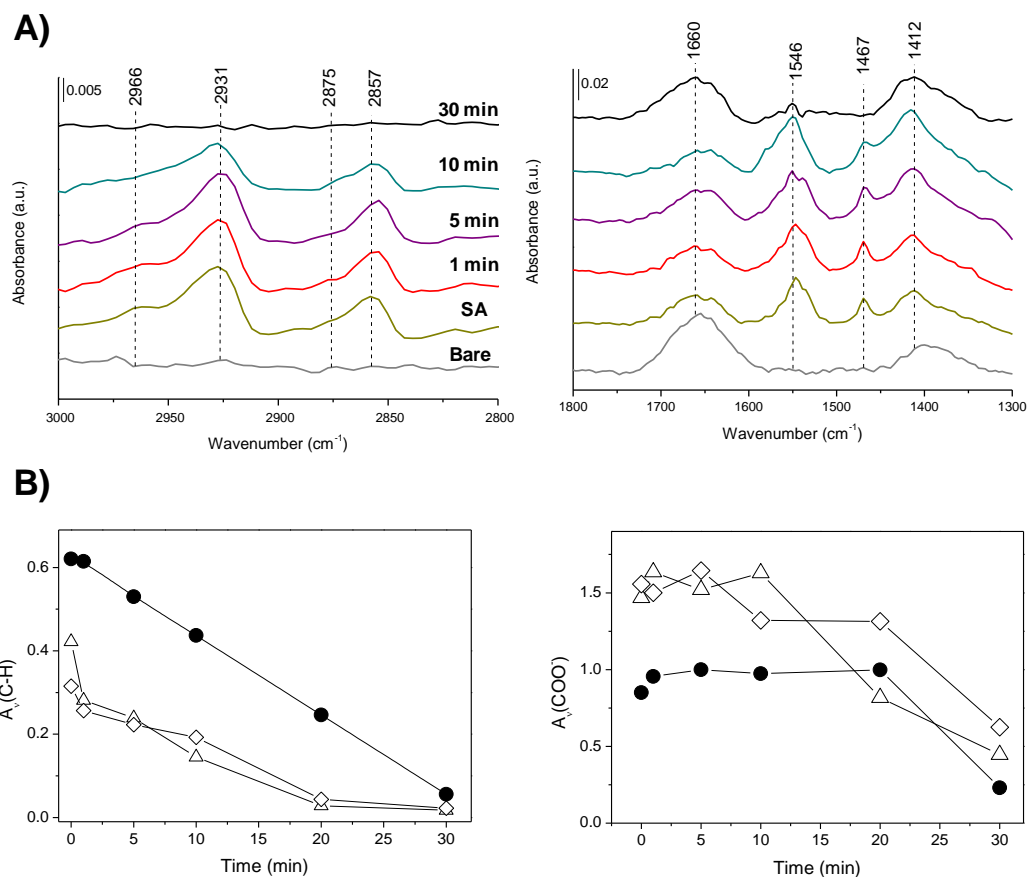


**Figure 3.13.** Panel A. PM-IRRAS spectra recorded in high (left) and low (right) frequency region on hydroxylated aluminum prior to and after the adsorption of SA and further UV/O<sub>3</sub> treatment for 1, 5, 10 and 30 min. Panel B. Evolution of A<sub>v</sub>(C-H) (left) and A<sub>v</sub>(COO<sup>-</sup>) (right), determined from PM-IRRAS data, as a function of UV/O<sub>3</sub> treatment time on hydroxylated aluminum surface after adsorption of SA (●), OA (△) and LA (◇).

The same trend was observed with OA and LA in both frequency regions (Figure 3.14).

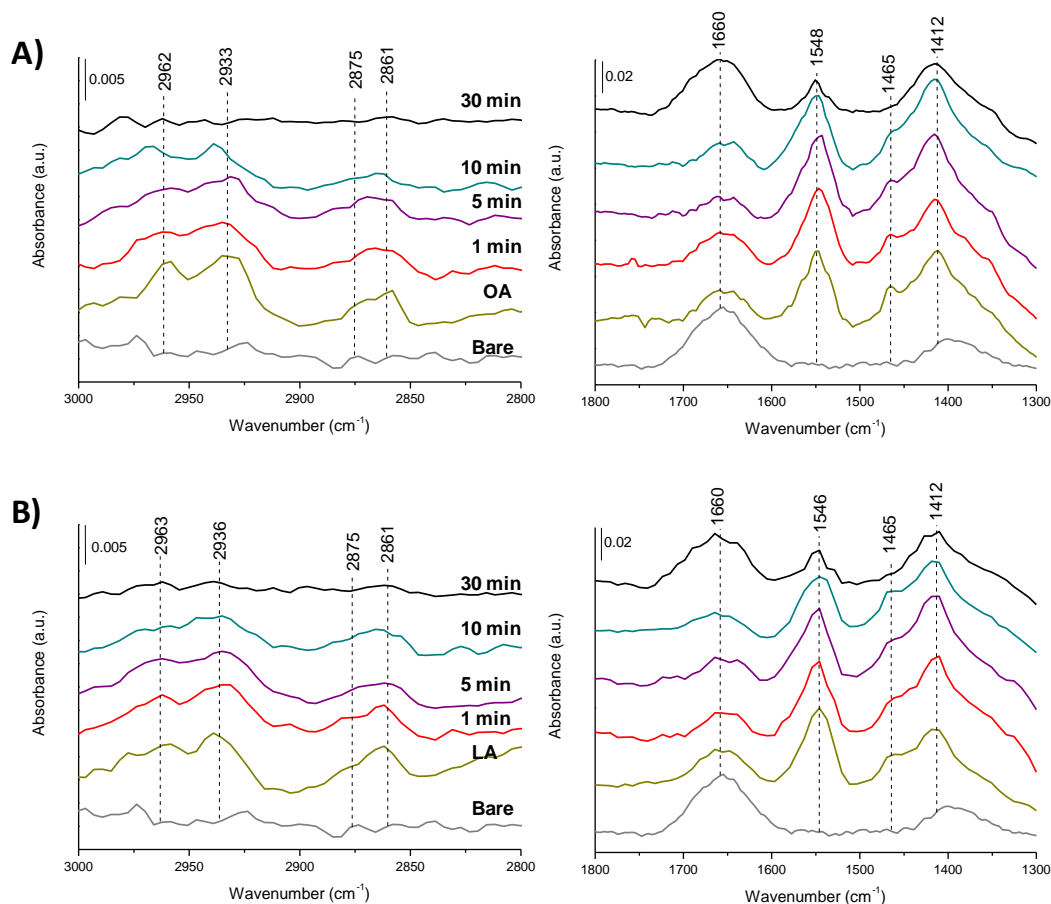


**Figure 3.14.** PM-IRRAS spectra recorded in high (left) and low (right) frequency region on hydroxylated aluminum prior to and after the adsorption of OA (Panel A) or LA (Panel B) and further UV/O<sub>3</sub> treatment for 1, 5, 10 and 30 min.

More direct evidence regarding the chemical composition of the treated surfaces may be obtained by exploring the area of bands from PM-IRRAS spectra which are characteristic of FA molecules, namely  $A_{\nu}(\text{C-H})$  and  $A_{\nu}(\text{COO}^-)$ . The results given in Figure 3.13B (left) evidenced that  $A_{\nu}(\text{C-H})$  decreased markedly as a function of the UV/O<sub>3</sub> treatment time for all FA. The trend is linear for the saturated FA, SA, indicating a zero-order kinetics which has also been observed by Ye et al. for octadecylsiloxane SAMs on SiO<sub>2</sub> [168]. In contrast, the decrease of  $A_{\nu}(\text{C-H})$  was fast at the early stages for both unsaturated FA and slowed down for higher durations (Figure 3.13B, left); in this case, the data are not precise enough to determine a reaction order. It is worth noting that the initial  $A_{\nu}(\text{C-H})$  value is significantly higher for SA than



for the other two FA, probably because of the formation of densely packed layers of SA, in contrast to unsaturated FA which probably form more disordered layers, as detailed above. The evolution of  $A_v(\text{COO}^-)$  did not follow the same trend as that of  $A_v(\text{C-H})$  (Figure 3.13B, right). The values initially remained at the same level and started to decrease markedly only after 20 and 30 min treatment for unsaturated and saturated FA, respectively. This result suggests that the carboxylate moieties remain stable for 20 min in our conditions of treatment, in contrast to  $-\text{CH}_x$  groups.

The evolution of the water contact angle as a function of the duration of UV/O<sub>3</sub> treatment is given in Figure 3.15. The results showed noticeable differences as a function of the level of unsaturation. On the SA-modified surface,  $\theta_w$  did not vary significantly up to 3 min UV/O<sub>3</sub> treatment and started to decrease only slightly after 4 and 5 min to reach values of about 120° and 112°, respectively. A significant decrease was achieved after 10 min treatment ( $\theta_w \sim 50^\circ$ , data not shown) and a complete spreading of the drop was observed after 30 min. By contrast, the decrease of  $\theta_w$  as a result of the UV/O<sub>3</sub> treatment occurred at earlier stages when the surfaces were modified with unsaturated FA, OA and LA (Figure 3.15), until the water drop spread completely on the surface after 4 and 5 min, respectively. The trend showed in Figure 3.15 reveal that the decrease of  $\theta_w$  is more rapid for LA compared to OA.

Under UV/O<sub>3</sub> treatment, unsaturated FA may be subject to two mechanisms of degradation (Chapter 1, section 1.2.2), ozonolysis [169] and autoxidation [53]. Ozonolysis is initiated through electrophilic addition of an ozone molecule to a double bond. The reactivity of bulk unsaturated FA in the presence of O<sub>3</sub> is well described in the literature [58-60]. O<sub>3</sub> inserts through the double bond (such as those in OA and LA, Chapter 2, Figure 2.1) and forms a primary ozonide, which decomposes leading to the formation of an aldehyde and a Criegee intermediate (a biradical). Criegee intermediates then form secondary ozonides (trioxolane rings) that are cleaved; depending on the place of the cleavage, they can form mono or diacids. The net result of this series of events

is a rupture of the fatty acid chain at the location of the double bond; the distal end of the chain is eliminated as a small-molecular weight molecule.

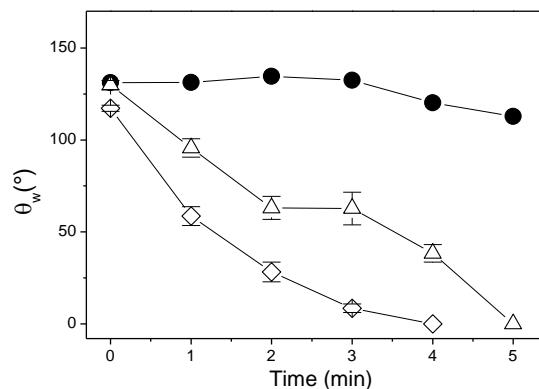


**Figure 3.15.** Evolution of the water contact angle ( $\theta_w$ ) as a function of UV/O<sub>3</sub> treatment time on hydroxylated aluminum surface after adsorption of SA (●), OA (△) and LA (◇).

The mechanism of degradation of the saturated FA, SA, must however be different, as ozonolysis only affects double bonds and this particular acid has none. It is likely due to autoxidation. The latter process is initiated by the formation of free radicals, which is caused by reactive oxygen species such as the OH• radical and atomic oxygen, the products of ozone dissociation under UV [168]. They abstract hydrogen from alkyl chains, leading to the formation of alkyl radicals, which further react to form alkoxy radicals and generate new reactive carbonyl group through oxidation. These carbonyl groups dissociate through photodecomposition or attacking by radicals with the loss of carbon, and therefore reduce the carbon chain length of fatty acids [83]. The key mechanistic step is the attack of a radical at a C-H bond, and it does not require double bonds.

The above results suggest the following view of FA layer degradation. In all cases the FA are strongly adsorbed to the hydroxylated Al surface through a coordination of their carboxylate groups to surface Al<sup>3+</sup>, with the (saturated or unsaturated) alkyl chains protruding away from the surface. For unsaturated

FA, the reaction with ozone is fast, and in particular the relatively loose packing of the layers does not impede ozone diffusion. Thus, large chunks of the FA chains are quickly removed by ozonolysis, leaving shorter-chain, fully saturated carboxylic acids still adsorbed through the carboxylate: the reaction then slows down because there are no further attack points for ozonolysis. The removal of  $\text{CH}_x$  groups is not complete when water starts spreading on the surface, judging from the evolution of PM-IRRAS bands; but the surface may become patchy after 5 minutes, with some of the underlying  $\text{AlOOH}$  groups available for interaction with water (see the discussion section for more details on this hypothesis).

In contrast, for the fully saturated SA layer, gas-phase radical species from ozone dissociation attack the C-H bonds in distal groups of the alkyl chain; since the latter are densely packed, the radical species cannot diffuse between the chains, which are eroded only from the distal end. The reactive surface exposed by the layer remains constant throughout this process, explaining the zero order, and it is only when most of the chain has been consumed that the carboxylate groups can be destroyed in turn.

AFM images were also recorded after the samples were treated with  $\text{UV/O}_3$  for 10 min. The bare hydroxylated Al surface kept almost the same surface morphology as before the  $\text{UV/O}_3$  treatment (Figure 3.16A and E). In contrast, on FA-modified surfaces the treatment caused a noticeable disturbance of the surface nanoscale organization. Indeed, the major alteration of the surface concerned the aligned patterns, which became less well discernible: they were enlarged and/or deformed. In fact, the phenomenon was apparently more pronounced when the level of unsaturation was higher, as the most severe alteration was observed with LA, while the SA-modified surface was subjected to the least disordering (Figure 3.16B-H). These findings showed the same trend as the sensitivity of FA to  $\text{UV/O}_3$  treatments, which was enhanced when increasing the level of unsaturation, as described above. Accordingly, there is evidence that the nature of the self-assembled molecules plays a major role not only on the formation of ordered nanostructures but also on their stability.

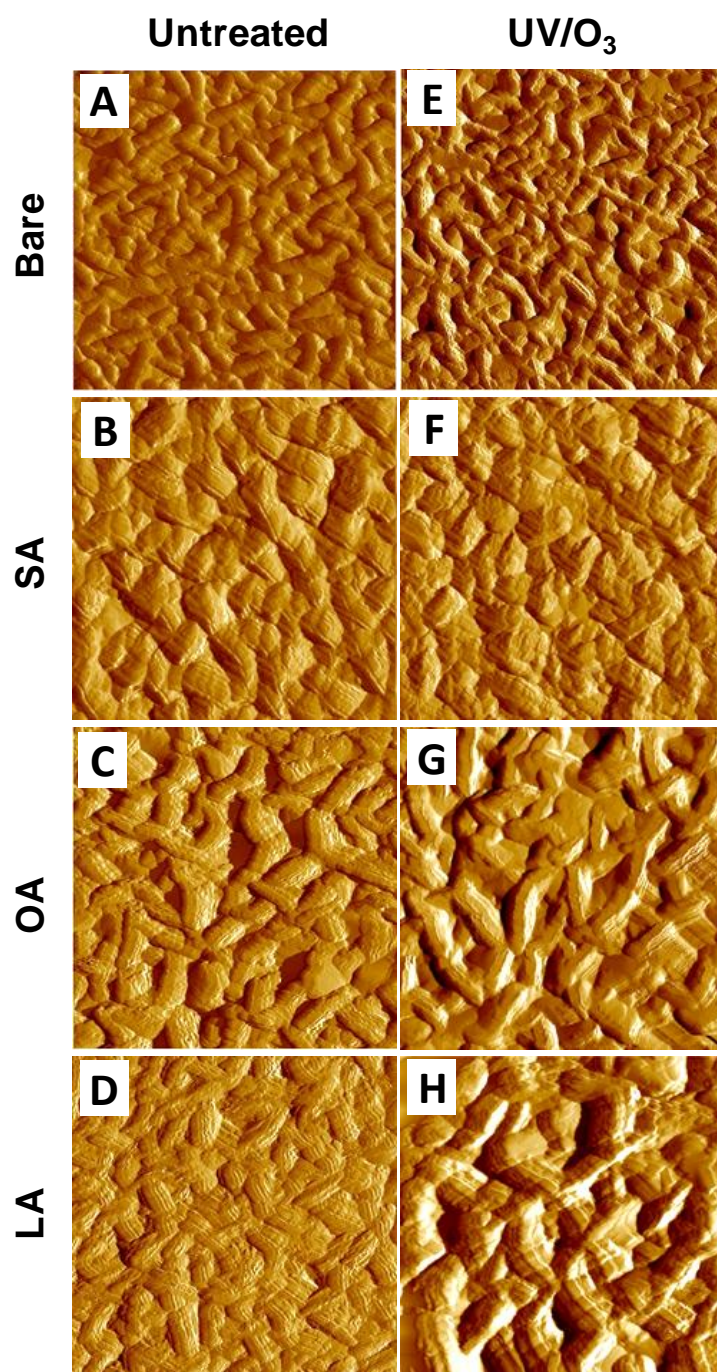


**Figure 3.16.** Representative AFM deflection images ( $1 \times 1 \mu\text{m}^2$ , Peak Force Tapping mode, in air) recorded on hydroxylated aluminum, prior to (A, B, C, D) and after UV/O<sub>3</sub> treatment for 10 min (E, F, G, H): bare hydroxylated surface (A, E), SA (B, F), OA (C, G) and LA (D, H).

### 3.2.2 Effect of conditioning

The stability of FA-modified surface was examined after conditioning in different media. To this end, after the adsorption of OA, the samples were incubated in air, in water or in other solutions simulating an environment of biological interest, namely solutions of sodium chloride (NaCl), hydrogen peroxide ( $\text{H}_2\text{O}_2$ ) or phosphate buffer saline (PBS). OA was chosen because it particularly induced a typical nanoscale organization, with an obvious presence of the ordered patterns (Figure 3.16C). PM-IRRAS spectra showed, in the lower frequency region (Figure 3.17, right) that the conditioning in air or in water did not affect the bands characteristic of the self-assembled OA, especially the one associated with the asymmetric stretching mode of the  $\text{COO}^-$  moiety at  $1548\text{ cm}^{-1}$ .

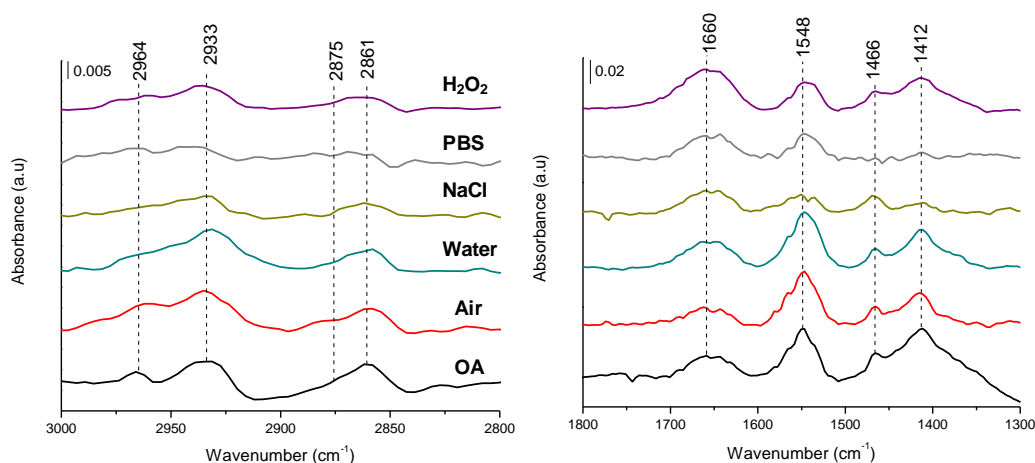


**Figure 3.17.** PM-IRRAS spectra recorded in high (left) and low (right) frequency region on hydroxylated aluminum surfaces modified with OA and conditioned for 24h in air, water, NaCl solution, PBS and  $\text{H}_2\text{O}_2$  solution.

In contrast, the intensity of this band decreased markedly as a result of conditioning in the other aqueous media, especially in NaCl solution and PBS. The same trend was also observed on the band at  $1412\text{ cm}^{-1}$ , the symmetric stretching mode of the  $\text{COO}^-$  moiety. In all spectra, the band at  $1466\text{ cm}^{-1}$  attributed to  $\delta(\text{CH}_2)$  was observed, except in PBS spectrum where it

disappeared totally (Figure 3.17, right). These findings are in agreement with spectra recorded in the high frequency region, showing that bands associated with  $\nu(\text{CH}_2)$  and  $\nu(\text{CH}_3)$  are much less obvious in PBS compared to the other spectra (Figure 3.17, left).

Water contact angle measurements bring additional insights into the stability of the self-assembled OA layer in the different media. The  $\theta_w$  value (Table 3.2) did not change markedly when the sample was conditioned in air. However, a significant decrease was observed after conditioning in water and solutions of  $\text{H}_2\text{O}_2$  and NaCl, while in PBS the surface reached a total wetting.

**Table 3.2.** Water contact angle,  $\theta_w$  ( $^\circ$ ) measured on hydroxylated Al surfaces after adsorption of OA and further conditioning in the different media.

	$\theta$ ( $^\circ$ )
Air	132.5 (2.5)
Water	103.5 (5.2)
NaCl	81.9 (2.6)
$\text{H}_2\text{O}_2$ (10 mM)	103.1 (1.4)
Phosphate buffer saline	bdl

PM-IRRAS results and the evolution of  $\theta_w$  as a function of the conditioning medium both showed that the self-assembled OA layer remains stable in air, but may be subjected to significant degradation in aqueous media, depending on the composition of the medium. In PBS, the instability of the FA layer is probably due to the phosphate ions which may displace the carboxylate groups as ligands for surface  $\text{Al}^{3+}$ .

AFM images showed that conditioning did not radically affect the surface morphology, although a few relevant changes are noticeable in some media (Figure 3.18).

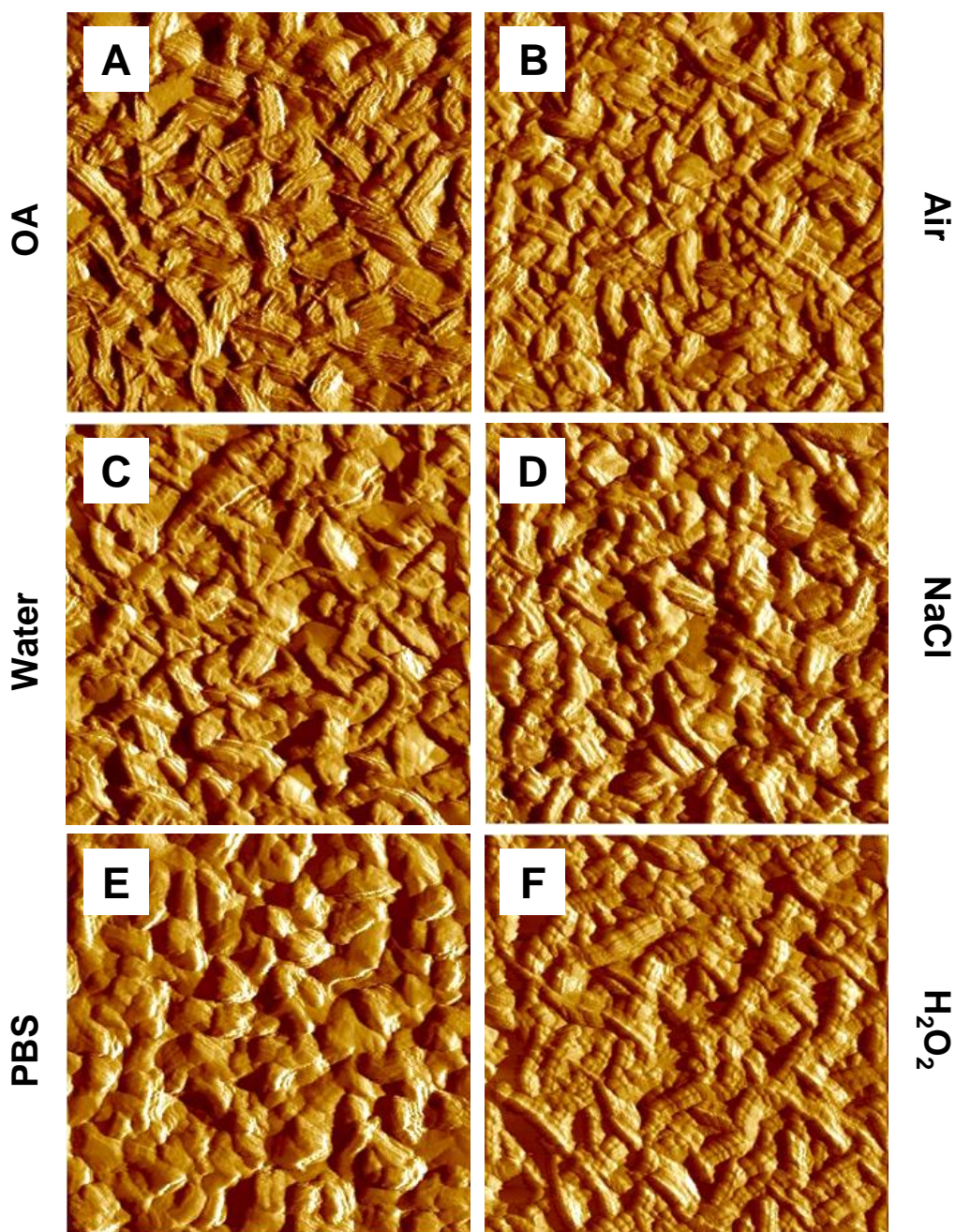


**Figure 3.18.** Representative AFM deflection images ( $1 \times 1 \mu\text{m}^2$ , Peak Force Tapping mode, in air) recorded on hydroxylated aluminum surfaces modified with OA (A) and conditioned for 24h in air (B), water (C), NaCl (D), PBS (E) and  $\text{H}_2\text{O}_2$  solution (F).

After incubation in air or in water the surface nanoscale organization remained almost unchanged, but the presence of the ordered patterns became less obvious, especially after conditioning in water (Figure 3.18B and C). This trend was more pronounced in NaCl solution (Figure 3.18D). In PBS, the surface morphology exhibited a significant change, namely an enlargement of

the nanostructures originating from the hydroxylation treatment, while the presence of the ordered patterns was not observed (Figure 3.18E). The situation after treatment in the H<sub>2</sub>O<sub>2</sub> solution is different. AFM images showed indeed that the whole nanoscale organization is similar to the one observed prior to the conditioning test (compare image F and A, Figure 3.18). However, the incubation in H<sub>2</sub>O<sub>2</sub> solution led to the formation of nanoparticles in close contact with each other.

### 3.2.3 “Chemistry” vs “Roughness”

One relevant way to confirm the involvement of self-assembled molecules on the observed nanoscale organization (formation of nano-patterns) consists in removing organic molecules without greatly altering the inorganic surface. UV/O<sub>3</sub> was used to this end as FA are difficult to remove with common washing procedures, when adsorbed on surfaces, due to their low solubility in water and their strong interaction with the AlOOH surface. The use of detergents may be efficient to remove the adsorbed fatty acids, but would typically lead to their replacement with detergent molecules i.e. to even further surface contamination. Accordingly, UV/O<sub>3</sub> treatment appears as a promising method as it cleaves the adsorbed molecules forming volatile products [164]. The impact of the UV/O<sub>3</sub> treatment on the surface morphology provides relevant information regarding the role of adsorbed FA on the nanoscale organization. Interestingly, AFM images showed more pronounced impact on the surface when the sensitivity of FA against UV/O<sub>3</sub> increased. For all FA, the surface organization was significantly altered, especially the ordered lines, when FA was removed partially or almost totally from the surface, suggesting that the nanoscale organization was not maintained when removing self-assembled molecules.

The second way used to modify the interface and check the evolution of the nanoscale organization consists in carrying out conditioning tests in aqueous media. In a previous study, the AlOOH surface itself was shown to be stable in water or in PBS buffer, in terms of chemical composition and morphological



features [140]. Therefore, the evolution of the surface morphology in PBS can only be due to the behavior of adsorbed FA. The latter were almost totally removed from the surface after incubation in this medium, as evidenced by water contact angle and PM-IRRAS. This result supports the role of self-assembled molecules in maintaining the nanoscale organization of the surface. Furthermore, when the removal of organic molecules was only partial, as observed after conditioning in water, but also in air, nano-patterns were preserved.

The mechanism in the  $\text{H}_2\text{O}_2$  solution is different. On bare hydroxylated Al surface, the effect of  $\text{H}_2\text{O}_2$  consists in the formation of larger Al oxyhydroxide nanostructures, while keeping a similar morphology. This is due to an oxidation to a larger depth of the Al substrate and an additional formation of Al oxyhydroxide compounds. In the presence of OA adlayer, the mechanism is modified because the oxidation process may be blocked in the sites where FA are assembled, leading to the growth of separated but closely packed nanostructures which exhibit a spherical-like shape (Figure 3.18F). In a different context, but for the same reasons, it has been evidenced that FA may play a role to improve the corrosion resistance of materials, likely through a blocking process of anodic sites present on the surface [109].

Regarding the wettability of the surface, the main issue is to clarify whether the presence of self-assembled FA or the surface roughness contributes to the observed trend. Concerning the surface roughness, finding the parameter which best describes the contribution of hierarchical substructures on the wetting properties of a surface is a key point, especially for surfaces showing specific and reproducible self-organized pattern. In our present data, the root-mean square roughness ( $R_{\text{rms}}$ ) usually employed to quantify the rugosity of a surface did not show any significant correlation with the equilibrium water contact angle regardless of the nature of the acids or the conditioning (Figure 3.19A).

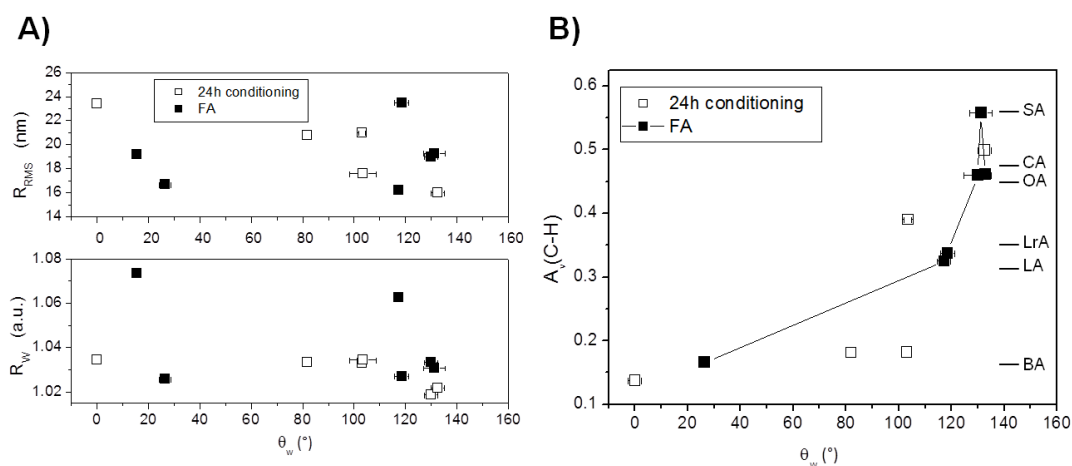


**Figure 3.19.** Correlation between (A) root-mean-square roughness ( $R_{RMS}$ ), Wenzel roughness ( $R_W$ ), (B) Area of bands associated with asymmetric stretching of C-H groups,  $A_v(C-H)$ , and water contact angle ( $\theta_w$ ) of hydroxylated Al samples after adsorption of FA (filled square) and further incubation in different conditioning media for 24 h (open square). In panel (B), 24 h conditioning specifications have been removed for clarity. The trend of the areas with respect to contact angle is as follows, from lower to higher values:  $PBS < NaCl < H_2O_2 < H_2O < OA < Air$ .

This result is not surprising: in the light of a previous study, it has been shown that surfaces with the same  $R_{rms}$  may have different wetting properties [170]. Furthermore, as  $R_{rms}$  is only sensitive to the height differences and does not contain information on the horizontal range fluctuations, if a substructure of the material governs the wettability properties of the surface, the  $R_{rms}$  parameter would not reveal its contribution.

Recently, the wetting properties of homogenous randomly rough surfaces were related to the contribution of sub-micrometer-scale protrusions via the Wenzel roughness ( $R_W$ ) [170]. In the Wenzel model, the water droplet covers the whole surface and  $\theta_w$  is expressed as a function of Young's angle and a roughness parameter defined as the ratio between the extended area of the surface, and the projected one obtained via AFM [171, 172].

This roughness parameter is expected to be a sensitive enough parameter to highlight whether a correlation exists between the 10-nm scaled high-frequency substructures and water contact angle.

Figure 3.19A shows the evolution of the Wenzel roughness  $R_w$  as a function of water contact angle,  $\theta_w$ . The results did not reveal any trend that might be linked to the Wenzel roughness ( $R_w$ ), suggesting that neither the structure nor the substructure including the 10 nm nanoscale pattern are the chief parameters determining the surface wettability. By contrast,  $A_v(\text{C-H})$ , which reflects the presence of adsorbed FA and to a lesser extent depends on their chemical nature, possibly through different packing densities of the FA layers, followed a clear trend as a function of  $\theta_w$ :  $A_v(\text{C-H})$  significantly increased at high  $\theta_w$  values (Figure 3.19B). Accordingly, it seems that the main origin of the hydrophobisation is the presence of  $-\text{CH}_x-$  groups exhibited by adsorbed FA. Support of this assumption may be found in the evolution of  $\theta_w$  after the adsorption of FA on “flat” (before hydroxylation) or “rough” (after hydroxylation) Al surface (Figure 3.8), indicating no effect of the surface roughness (modulated by the hydroxylation treatment) on the wettability for long chain FA.

However, in addition to the chemical nature of the exposed groups, another factor related to the “in depth” localization of adsorbed molecules may play a role in wettability. Indeed, as already discussed, on OA and LA-modified surfaces exposed to UV/O<sub>3</sub>, complete wetting was achieved, even with treatments of intermediate duration where C-H groups were still present on the surface (observed in PM-IRRAS spectra, Figure 3.13B). Actually, owing to the surface roughness (Figure 3.20A), the difference in the depth scales probed by each technique has to be taken into account, as depicted in Figure 3.20B. It is expected that molecules adsorbed on the outermost surface (on the ridges, Figure 3.20B) are more sensitive to UV/O<sub>3</sub> irradiation, as compared to those present within the “valleys” (technically, mesopores in the AlOOH surface), and therefore are removed first. This would lead to the exposure of hydrophilic surface groups (Al-OH) and to  $\theta_w$  values equal to zero, even though some FA molecules would remain present in the mesopores.

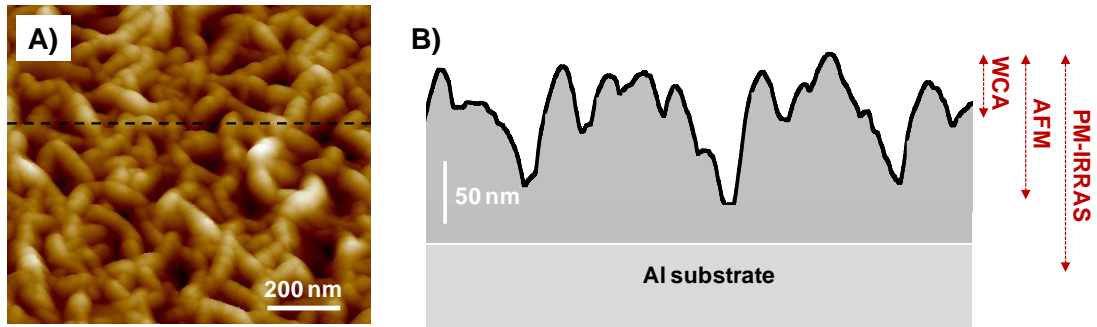


**Figure 3.20.** (A) Representative AFM 3D height image recorded on hydroxylated aluminum surface. (B) Schematic representation of the interface based on cross section taken at the position indicated by dashed lines in panel (A). The thickness probed by each technique is indicated.

As seen from this example, a complete picture of the interface may only be provided if the appropriate parameter of surface roughness is used and two directions are considered for the exploration of surface morphology, i.e. surface organization both perpendicular and parallel to the surface plane.

### **3.3. Mechanism of adsorption of DPPC on nanostructured Al substrate:**

#### **Influence of surface hydrophobicity**

This chapter will detail the adsorption of a phospholipid (DPPC) on the nanostructured hydroxylated Al surface prior to and after modification with SA, as described previously (Chapter 3.1.). The main purpose of this chapter is to investigate the adsorption behavior of DPPC whether the surface is hydrophilic (AlOOH) or hydrophobic (SA-modified surface) with a view to designing a hybrid phospholipid/fatty acid “bilayer”. A variety of techniques were used to probe the properties of the layer (chemical, wetting) and to evaluate its stability in aqueous medium.

#### *3.3.1 Adsorption of DPPC*

The adsorption of DPPC was performed on hydroxylated Al (AlOOH) and SA-modified hydroxylated Al (SA-AlOOH) surfaces. The surface modification with SA was performed according to the procedure described in the previous chapter, leading to the formation of self-assembled layer.

The adsorption of DPPC was performed using two different procedures, as detailed in chapter 2 (section 2.2.5):

***Procedure I:*** 20  $\mu$ l drop of DPPC solution was deposited on the Al substrate and left into the vacuum for 2 h. The samples prepared with this procedure were called “AlOOH-DPPC I” and “SA-AlOOH-DPPC I” depending whether the substrate was AlOOH or SA-AlOOH, respectively.

***Procedure II:*** 40  $\mu$ l of DPPC solution was spread on the sample and rotated at 3000 rpm for 40 s by using spin-coater, and before further analysis left in the vacuum for 2 h. The samples prepared with this procedure were called “AlOOH-DPPC II” and “SA-AlOOH-DPPC II”, as specified above.

#### a) PM-IRRAS

As discussed in the previous chapters, PM-IRRAS spectra recorded on the hydroxylated Al substrates are characteristics of AlOOH compound (Figure 3.1). The adsorption of DPPC led to the apparition of new bands as shown in

(Figure 3.22A, spectrum b). In the C-H stretching region, the vibrational features due to the alkyl chains of the adsorbed DPPC molecules were observed. The symmetric and asymmetric stretching modes of methylene groups,  $\nu_s(\text{CH}_2)$  and  $\nu_{as}(\text{CH}_2)$ , at 2855 and 2925  $\text{cm}^{-1}$ , respectively can be observed. The asymmetric stretching mode of  $\text{CH}_3$  moieties,  $\nu_{as}(\text{CH}_3)$ , as well as the corresponding symmetric mode,  $\nu_s(\text{CH}_3)$  are also visible at 2962  $\text{cm}^{-1}$ , and 2876  $\text{cm}^{-1}$ , respectively. Methylene groups are dominating because DPPC molecule has 28 methylene groups in the two acyl chains and 2 methylene groups in its glycerol part.

In the low frequency region, relevant vibrational features related to the adsorbed DPPC were observed. The band at 1741  $\text{cm}^{-1}$  is attributed to  $\nu(\text{C}=\text{O})$  due to the ester group of the glycerol backbone. The asymmetric bending ( $\delta_{as}$ ) modes of the methyl groups attached to the nitrogen atom in the choline moiety ( $(\text{CH}_3)_3\text{-N}^+$ ) appeared at 1492  $\text{cm}^{-1}$  and its symmetric modes was observed at 1416  $\text{cm}^{-1}$ . The bands at 1469  $\text{cm}^{-1}$  and 1378  $\text{cm}^{-1}$  can be attributed to methylene scissoring mode  $\delta(\text{CH}_2)$  and symmetric  $\text{CH}_3$  deformation  $\delta_s(\text{CH}_3)$ , respectively (Figure 3.22A, spectrum b).

The characteristic band due to phosphate group, which appears around 1125-1000  $\text{cm}^{-1}$  could not be observed in this case, as it overlaps with the intense band at 1091  $\text{cm}^{-1}$  due to Al-OH hydroxyl bending mode  $\delta(\text{OH})$  in AlOOH compounds. However, the asymmetric stretch of phosphate group was observed at 1256  $\text{cm}^{-1}$ . The C-O-C stretch of the ester groups is recorded at 1174  $\text{cm}^{-1}$  and the band at 975  $\text{cm}^{-1}$  is due to the asymmetric stretching vibration of C-N group,  $\nu_{as}(\text{C-N}^+(\text{CH}_3))$ , and its symmetric one at 926  $\text{cm}^{-1}$ .

When the adsorption was performed on SA-modified AlOOH surface (SA-AlOOH), no significant differences were observed (Figure 3.22B), except that bands due to self-assembled SA molecules were visible, i.e. bands at about 1417 and 1547  $\text{cm}^{-1}$  associated with the symmetric and asymmetric stretching modes of the  $\text{COO}^-$  moiety, respectively.

All the vibrational features recorded in the present study after the adsorption of DPPC on AlOOH and SA-AlOOH surfaces are summarized in Table 3.3.

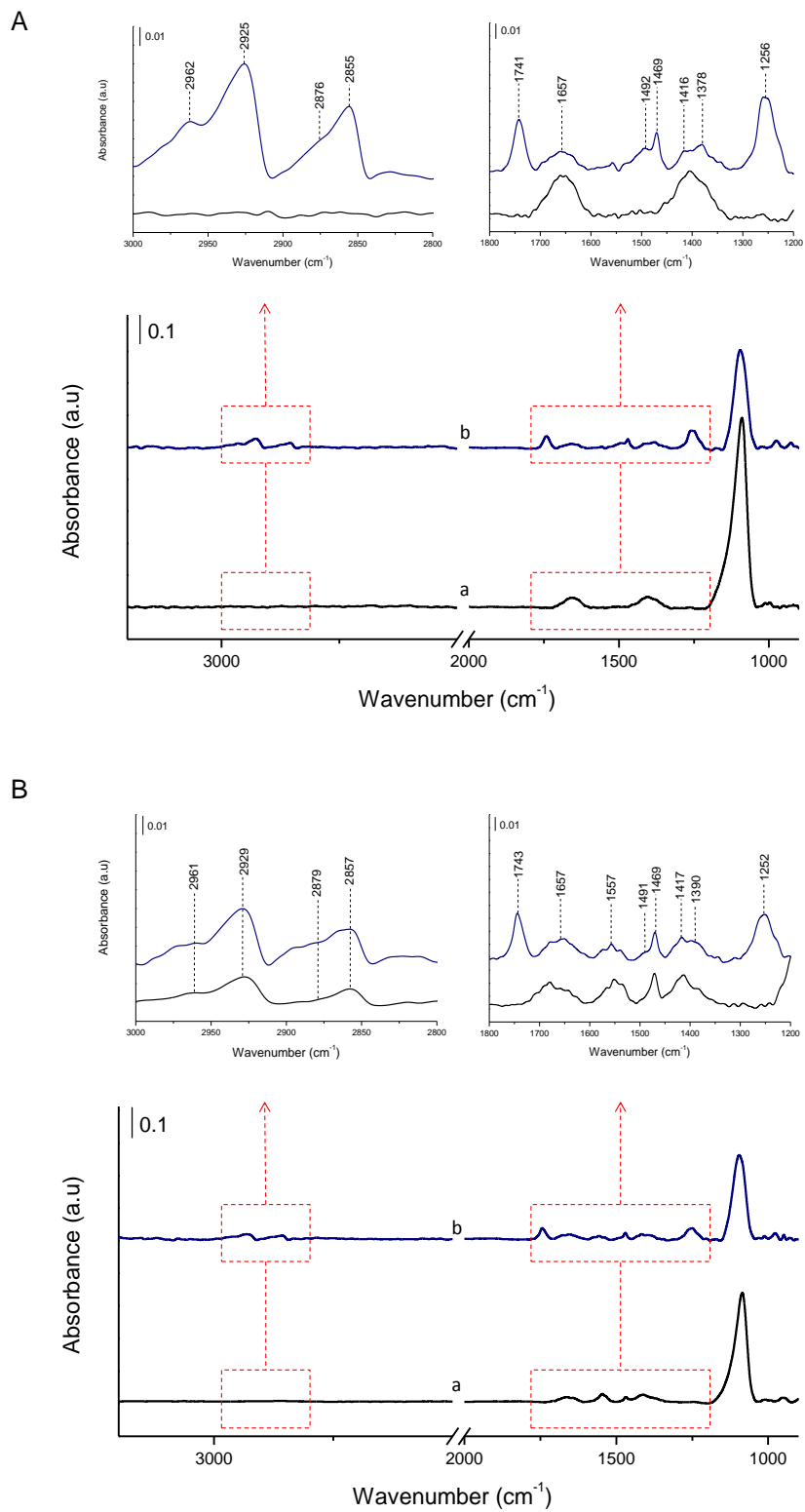


**Figure 3.22.** PM-IRRAS spectra recorded on (A) AlOOH and (B) SA-AlOOH substrates (a) prior to and (b) after the adsorption of DPPC.

**Table 3.3.** Assignment of IR bands relative to phospholipid molecules. For sake of comparison, data from the literature [115, 120, 173, 174] were also presented, showing vibrational features of DPPC molecules free in the solution or in the adsorbed state.

chemical group	vibrational type	Literature		This study			
		liquid	adsorbed state	Procedure I		Procedure II	
		$\lambda$ (cm <sup>-1</sup> )	$\lambda$ (cm <sup>-1</sup> )	$\lambda$ (cm <sup>-1</sup> )	$\lambda$ (cm <sup>-1</sup> )	$\lambda$ (cm <sup>-1</sup> )	$\lambda$ (cm <sup>-1</sup> )
CH <sub>3</sub>	$\nu_{as}$ (C-H)	2956	2956	2962	2965	2962	2961
CH <sub>2</sub>	$\nu_{as}$ (C-H)	2920	2920	2925	2927	2925	2929
CH <sub>3</sub>	$\nu_s$ (C-H)	2870	2873	2876	2871	2876	2879
CH <sub>2</sub>	$\nu_s$ (C-H)	2850	2850	2855	2858	2855	2857
COOR	$\nu$ (C=O)	1735	1740	1741	1744	1741	1744
COO <sup>-</sup>	$\nu_s$ (COO <sup>-</sup> )	-	-	-	1557	-	1550
(CH <sub>3</sub> ) <sub>3</sub> N <sup>+</sup>	$\delta_{as}$ ((CH <sub>3</sub> ) <sub>3</sub> N <sup>+</sup> )	1490, 1480	1491, 1480	1492	1491	1492	1491
CH <sub>2</sub>	$\delta$ (CH <sub>2</sub> )	1473, 1472, 1468, 1463	1468	1469	1469	1469	1469
CH <sub>3</sub>	$\nu_{as}$ (C-H)	1460	1457	-	-	-	-
COO <sup>-</sup>	$\nu_s$ (COO <sup>-</sup> )	-	-	-	1417	-	1421
(CH <sub>3</sub> ) <sub>3</sub> N <sup>+</sup>	$\delta_s$ ((CH <sub>3</sub> ) <sub>3</sub> N <sup>+</sup> )	1418, 1378	-	1416	-	1416	-
CH <sub>3</sub>	$\delta_s$ (C-H)	1378	1378	1378	1390	1378	1378
PO <sub>2</sub> <sup>-</sup>	$\nu_{as}$ (PO <sub>2</sub> <sup>-</sup> )	1230	1250	1256	1252	1247	1251
CO-O-C	$\nu_{as}$ (C-O-C)	1175	1190	1174	1174	1174	1174
PO <sub>2</sub> <sup>-</sup>	$\nu_s$ (PO <sub>2</sub> <sup>-</sup> )	1085	1092	-	-	-	-
CO-O-C	$\nu_s$ (C-O-C)	1070	1070	-	-	-	-
C-O-P	$\nu_{as}$ (C-O-[P])	1055; 1068	1056; 1070	-	-	-	-
C-N	$\nu_{as}$ (C-N <sup>+</sup> - (CH <sub>3</sub> ) <sub>3</sub> )	972	970	975	976, 949	975	977, 952
C-N	$\nu_s$ (C-N <sup>+</sup> - (CH <sub>3</sub> ) <sub>3</sub> )	-	950, 920	926	926	926	933
P-O	$\nu_{as}$ (P-O)	820	-	-	-	-	-

There was the same tendency for both procedures – increasing concentrations increasing the amount of adsorbed molecule. This could be observed from measurements of area of band at 1741 cm<sup>-1</sup> of C=O stretching due to the ester group (Figure 3.23.A). However, the evolution was noticeably different for the two procedures. Using Procedure I,  $A_\nu(C=O)$  increased markedly when increasing the concentration of DPPC, while, the trend was less pronounced using procedure II. The parameter  $A_\nu(C=O)$ , extracted from PM-IRRAS data, may be related to the adsorbed amount of DPPC in a semi-quantitative way. Accordingly, the evolution observed in Figure 3.23A suggests that DPPC adsorbed in a higher amount when procedure I was used.

#### b) Water contact angle

Water contact angle measurements were performed on the hydrophilic AIOOH ( $\theta_w \sim 15^\circ$ ) and hydrophobic SA-modified AIOOH ( $\theta_w \sim 130^\circ$ ) substrates after adsorption of DPPC.



By using procedure I, the adsorption of DPPC on AlOOH surface did not induce significant changes in  $\theta_w$ , regardless of DPPC concentration (Figure 3.23B). By contrast, on SA-modified surface,  $\theta_w$  decreased markedly after the adsorption of DPCC at 1 mg/mL, to reach the same level of hydrophilicity than AlOOH. The situation is different when the adsorption was performed using spin coating (procedure II). Results showed a progressive increase of  $\theta_w$  after DPPC adsorption on AlOOH and an opposite trend on SA-AlOOH surface (Figure 3.23C). It is noteworthy that in both procedures, the evolution of  $\theta_w$  was only noticeable in the range of high concentrations of DPPC (from 1 to 10 mg/mL, Figure 3.23C).

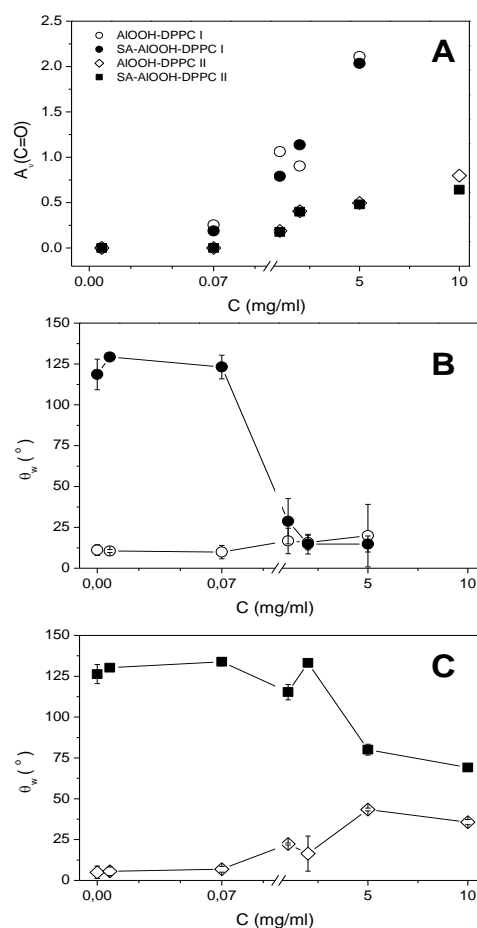


**Figure 3.23.** Evolution of the band at 1741 cm<sup>-1</sup> recorded by PM-IRRAS and the water contact angle ( $\theta_w$ ) as a function of the concentration of DPPC solution, after adsorption on AlOOH (open symbols) and SA-AlOOH (filled symbols) surfaces by using the adsorption procedures I (B) or II (C)

### 3.3.2 Effect of hydration

The hydration of the adsorbed DPPC layers may provide insights regarding its stability in aqueous media. In this work, the hydration was performed at room temperature, by incubating the samples in Tris-HCl buffer (pH 7.4) during 2 h. The experimental conditions of hydration were chosen in a manner to keep the self-assembled fatty acid layer intact. For this purpose and prior to the DPPC adsorption, a series of immersion tests were carried out in different common buffers: phosphate buffer saline (pH ~ 7.4), Tris-HCl (pH ~ 7.4, ~ 9.4) and carbonate buffer (pH ~ 9.4). Furthermore, for sake of comparison, the same tests were also performed on oleic acid-modified ALOOH. Based on water contact angle measurements, results, given in Figure 3.24, showed that (i) the SA layer is more stable than oleic acid, (ii) after 2 h immersion in Tris-HCl (pH ~ 7.4), the SA layer seems to be kept unchanged. The latter medium was, thus, chosen for hydration tests performed after the adsorption of DPPC.

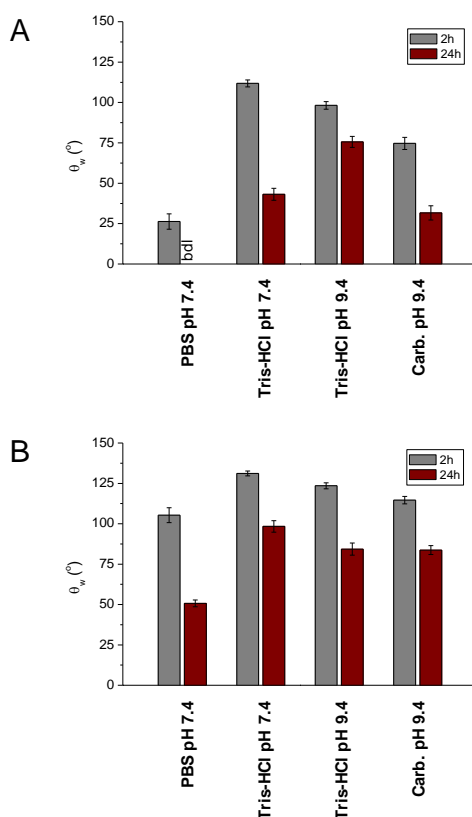


**Figure 3.24.** Histograms of WCA of adsorbed on ALOOH A) OA and B) SA after incubating in various buffers for 2 and 24 h.

The effect of hydration of the adsorbed DPPC layers was investigated by means of X-ray photoelectron spectroscopy (XPS). The use of XPS analysis is more appropriate in this context, as the technique is very sensitive to evidence and quantify weak variations when investigating the composition of thin solid films. Typical C 1s and N 1s peaks recorded on the different samples are presented in Figure 3.25. C 1s peak can be safely decomposed into four contributions on the basis of data obtained from biocomponents [144]: (i) a component at 284.8 eV due to carbon only bound to carbon and hydrogen [ $\underline{\text{C}}$ -(C,H)], (ii) a component at 286.3 eV due to carbon bound to oxygen or nitrogen [ $\underline{\text{C}}$ -(O,N)], including alcohol, amide, acetal or hemiacetal, (iii) a component at about 287.8 eV due to carbon making one double bond [ $\underline{\text{C}}=\text{O}$ ] or two single bonds with oxygen [ $\text{O}-\underline{\text{C}}-\text{O}$ ], including amide, acetal and hemiacetal and finally (iv) a component found near 288.7 eV due to carboxylic acid and ester ( $\text{O}=\underline{\text{C}}-\text{O}$ ). All components were imposed to have the same full width at half maximum (FWHM). The N 1s peak exhibited a component at 399.8 eV attributed to amide or amine functions ( $\text{C}-\underline{\text{N}}$ ), on bare AlOOH which may originate from adventitious contamination. After the adsorption of DPPC a contribution at higher binding energies (~402.3 eV) appeared and may be related to the presence of quaternary amine groups ( $\text{C}-\underline{\text{N}}^+$ ) (see molecular structure of DPPC, Figure 2.2). The molar fractions associated all the elements detected with XPS are given in Table 3.4, where the name of an element designates its concentration and the number in subscript designates the binding energy of the peak component.

Based on the evolution of nitrogen, in quaternary amine group, and phosphor, which are specific markers of DPPC molecules, it is clearly shown that the adsorbed amount of DPPC did not vary markedly after the hydration of the layer (Table 3.4). Indeed, even some slight variations can be observed, it appears that the hydration did not greatly affect the adsorbed amount on both AlOOH and SA-AlOOH surfaces, regardless of the procedure used (DPPC I vs DPPC II).

Another practical way to evaluate the effect of hydration on the amount of adsorbed DPPC molecules consists in exploring the  $N_{402.2}/C_{tot}$  molar concentration ratios (data from Table 3.4) which reflect a possible enrichment/depletion of the organic adlayer with DPPC molecules. This parameter showed indeed that the amount of DPPC is significantly higher when using procedure I, compared to procedure II (Figure 3.26A). Furthermore, no significant variations were noticeable after hydration, except when DPPC adsorption was performed on AlOOH surface using the procedure I. This result suggests that hydration leads to the partial desorption of DPPC molecules.

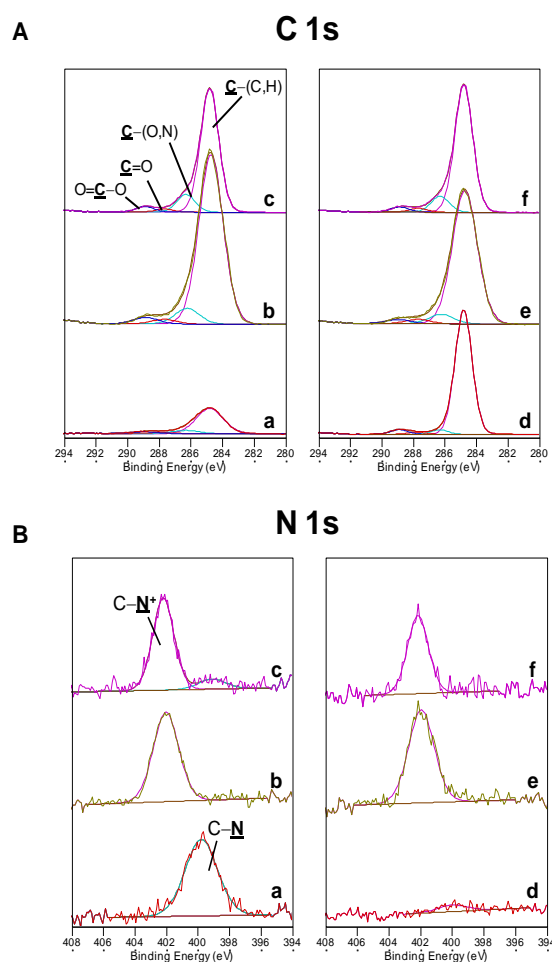


**Figure 3.25.** Decomposition of *N* 1s, and *C* 1s peaks recorded on the (a) AlOOH, (b) AlOOH-DPPC I, (c) AlOOH-DPPC II, (d) SA-AlOOH, (e) SA-AlOOH-DPPC I and (f) SA-AlOOH-DPPC II. (Chosen DPPC concentrations for procedure I and procedure II were 1mg/ml and 5mg/ml, respectively).

**Table 3.4.** Surface concentration (mole percentage computed over all elements except hydrogen) of elements determined by XPS. (Chosen DPPC concentrations for procedure I and procedure II were 1mg/ml and 5mg/ml, respectively).

	Al 2p	P 2p	Cl 2p	C 1s					N 1s			O 1s
				C <sub>284.8</sub>	C <sub>286.3</sub>	C <sub>287.9</sub>	C <sub>288.7</sub>	C <sub>tot</sub>	N <sub>399.8</sub>	N <sub>402.3</sub>	N <sub>tot</sub>	
<b>Adsorption</b>												
AIOOH	29.94	0.00	0.00	13.46	1.76	0.60	0.95	16.77	0.57	0.00	0.57	52.71
AIOOH-DPPC I	1.11	1.91	0.00	72.69	6.76	2.00	2.78	84.23	0.00	1.42	1.42	11.33
AIOOH-DPPC II	14.00	1.04	0.00	49.57	7.09	1.22	2.19	60.07	0.12	0.81	0.93	23.96
SA-AIOOH	20.09	0.00	0.00	46.77	1.71	0.83	1.77	51.08	0.06	0.00	0.06	28.77
SA-AIOOH-DPPC I	5.64	1.52	0.00	67.56	4.84	2.25	2.09	76.74	0.00	1.11	1.11	14.99
SA-AIOOH-DPPC II	14.96	0.73	0.00	48.79	6.18	1.51	1.98	58.46	0.00	0.58	0.58	25.27
<b>Hydration</b>												
AIOOH	5.77	0.00	0.03	71.33	6.84	2.85	3.96	84.98	0.05	0.00	0.05	9.18
AIOOH-DPPC I	8.61	1.44	0.07	66.92	9.54	1.24	3.08	80.78	0.26	1.14	1.40	7.71
AIOOH-DPPC II	16.29	1.20	0.12	51.86	2.54	2.10	1.20	57.70	0.16	0.78	0.94	23.77
SA-AIOOH	4.11	0.00	0.02	78.16	6.02	2.14	3.18	89.50	0.05	0.00	0.05	6.33
SA-AIOOH-DPPC I	2.83	1.74	0.00	70.49	6.19	2.52	2.30	81.50	0.00	1.31	1.31	12.62
SA-AIOOH-DPPC II	10.34	1.24	0.00	61.89	6.84	1.66	2.38	72.77	0.00	0.89	0.89	14.77

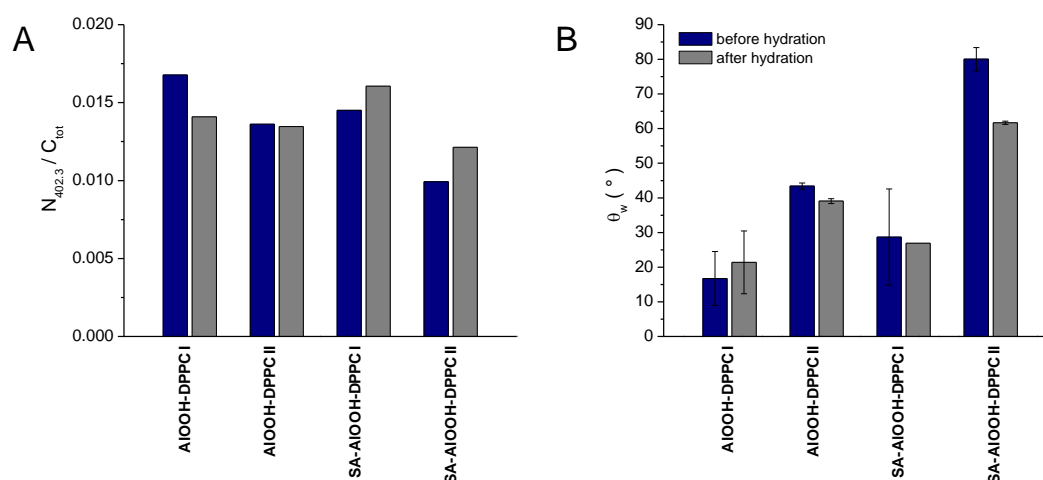


**Figure 3.26.** Evolution of (A) water contact angle ( $\theta_w$ ) and (B) ratio  $N_{402.3}/C_{tot}$  got by XPS of DPPC on AIOOH and SA-AIOOH surfaces before and after hydration for different procedures (Chosen DPPC concentrations for procedure I and procedure II were 1mg/ml and 5mg/ml, respectively).

### 3.3.3 Discussion

Generally, the adsorption of DPPC using drop spreading/evaporation or spin-coating method leads to the formation of multilayers [124]. The amount of adsorbed DPPC may significantly vary as a function of the solution concentration, as also observed in our study.

The main difference between procedure I and II, used in the present study, seems to be related to the amount of adsorbed DPPC molecule, as revealed by PM-IRRAS analyses. It appears, moreover, that the film formed from drop deposition (procedure I) is more stack than the one obtained by spin-coating. Indeed, in contrast to the latter procedure, when the drop is deposited (procedure I), no tossing of lipid solution occurs and the amount of phospholipids remains entirely on the sample surface, leading to the formation of a film with a higher thickness, in agreement with observations made on flat “smooth” surfaces [124]. However, this may induce less uniformity of the film and more holes, while in spin-coating process the sample thickness is almost uniform between defects [122, 124]. It is noteworthy that it is possible to get homogeneous and desired thick films with drop deposition method by choosing suitable combination and concentration of phospholipids, the solvent which wets the surface and substrate [127, 175].

The main complexity of this work is related to the fact that the surface used exhibit a high level of roughness, owing to the nanoscale organization of the superficially hydroxylated alumina surface and further modification with SA (see chapter 3.1). By contrast, the main investigations reported in the literature have been carried out on model flat substrate with low roughness, such as mica, silicon wafer, glass, etc. accordingly, the number of adsorbed phospholipid layers (multilayered film) can be determined easily by means of ellipsometry, reflectometry, or other techniques [123, 124, 127, 128]. In the present study, it is difficult to conclude about the number of DPPC layers, however, water contact angle measurements may provide relevant information regarding the orientation of adsorbed molecules. Simplified configurations corresponding to the different surfaces and the adsorption procedures are

illustrated in Figure 3.27. Even these configurations do not take into account the exact number of layers, it may provide a rough idea about how DPPC molecules may self-organize in the adsorbed state whether the surface is hydrophilic (AlOOH) or hydrophobic (SA-AlOOH), depending on the adsorption procedure (drop deposition vs spin-coating).

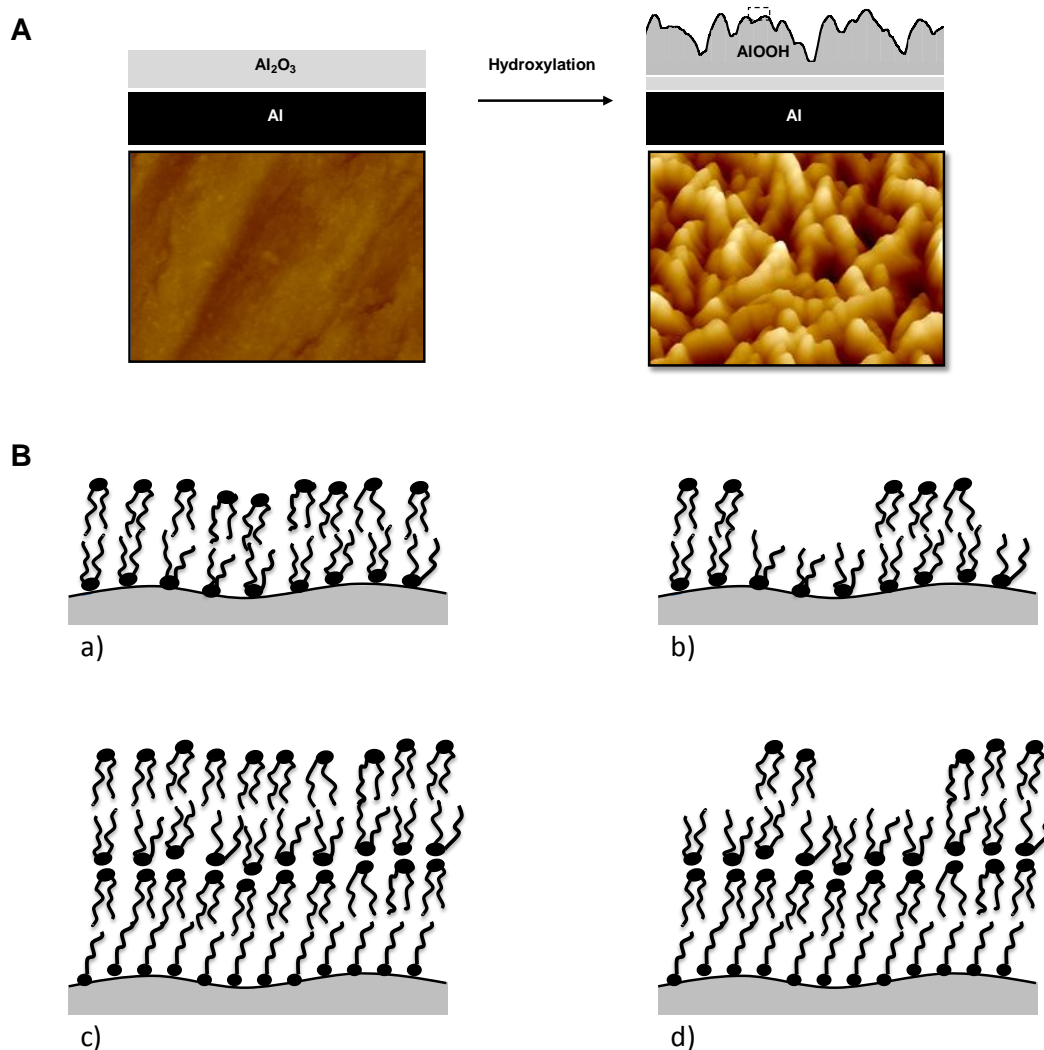


**Figure 3.27.** (A) Surface morphology before and after hydroxylation; (B) zoom part of hydroxylated surface with simplified configurations of adsorbed DPPC on the AlOOH (a), (b) and SA-AlOOH (c), (d); by the adsorption procedure I (a), (c) and procedure II (b), (d).

The stability of phospholipids' layers is usually examined in contact with water vapor at different temperatures and humidity level, or by a direct immersion in

aqueous solution, mostly buffers (with biological interest). During the hydration, the phospholipids' layers may re-organize. Moreover, the first single bilayer which is in a direct contact with the substrate is commonly left stable, whereas top layers could be detached [122, 123]. The stability of the adsorbed layers may also increase when the film thickness is higher, because interaction force between the liquid/vapor and solid/liquid interface becomes more attractive when the thickness decreases [123]. In the present study, the hydration has no drastic effect on the DPPC film, on the basis of XPS results and the evolution of  $\theta_w$ . However, using procedure I is used, the film seems to be more sensitive to hydration, when the adsorption was performed on the hydrophilic AlOOH surface.

Although further investigations are needed regarding structural features of the adsorbed film, our study revealed promising results on the possibility to form a stable “hybrid film” made with one fatty acid (SA) and one phospholipid (DPPC), which could be used for tuning surface properties (especially wettability) and interaction with different environment.



## Conclusions and perspectives

The self-assembly of lipids on the surfaces of inorganic materials is a relevant way to control their properties. While the mechanism of adsorption on model flat substrate is well described in the literature, interfacial processes remain poorly documented on nanostructured surfaces. The mechanism of interaction of several lipids with an AlOOH surface has been investigated. Different FA varying by their chain length and level of unsaturation, one fatty acid methyl ester were adsorbed on hydroxylated Al surface from alkane solution. Long fatty acids impact on the organization and wettability of the surface. The stability of the FA self-assembled layers was examined under UV/O<sub>3</sub> or conditioning in different media (air or aqueous solutions). This strategy aimed to examine the role of adsorbed FA on the changes of surface properties, in terms of morphology and wettability. DPPC also was as adsorbed from organic solution by drop deposition or spin-coating techniques on two kind of surfaces AlOOH and SA-AlOOH. After all these investigation we can conclude that:

1. FA interact strongly with the hydroxylated Al through their deprotonated carboxylic acid head groups, leading to the formation of coordinative carboxylate–surface bonds, as evidenced by PM-IRRAS analyses. MO on the other hand, when contacting the AlOOH surface, is subjected to a chemical transformation which presumably consists of saponification of the methyl ester group, leading to the formation of carboxylate species. The latter then interact with the surface in a manner similar to that evidenced for FA.
2. The changes of surface morphology, using the AFM recently developed peak force tapping mode, were observed after adsorption of FA and MO. High resolution images revealed the existence of highly ordered nanostructures through the self-assembly of FA. AFM results revealed a peculiar fingerprint due to the FA self-assembly which consists in the formation of aligned nanopatterns in a state of hierarchical nanostructuration, regardless of the molecular structure of the FA (chain

length, level of unsaturation). By contrast, no comparable organization was observed with MO.

3. UV/O<sub>3</sub> treatments led to the degradation of adsorbed FA by different mechanisms mainly involving ozonolysis and autoxidation processes, depending on the level of unsaturation of the FA. These tests evidenced the pivotal role played by the self-assembled molecules to form and maintain the obtained nano-patterns. On the contrary, a strong increase of  $\theta_w$  was observed when increasing the amount of C-H groups, estimated by PM-IRRAS data (area of  $\nu(\text{C-H})$  bands) These findings suggest that the main origin of hydrophobisation is due to the alkyl chains of self-assembled FA and that the nanoscale organization only has a small contribution.
4. After the adsorption of FA and further conditioning in different media, the surface properties were subjected to significant effects regarding both nanoscale organization and wettability. To quantify the contribution of the surface roughness on the wetting properties, the Wenzel roughness, defined as the third moment of power spectral density (PSD), appears to be more relevant than the root-mean-square roughness ( $R_{\text{rms}}$ ) as it also includes information on the horizontal range fluctuations. Results did not show any trend that might correlate wettability ( $\theta_w$ ) and Wenzel roughness ( $R_w$ ).
5. The mechanisms of adsorption of phospholipids are more complicated than FA, knowing their ability to form bilayers in the presence of water. DPPC differently interacts with AlOOH and SA-AlOOH surfaces, because of their hydrophilicity and hydrophobicity, respectively. The surface properties, adsorption procedures (drop deposition v.s. spin-coating) strongly effect the orientation and organization of self-assembled molecules. The main effect of adsorption could be described as an evolution of the surface wettability, which in agreement with other results shows the formation of DPPC multilayers. However, it is

extremely difficult to conclude about the number of (bi)layers owning nano-roughness of hydroxylated surface.

The complexity of interfacial processes involved in the adsorption of lipids on metal oxide and hydroxides is inherent in the multiplicity of the parameters influencing this process. The FA self-organization principles can be extended to other macromolecules of biological interest, phospholipids in particular, and have a particular interest in applications such as the control of cell adhesion.

**List of publications which are involved in the dissertation:**

I. Liascukiene, M. Steffenhagen , S. J. Asadauskas, J-F. Lambert, J. Landoulsi, Self-assembly of fatty acids on hydroxylated Al surface and effects of their stability on wettability and nanoscale organization, Langmuir 2014, accepted,

**DOI:** 10.1021/la404756y

I. Liascukiene, N. Aissaoui, S. J. Asadauskas, J. Landoulsi, J-F. Lambert, Highly ordered nanostructures on hydroxylated aluminum surface through the self-assembly of fatty acids, Langmuir 2012, 28, 5116-5124

Sections 3.1 and 3.2 were derived with permission from our publications listed above.

**List of publications which are not involved in the dissertation:**

A. Stoncius, I. Liascukiene, S. Jankauskas, S. Asadauskas, Volatiles from Thin Film Degradation of Bio-based, Synthetic and Mineral Basestocks, Industrial Lubrication and Tribology 2013, 65(3), 209-215

**Others:**

I. Liascukiene, S. J. Asadauskas, N. Aissaoui, J-F. Lambert, J. Landoulsi, Self-assembly of fatty acids on hydroxylated aluminum surface: Nanoscale organization and effect on protein, European Cells and Materials 2013, 26(6), 47

I. Liascukiene, J. Landoulsi, N. Aissaoui, J-F. Lambert, S. J. Asadauskas, “The complexity of interfacial processes between metallic surface and free fatty acids / esters“, 2012, Online Only Supplement –Book of abstracts of the 10th EuroFed Lipid Congress, Cracow, Poland 2326 September 2012. Eur. J. Lipid Sci. Technol.,114:n/a.DOI:10.1002/ejlt.202390034, pp. 151

Irma Liaščukienė, Arvydas Stončius, S. Asadauskas, "Formation of solid residues in bio-based esters during oxidation and their dissolution in organic solvents" Proc. BaltTrib 2011, ISSN 1822-8801, A. Stulginskis University, Kaunas, 17-18 November 2011, pp. 37-42

I. Liascukiene, Jurate Vaiciuniene, Asta Griguceviciene, S. Asadauskas „Dissolution of Iron in Biodiesel Films on Steel Surface under Oxidative Stress“, 2011, Proceedings of COST CM0901 2st Annual meeting, Zaragoza, Spain, pp. 102-104

S. Asadauskas, A. Grigucevičienė, D. Bražinskienė, I. Liaščukienė, A. Stončius „Dissolved Metals as Soot Precursors -- Review of Dissolution Mechanisms in Thin Biofuel Films“, 2010, Proceedings of COST CM0901 1st Annual meeting, Nancy, France, pp. 55-56

**Scientific conferences:**

I. Liascukiene\*, S. J. Asadauskas, N. Aissaoui, J-F. Lambert, J. Landoulsi, “Self-assembly of fatty acids on hydroxylated aluminum surface: Nanoscale organization and effect on protein”, ISSIB 2013 The 4th International Symposium of Surface and Interface of Biomaterials, Roma, Italy, September 25, 2013 (oral presentation)

I. Liascukiene\*, J. Landoulsi, N. Aissaoui, J-F. Lambert, S. J. Asadauskas, “The complexity of interfacial processes between metallic surface and free fatty acids / esters“, 104th AOCS Annual Meeting & Expo, Montréal, Canada, May 1, 2013 (oral presentation)

I. Liascukiene\*, J. Landoulsi, N. Aissaoui, J-F. Lambert, S. J. Asadauskas, “Adsorption behavior of fatty acids on AlOOH surface: from self-assembly to surface nanostructuring“, 10<sup>th</sup> Euro Fed Lipid congress, Cracow, Poland, 2012, September 26d. (oral presentation)

I. Liaščukienė \*, J. Landoulsi, G. Bikulčius, I. Demčenko, S. Jankauskas, S. Asadauskas, “ Fatty acid interaction with Al surfaces and their Anti-Wear effects”, FTMC doctoral conference, Vilnius, 2011m. November 24 d. (oral presentation)

I. Liaščukienė\*, A. Stončius, A. Asadauskas, “Formation of solid residues in bio-based esters during oxidation and their dissolution in organic solvents”, International Conference BALTTTRIB'2011, Kaunas, 2011m. November 17d. (oral presentation)

I. Liascukiene, J. Vaiciuniene, A. Grigucevičienė, S. Asadauskas\* „ Dissolution of Iron in Biodiesel Films on Steel Surface under Oxidative Stress “, COST CM0901 2st Annual meeting, Zaragoza, Spain, 2011 (oral presentation)

I. Liaščukienė \* , A. Grigucevičienė, S. Asadauskas, “Biodegalų ir plieno tarpfazyje vykstančių oksidacijos ir korozijos mechanizmų tyrimai”, Lithuanian scientific concul (LMT) young scientist conference „Fizinių ir Technologijos mokslų tarpdalykiniai tyrimai“, Vilnius 2010m. February 8 d. (oral presentation)

I. Liaščukienė \*, S. Asadauskas, J. Vaičiūnienė „Metalų tirpimas biodegaluose“ FTMC doctoral conference, Vilnius, 2010 m. November 18 d. (oral presentation)

S. J. Asadauskas \*, A. Grigucevičienė, D. Bražinskienė, I. Liaščukienė, A. Stončius „Dissolved Metals as Soot Precursors -- Review of Dissolution Mechanisms in Thin Biofuel Films“, COST CM0901 1st Annual meeting, Nancy, France, 2010 (oral presentation)

\* *presenting author*

## References

1. Sharma, B.K., A. Adhvaryu, and S.Z. Erhan, *Friction and wear behavior of thioether hydroxy vegetable oil*. Tribology International, 2009. **42**(2): p. 353-358.
2. Knothe, G., J.V. Gerpen, and J. Krahl, *The Biodiesel Handbook 2005*: AOCS Press.
3. Largueze, J.-B., K.E. Kirat, and S. Morandat, *Preparation of an electrochemical biosensor based on lipid membranes in nanoporous alumina*. Colloids and Surfaces B: Biointerfaces, 2010. **79**(1): p. 33-40.
4. Castellana, E.T. and P.S. Cremer, *Solid supported lipid bilayers: From biophysical studies to sensor design*. Surface Science Reports, 2006. **61**(10): p. 429-444.
5. Mourtas, S., et al., *Covalent immobilization of liposomes on plasma functionalized metallic surfaces*. Colloids and Surfaces B: Biointerfaces, 2011. **84**(1): p. 214-220.
6. Trommer, H., et al., *The examination of skin lipid model systems stressed by ultraviolet irradiation in the presence of transition metal ions*. European Journal of Pharmaceutics and Biopharmaceutics, 2001. **51**(3): p. 207-214.
7. Alberts, B., et al., *Molecular Biology of the Cell*. 4th ed2002, USA: Garland Science, Taylor & Francis Group.
8. Sackmann, E., *Chapter 1 Biological membranes architecture and function*, in *Handbook of Biological Physics*, R. Lipowsky and E. Sackmann, Editors. 1995, North-Holland. p. 1-63.
9. Risse, T., et al., *Investigation of the Molecular Motion of Self-Assembled Fatty Acid Films*. The Journal of Physical Chemistry B, 1998. **102**(15): p. 2668-2676.
10. Nishinaga, O., et al., *Rapid fabrication of self-ordered porous alumina with 10-/sub-10-nm-scale nanostructures by selenic acid anodizing*. Sci. Rep., 2013. **3**.

11. Richter, R.P., R. Bérat, and A.R. Brisson, *Formation of Solid-Supported Lipid Bilayers: An Integrated View*. Langmuir, 2006. **22**(8): p. 3497-3505.
12. Ulman, A., *Formation and Structure of Self-Assembled Monolayers*. Chemical Reviews, 1996. **96**(4): p. 1533-1554.
13. Picardo, M., et al., *Sebaceous gland lipids*. Dermato-endocrinology, 2009. **1**(2): p. 68-71.
14. T. J. Keene, M., R. Denoyel, and P. L. Llewellyn, *Ozone treatment for the removal of surfactant to form MCM-41 type materials*. Chemical Communications, 1998(20): p. 2203-2204.
15. Chen, S.H. and C.W. Frank, *Infrared and fluorescence spectroscopic studies of self-assembled n-alkanoic acid monolayers*. Langmuir, 1989. **5**(4): p. 978-987.
16. Folkers, J.P., et al., *Self-Assembled Monolayers of Long-Chain Hydroxamic Acids on the Native Oxide of Metals*. Langmuir, 1995. **11**(3): p. 813-824.
17. Gun, J., R. Iscovici, and J. Sagiv, *On the formation and structure of self-assembling monolayers: II. A comparative study of Langmuir-Blodgett and adsorbed films using ellipsometry and IR reflection-absorption spectroscopy*. Journal of Colloid and Interface Science, 1984. **101**(1): p. 201-213.
18. Lim, M.S., et al., *Adsorption and Desorption of Stearic Acid Self-Assembled Monolayers on Aluminum Oxide*. Langmuir, 2007. **23**(5): p. 2444-2452.
19. Tao, Y.T., *Structural comparison of self-assembled monolayers of n-alkanoic acids on the surfaces of silver, copper, and aluminum*. Journal of the American Chemical Society, 1993. **115**(10): p. 4350-4358.
20. Taylor, C.E. and D.K. Schwartz, *Octadecanoic Acid Self-Assembled Monolayer Growth at Sapphire Surfaces*. Langmuir, 2003. **19**(7): p. 2665-2672.



21. Allara, D.L. and R.G. Nuzzo, *Spontaneously organized molecular assemblies. 1. Formation, dynamics, and physical properties of n-alkanoic acids adsorbed from solution on an oxidized aluminum surface*. Langmuir, 1985. **1**(1): p. 45-52.
22. Allara, D.L. and R.G. Nuzzo, *Spontaneously organized molecular assemblies. 2. Quantitative infrared spectroscopic determination of equilibrium structures of solution-adsorbed n-alkanoic acids on an oxidized aluminum surface*. Langmuir, 1985. **1**(1): p. 52-66.
23. Wefers, K. and C. Misra, *Oxides and hydroxides of aluminium*; . Alcoa Technical Paper 1987. **No. 19**.
24. Feng, L., et al., *Formation process of a strong water-repellent alumina surface by the sol-gel method*. Applied Surface Science, 2010. **256**(10): p. 3191-3196.
25. Hozumi, A., B. Kim, and T.J. McCarthy, *Hydrophobicity of Perfluoroalkyl Isocyanate Monolayers on Oxidized Aluminum Surfaces*. Langmuir, 2009. **25**(12): p. 6834-6840.
26. Ranau, R., J. Oehlenschläger, and H. Steinhart, *Aluminium levels of fish fillets baked and grilled in aluminium foil*. Food Chemistry, 2001. **73**(1): p. 1-6.
27. Sadettin, T., *Aluminium contents in baked meats wrapped in aluminium foil*. Meat Science, 2006. **74**(4): p. 644-647.
28. Fahy, E., et al., *A comprehensive classification system for lipids*. Journal of lipid research, 2005. **46**(5): p. 839-862.
29. Jones, P.J.H. and S. Kubow, *Chapter 5. Lipids, sterols , and their metabolites*. 10th ed. Modern Nutrition in Health and Disease, ed. M.E. Shils, et al.2006: Lippincott Williams & Wilkins.
30. Merrill Jr, A.H. and K. Sandhoff, *Chapter 14 Sphingolipids: metabolism and cell signaling*, in *New Comprehensive Biochemistry*, J.E.V. Dennis E. Vance, Editor 2002, Elsevier. p. 373-407.
31. Taniguchi, N., K. Honke, and M. Fukuda, *Handbook for glycosyltransferases and related genes*2002: Springer.

32. Bach, D. and E. Wachtel, *Phospholipid/cholesterol model membranes: formation of cholesterol crystallites*. *Biochimica et Biophysica Acta (BBA) - Biomembranes*, 2003. **1610**(2): p. 187-197.
33. Tsai, M. and B.W. O'Malley, *Molecular mechanisms of action of steroid/thyroid receptor superfamily members*. *Annual review of biochemistry*, 1994. **63**(1): p. 451-486.
34. Dubiel, E.A., Y. Martin, and P. Vermette, *Bridging the Gap Between Physicochemistry and Interpretation Prevalent in Cell– Surface Interactions*. *Chemical reviews*, 2011. **111**(4): p. 2900-2936.
35. Moser, B.R., *Influence of extended storage on fuel properties of methyl esters prepared from canola, palm, soybean and sunflower oils*. *Renewable Energy*, 2011. **36**(4): p. 1221-1226.
36. Meher, L., D. Vidya Sagar, and S. Naik, *Technical aspects of biodiesel production by transesterification—a review*. *Renewable and sustainable energy reviews*, 2006. **10**(3): p. 248-268.
37. Pimentel, D., et al., *Food Versus Biofuels: Environmental and Economic Costs*. *Human Ecology*, 2009. **37**(1): p. 1-12.
38. van der Horst, D. and S. Vermeulen, *Spatial scale and social impacts of biofuel production*. *Biomass and Bioenergy*, 2011. **35**(6): p. 2435-2443.
39. Şensöz, S. and İ. Kaynar, *Bio-oil production from soybean (*Glycine max* L.); fuel properties of Bio-oil*. *Industrial Crops and Products*, 2006. **23**(1): p. 99-105.
40. Xie, W., H. Peng, and L. Chen, *Transesterification of soybean oil catalyzed by potassium loaded on alumina as a solid-base catalyst*. *Applied Catalysis A: General*, 2006. **300**(1): p. 67-74.
41. Cvengroš, J. and F. Považanec, *Production and treatment of rapeseed oil methyl esters as alternative fuels for diesel engines*. *Bioresource Technology*, 1996. **55**(2): p. 145-150.
42. Peterson, C.L., et al., *Ethyl ester of rapeseed used as a biodiesel fuel—a case study*. *Biomass and Bioenergy*, 1996. **10**(5–6): p. 331-336.

43. Kalam, M.A. and H.H. Masjuki, *Biodiesel from palmoil—an analysis of its properties and potential*. Biomass and Bioenergy, 2002. **23**(6): p. 471-479.
44. Antolín, G., et al., *Optimisation of biodiesel production by sunflower oil transesterification*. Bioresource Technology, 2002. **83**(2): p. 111-114.
45. Vicente, G., et al., *Kinetics of Sunflower Oil Methanolysis*. Industrial & Engineering Chemistry Research, 2005. **44**(15): p. 5447-5454.
46. Helwani, Z., et al., *Solid heterogeneous catalysts for transesterification of triglycerides with methanol: A review*. Applied Catalysis A: General, 2009. **363**(1–2): p. 1-10.
47. Harwood, J.L. and C.M. Scrimgeour, *Fatty Acid and Lipid Structure*, in *The Lipid Handbook with CD-ROM, Third Edition* 2007, CRC Press. p. 1-36.
48. Crawford, M.A., *The Role of Dietary Fatty Acids in Biology: Their Place in the Evolution of the Human Brain*. Nutrition Reviews, 1992. **50**(4): p. 3-11.
49. Stryer, L., *Biochemistry*, 1981. p. 403.
50. Bloom, M. and O.G. Mourtsen, *Chapter 2 The evolution of membranes*, in *Handbook of Biological Physics*, R. Lipowsky and E. Sackmann, Editors. 1995, North-Holland. p. 65-95.
51. Sahoo, R.R. and S.K. Biswas, *Frictional response of fatty acids on steel*. Journal of Colloid and Interface Science, 2009. **333**(2): p. 707-718.
52. Knothe, G., *Some aspects of biodiesel oxidative stability*. Fuel Processing Technology, 2007. **88**(7): p. 669-677.
53. Privett, O., *Autoxidation and autoxidative polymerization*. Journal of the American Oil Chemists' Society, 1959. **36**(10): p. 507-512.
54. Stoncius, A., et al., *"Volatiles from thin film degradation of bio-based, synthetic and mineral basestocks"*. Industrial Lubrication and Tribology, 2013. **65**(3): p. 209-215.

55. Asadauskas, S.J., et al., *Application of three-electrode electrolytic cell to evaluate thin films of vegetable and mineral oils*. Tribology International, 2011. **44**(5): p. 557-564.
56. Murray, R.W., *Mechanism of ozonolysis*. Accounts of Chemical Research, 1968. **1**(10): p. 313-320.
57. Razumovskii, S.D. and G.E. Zaikov, *Ozone and its reactions with organic compounds*. Studies in organic chemistry (Elsevier Science Publishers) ed. Vol. 15. 1984, Amsterdam; New York; New York, NY: Elsevier Science Publishers ; Distributors for the U.S. and Canada, Elsevier Science Pub. Co.
58. Moise, T. and Y. Rudich, *Reactive Uptake of Ozone by Aerosol-Associated Unsaturated Fatty Acids: Kinetics, Mechanism, and Products*. The Journal of Physical Chemistry A, 2002. **106**(27): p. 6469-6476.
59. Lee, A.K.Y. and C.K. Chan, *Heterogeneous Reactions of Linoleic Acid and Linolenic Acid Particles with Ozone: Reaction Pathways and Changes in Particle Mass, Hygroscopicity, and Morphology*. The Journal of Physical Chemistry A, 2007. **111**(28): p. 6285-6295.
60. Rani, M.A.A., et al., *Ozonolysis of Oleic Acid Over a Nano Vanadium Pentoxide (V<sub>2</sub>O<sub>5</sub>) Catalyst*. European Journal of Scientific Research, 2008. **24**(3): p. 428-432.
61. El Kirat, K., S. Morandat, and Y.F. Dufrêne, *Nanoscale analysis of supported lipid bilayers using atomic force microscopy*. Biochimica et Biophysica Acta (BBA) - Biomembranes, 2010. **1798**(4): p. 750-765.
62. Peterson, I.R., *Langmuir-Blodgett films*. Journal of Physics D: Applied Physics, 1990. **23**(4): p. 379.
63. Peltonen, J.P.K., H. Pingsheng, and J.B. Rosenholm, *The polymerization of monolayers of some unsaturated fatty acids*. Thin Solid Films, 1992. **210–211**, Part 1(0): p. 372-374.
64. Peltonen, J.P.K., P. He, and J.B. Rosenholm, *Influence of UV irradiation on unsaturated fatty acid monolayers and multilayer films:*

- x-ray diffraction and atomic force microscopy study*. Langmuir, 1993. **9**(9): p. 2363-2369.
65. Yang, J. and J.M. Kleijn, *Order in Phospholipid Langmuir-Blodgett Layers and the Effect of the Electrical Potential of the Substrate*. Biophysical journal, 1999. **76**(1): p. 323-332.
  66. Hui, S.W., et al., *The structure and stability of phospholipid bilayers by atomic force microscopy*. Biophysical journal, 1995. **68**(1): p. 171-178.
  67. Seidel, M.T., S. Chen, and A.H. Zewail, *Ultrafast Electron Crystallography. 2. Surface Adsorbates of Crystalline Fatty Acids and Phospholipids*. The Journal of Physical Chemistry C, 2007. **111**(13): p. 4920-4938.
  68. Kaganer, V.M., H. Möhwald, and P. Dutta, *Structure and phase transitions in Langmuir monolayers*. Reviews of Modern Physics, 1999. **71**(3): p. 779-819.
  69. Peruchon, L., et al., *Characterization of self-cleaning glasses using Langmuir-Blodgett technique to control thickness of stearic acid multilayers: Importance of spectral emission to define standard test*. Journal of Photochemistry and Photobiology A: Chemistry, 2008. **197**(2-3): p. 170-176.
  70. Wiącek, A.E., *Changes in wetting properties of alumina surface treated with DPPC in the presence of phospholipase A2 enzyme*. Colloids and Surfaces B: Biointerfaces, 2011. **87**(1): p. 54-60.
  71. Glasmästar, K., et al., *Protein Adsorption on Supported Phospholipid Bilayers*. Journal of Colloid and Interface Science, 2002. **246**(1): p. 40-47.
  72. Schreiber, F., *Structure and growth of self-assembling monolayers*. Progress in Surface Science, 2000. **65**(5-8): p. 151-257.
  73. Lee, S., et al., *The Influence of Packing Densities and Surface Order on the Frictional Properties of Alkanethiol Self-Assembled Monolayers (SAMs) on Gold: A Comparison of SAMs Derived from Normal and Spiroalkanedithiols*. Langmuir, 2000. **16**(5): p. 2220-2224.

74. Shon, Y.-S. and T.R. Lee, *Desorption and Exchange of Self-Assembled Monolayers (SAMs) on Gold Generated from Chelating Alkanedithiols*. The Journal of Physical Chemistry B, 2000. **104**(34): p. 8192-8200.
75. Rieley, H., et al., *X-ray Studies of Self-Assembled Monolayers on Coinage Metals. 1. Alignment and Photooxidation in 1,8-Octanedithiol and 1-Octanethiol on Au*. Langmuir, 1998. **14**(18): p. 5147-5153.
76. Rieley, H. and G.K. Kendall, *X-ray Studies of Self-Assembled Monolayers on Coinage Metals. 3. Angularly Resolved Near Edge X-ray Absorption Fine Structure Determination of the Orientation in 1-Octanethiol SAMs on Ag(111) and Cu(111)*. Langmuir, 1999. **15**(26): p. 8867-8875.
77. Sackmann, E. and M. Tanaka, *Supported membranes on soft polymer cushions: fabrication, characterization and applications*. Trends in Biotechnology, 2000. **18**(2): p. 58-64.
78. Safinya, C.R., *Biomolecular materials: structure, interactions and higher order self-assembly*. Colloids and Surfaces A: Physicochemical and Engineering Aspects, 1997. **128**(1-3): p. 183-195.
79. Barthlott, W. and C. Neinhuis, *Purity of the sacred lotus, or escape from contamination in biological surfaces*. Planta, 1997. **202**(1): p. 1-8.
80. Bhushan, B., Y.C. Jung, and K. Koch, *Self-Cleaning Efficiency of Artificial Superhydrophobic Surfaces*. Langmuir, 2009. **25**(5): p. 3240-3248.
81. Badre, C., et al., *Effects of nanorod structure and conformation of fatty acid self-assembled layers on superhydrophobicity of zinc oxide surface*. Journal of Colloid and Interface Science, 2007. **316**(2): p. 233-237.
82. Badre, C., et al., *A ZnO nanowire array film with stable highly water-repellent properties*. Nanotechnology, 2007. **18**(36): p. 365705.
83. Kwak, G., et al., *Superhydrophobic ZnO Nanowire Surface: Chemical Modification and Effects of UV Irradiation*. The Journal of Physical Chemistry C, 2009. **113**(28): p. 12085-12089.

84. Ren, S., et al., *Preparation and characterization of an ultrahydrophobic surface based on a stearic acid self-assembled monolayer over polyethyleneimine thin films*. *Surface Science*, 2003. **546**(2–3): p. 64-74.
85. Lundgren, S.M., et al., *Unsaturated Fatty Acids in Alkane Solution: Adsorption to Steel Surfaces*. *Langmuir*, 2007. **23**(21): p. 10598-10602.
86. Ratoi, M., et al., *Mechanisms of oiliness additives*. *Tribology International*, 2000. **33**(3–4): p. 241-247.
87. Murase, A. and T. Ohmori, *ToF-SIMS analysis of model compounds of friction modifier adsorbed onto friction surfaces of ferrous materials*. *Surface and Interface Analysis*, 2001. **31**(3): p. 191-199.
88. Cong, P., T. Igari, and S. Mori, *Effects of film characteristics on frictional properties of carboxylic acid monolayers*. *Tribology Letters*, 2001. **9**(3-4): p. 175-179.
89. Tsukruk, V.V., et al., *Organic Molecular Films under Shear Forces: Fluid and Solid Langmuir Monolayers*. *Langmuir*, 1996. **12**(20): p. 4840-4849.
90. Ruths, M., et al., *Friction of Fatty Acids in Nanometer-Sized Contacts of Different Adhesive Strength*. *Langmuir*, 2007. **24**(4): p. 1509-1516.
91. Chapman, D., *Biomembranes and new hemocompatible materials*. *Langmuir*, 1993. **9**(1): p. 39-45.
92. Sackmann, E., *Supported Membranes: Scientific and Practical Applications*. *Science*, 1996. **271**(5245): p. 43-48.
93. Buijs, J., D.W. Britt, and V. Hlady, *Human Growth Hormone Adsorption Kinetics and Conformation on Self-Assembled Monolayers*. *Langmuir*, 1998. **14**(2): p. 335-341.
94. Lazzara, T.D., et al., *Phospholipids as an alternative to direct covalent coupling: Surface functionalization of nanoporous alumina for protein recognition and purification*. *Journal of Colloid and Interface Science*, 2012. **366**(1): p. 57-63.

95. Bakshi, M.S., F. Possmayer, and N.O. Petersen, *Role of Different Phospholipids in the Synthesis of Pearl-Necklace-Type Gold–Silver Bimetallic Nanoparticles as Bioconjugate Materials*. *The Journal of Physical Chemistry C*, 2007. **111**(38): p. 14113-14124.
96. He, P. and M.W. Urban, *Phospholipid-Stabilized Au–Nanoparticles*. *Biomacromolecules*, 2005. **6**(3): p. 1224-1225.
97. Zhu, H., et al., *One step synthesis and phase transition of phospholipid-modified Au particles into toluene*. *Colloids and Surfaces A: Physicochemical and Engineering Aspects*, 2005. **257–258**(0): p. 411-414.
98. Lin, S.-Y., et al., *Structures of Self-Assembled Monolayers of n-Alkanoic Acids on Gold Surfaces Modified by Underpotential Deposition of Silver and Copper: Odd–Even Effect*. *Langmuir*, 2002. **18**(14): p. 5473-5478.
99. Shustak, G., A.J. Domb, and D. Mandler, *Preparation and Characterization of n-Alkanoic Acid Self-Assembled Monolayers Adsorbed on 316L Stainless Steel*. *Langmuir*, 2004. **20**(18): p. 7499-7506.
100. Chang, C.-S. and S.-Y. Suen, *Modification of porous alumina membranes with n-alkanoic acids and their application in protein adsorption*. *Journal of Membrane Science*, 2006. **275**(1–2): p. 70-81.
101. Thompson, W.R. and J.E. Pemberton, *Characterization of Octadecylsilane and Stearic Acid Layers on Al<sub>2</sub>O<sub>3</sub> Surfaces by Raman Spectroscopy*. *Langmuir*, 1995. **11**(5): p. 1720-1725.
102. Pertays, K.M., G.E. Thompson, and M.R. Alexander, *Self-assembly of stearic acid on aluminium: the importance of oxide surface chemistry*. *Surface and Interface Analysis*, 2004. **36**(10): p. 1361-1366.
103. Smith, E.L. and M.D. Porter, *Structure of monolayers of short chain n-alkanoic acids (CH<sub>3</sub>(CH<sub>2</sub>)<sub>n</sub>COOH, n = 0-9) spontaneously adsorbed from the gas phase at silver as probed by infrared reflection*



- spectroscopy*. The Journal of Physical Chemistry, 1993. **97**(30): p. 8032-8038.
104. Aronoff, Y.G., et al., *Stabilization of Self-Assembled Monolayers of Carboxylic Acids on Native Oxides of Metals*. Journal of the American Chemical Society, 1997. **119**(2): p. 259-262.
  105. Maoz, R. and J. Sagiv, *On the formation and structure of self-assembling monolayers. I. A comparative atr-wettability study of Langmuir—Blodgett and adsorbed films on flat substrates and glass microbeads*. Journal of Colloid and Interface Science, 1984. **100**(2): p. 465-496.
  106. Öberg, K., et al., *Comparison of monolayer films of stearic acid and methyl stearate on an Al<sub>2</sub>O<sub>3</sub> surface*. Thin Solid Films, 2001. **397**(1–2): p. 102-108.
  107. Schlotter, N.E., et al., *Formation and structure of a spontaneously adsorbed monolayer of arachidic on silver*. Chemical Physics Letters, 1986. **132**(1): p. 93-98.
  108. Samant, M.G., C.A. Brown, and J.G. Gordon, *An epitaxial organic film. The self-assembled monolayer of docosanoic acid on silver(111)*. Langmuir, 1993. **9**(4): p. 1082-1085.
  109. Bommarito, G.M. and A.V. Pocius, *An electrochemical study of the changes in the passivation of an aluminum alloy surface induced by the presence of a self-assembled monolayer*. Thin Solid Films, 1998. **327–329**(0): p. 481-485.
  110. Alexander, M.R., et al., *Interaction of carboxylic acids with the oxyhydroxide surface of aluminium: poly(acrylic acid), acetic acid and propionic acid on pseudoboehmite*. Journal of Electron Spectroscopy and Related Phenomena, 2001. **121**(1–3): p. 19-32.
  111. van den Brand, J., et al., *Interaction of Anhydride and Carboxylic Acid Compounds with Aluminum Oxide Surfaces Studied Using Infrared Reflection Absorption Spectroscopy*. Langmuir, 2004. **20**(15): p. 6308-6317.

112. Raman, A. and E.S. Gawalt, *Self-Assembled Monolayers of Alkanoic Acids on the Native Oxide Surface of SS316L by Solution Deposition*. Langmuir, 2007. **23**(5): p. 2284-2288.
113. Boerio, F.J. and S.L. Chen, *Infrared spectra of adsorbed films on metal mirrors*. Journal of Colloid and Interface Science, 1980. **73**(1): p. 176-185.
114. Dacre, B. and P.A. Wheeler, *Kinetics of fatty acid adsorption from non-aqueous solutions onto metal surfaces. Part 1.-Linoleic acid*. Journal of the Chemical Society, Faraday Transactions 1: Physical Chemistry in Condensed Phases, 1981. **77**(6): p. 1285-1296.
115. Bin, X., et al., *Electrochemical and PM-IRRAS Studies of the Effect of the Static Electric Field on the Structure of the DMPC Bilayer Supported at a Au(111) Electrode Surface*. Langmuir, 2004. **21**(1): p. 330-347.
116. Lang, H., C. Duschl, and H. Vogel, *A new class of thiolipids for the attachment of lipid bilayers on gold surfaces*. Langmuir, 1994. **10**(1): p. 197-210.
117. Plant, A.L., *Supported Hybrid Bilayer Membranes as Rugged Cell Membrane Mimics*. Langmuir, 1999. **15**(15): p. 5128-5135.
118. Silin, V.I., et al., *The Role of Surface Free Energy on the Formation of Hybrid Bilayer Membranes*. Journal of the American Chemical Society, 2002. **124**(49): p. 14676-14683.
119. Terrettaz, S., M. Mayer, and H. Vogel, *Highly Electrically Insulating Tethered Lipid Bilayers for Probing the Function of Ion Channel Proteins*. Langmuir, 2003. **19**(14): p. 5567-5569.
120. Parikh, A.N., et al., *Infrared Spectroscopic Characterization of Lipid-Alkylsiloxane Hybrid Bilayer Membranes at Oxide Substrates*. Langmuir, 1999. **15**(16): p. 5369-5381.
121. Reviakine, I. and A. Brisson, *Formation of Supported Phospholipid Bilayers from Unilamellar Vesicles Investigated by Atomic Force Microscopy*. Langmuir, 2000. **16**(4): p. 1806-1815.

122. Simonsen, A.C. and L.A. Bagatolli, *Structure of Spin-Coated Lipid Films and Domain Formation in Supported Membranes Formed by Hydration*. Langmuir, 2004. **20**(22): p. 9720-9728.
123. Perino-Gallice, L., et al., *Dewetting of solid-supported multilamellar lipid layers*. The European Physical Journal E, 2002. **8**(3): p. 275-282.
124. Mennicke, U. and T. Salditt, *Preparation of Solid-Supported Lipid Bilayers by Spin-Coating*. Langmuir, 2002. **18**(21): p. 8172-8177.
125. Jurak, M. and E. Chibowski, *Wettability and Topography of Phospholipid DPPC Multilayers Deposited by Spin-Coating on Glass, Silicon, and Mica Slides*. Langmuir, 2007. **23**(20): p. 10156-10163.
126. Heredia, A., et al., *Preferred deposition of phospholipids onto ferroelectric P(VDF-TrFE) films via polarization patterning*. Journal of Physics D: Applied Physics, 2010. **43**(33): p. 335301.
127. Seul, M. and M.J. Sammon, *Preparation of surfactant multilayer films on solid substrates by deposition from organic solution*. Thin Solid Films, 1990. **185**(2): p. 287-305.
128. Le Berre, M., Y. Chen, and D. Baigl, *From Convective Assembly to Landau–Levich Deposition of Multilayered Phospholipid Films of Controlled Thickness*. Langmuir, 2009. **25**(5): p. 2554-2557.
129. Jurak, M. and E. Chibowski, *Topography and Surface Free Energy of DPPC Layers Deposited on a Glass, Mica, or PMMA Support*. Langmuir, 2006. **22**(17): p. 7226-7234.
130. Muro, M., Y. Itoh, and T. Hasegawa, *A Conformation and Orientation Model of the Carboxylic Group of Fatty Acids Dependent on Chain Length in a Langmuir Monolayer Film Studied by Polarization-Modulation Infrared Reflection Absorption Spectroscopy*. The Journal of Physical Chemistry B, 2010. **114**(35): p. 11496-11501.
131. Frey, B.L., R.M. Corn, and S.C. Weibel, *Polarization-Modulation Approaches to Reflection–Absorption Spectroscopy*, in *Handbook of Vibrational Spectroscopy* 2006, John Wiley & Sons, Ltd.

132. Buffeteau, T., B. Desbat, and J.M. Turllet, *Polarization Modulation FT-IR Spectroscopy of Surfaces and Ultra-thin Films: Experimental Procedure and Quantitative Analysis*. Appl. Spectrosc., 1991. **45**(3): p. 380-389.
133. De Gennes, P.-G., F. Brochard-Wyart, and D. Quéré, *Capillarity and wetting phenomena: drops, bubbles, pearls, waves*2004: Springer.
134. Yuan, Y. and T.R. Lee, *Contact Angle and Wetting Properties*, in *Surface Science Techniques*, G. Bracco and B. Holst, Editors. 2013, Springer Berlin Heidelberg. p. 3-34.
135. Erbil, H.Y., *Surface chemistry of solid and liquid interfaces*2006: Blackwell Pub.
136. Nakajima, A., K. Hashimoto, and T. Watanabe, *Recent Studies on Super-Hydrophobic Films*. Monatshefte für Chemie / Chemical Monthly, 2001. **132**(1): p. 31-41.
137. Binnig, G., C.F. Quate, and C. Gerber, *Atomic force microscope*. Physical review letters, 1986. **56**(9): p. 930.
138. Braet, F., et al., *Comparison of fixed and living liver endothelial cells by atomic force microscopy*. Applied Physics A, 1998. **66**(1): p. S575-S578.
139. Higgins, M.J., et al., *Structured Water Layers Adjacent to Biological Membranes*. Biophysical journal, 2006. **91**(7): p. 2532-2542.
140. Landoulsi, J. and V. Dupres, *Direct AFM force mapping of surface nanoscale organization and protein adsorption on an aluminum substrate*. Physical Chemistry Chemical Physics, 2013. **15**(21): p. 8429-8440.
141. Jalili, N. and K. Laxminarayana, *A review of atomic force microscopy imaging systems: application to molecular metrology and biological sciences*. Mechatronics, 2004. **14**(8): p. 907-945.
142. Spadavecchia, J., et al., *nPEG-TiO<sub>2</sub> Nanoparticles: A Facile Route to Elaborate Nanostructured Surfaces for Biological Applications*. ACS Applied Materials & Interfaces, 2011. **3**(7): p. 2637-2642.

143. Adamcik, J., A. Berquand, and R. Mezzenga, *Single-step direct measurement of amyloid fibrils stiffness by peak force quantitative nanomechanical atomic force microscopy*. *Applied Physics Letters*, 2011. **98**(19): p. 193701-3.
144. Genet, M.J., C.C. Dupont-Gillain, and P.G. Rouxhet, *XPS analysis of biosystems and biomaterials*. *Medical Applications of Colloids*, 2008: p. 177-307.
145. Watts, J.F. and J. Wolstenholme, *An introduction to surface analysis by XPS and AES*. *An Introduction to Surface Analysis by XPS and AES*, by John F. Watts, John Wolstenholme, pp. 224. ISBN 0-470-84713-1. Wiley-VCH, May 2003., 2003. **1**.
146. van den Brand, J., et al., *Acid-Base Characterization of Aluminum Oxide Surfaces with XPS*. *The Journal of Physical Chemistry B*, 2004. **108**(19): p. 6017-6024.
147. Alwitt, R.S., *Oxides and oxide films*. Vol. Vol. 4. 1976, New York: Dekker.
148. Delebecque, A., et al., *Reactivity of a Hydroxylated Alumina Surface in the Presence of NO Diluted in N<sub>2</sub>: A PM-IRRAS in Situ Investigation*. *The Journal of Physical Chemistry C*, 2008. **112**(8): p. 2964-2971.
149. Alexander, M.R., G.E. Thompson, and G. Beamson, *Characterization of the oxide/hydroxide surface of aluminium using x-ray photoelectron spectroscopy: a procedure for curve fitting the O 1s core level*. *Surface and Interface Analysis*, 2000. **29**(7): p. 468-477.
150. van den Brand, J., et al., *Interaction of Ester Functional Groups with Aluminum Oxide Surfaces Studied Using Infrared Reflection Absorption Spectroscopy*. *Langmuir*, 2004. **20**(15): p. 6318-6326.
151. Delebecque, A., et al., *On the reactivity of NO/N<sub>2</sub> mixtures with aluminum surfaces: A combined PM-IRRAS and QCM investigation*. *Surface Science*, 2008. **602**(1): p. 283-290.
152. Misra, R.M., et al., *Normal mode analysis of  $\hat{I}^3$  form of oleic acid*. *Chemistry and Physics of Lipids*, 2006. **142**(1-2): p. 70-83.

153. Pi, F., et al., *Self-assembling of oleic acid (cis-9-octadecenoic acid) and linoleic acid (cis-9, cis-12-octadecadienoic acid) in ethanol studied by time-dependent attenuated total reflectance (ATR) infrared (IR) and two-dimensional (2D) correlation spectroscopy*. Journal of Molecular Structure, 2010. **974**(1-3): p. 40-45.
154. Roonasi, P., X. Yang, and A. Holmgren, *Competition between sodium oleate and sodium silicate for a silicate/oleate modified magnetite surface studied by in situ ATR-FTIR spectroscopy*. Journal of Colloid and Interface Science, 2010. **343**(2): p. 546-552.
155. Yang, Z., et al., *Electrochemical characterisation of mixed monolayer assemblies of thiol analogues of cholesterol and fatty acids on gold*. Journal of Electroanalytical Chemistry, 1997. **430**(1-2): p. 189-195.
156. Evans, K.O. and G. Biresaw, *Quartz crystal microbalance investigation of the structure of adsorbed soybean oil and methyl oleate onto steel surface*. Thin Solid Films, 2010. **519**(2): p. 900-905.
157. Douillard, J.-M., *Experimental approach of the relation between surface tension and interfacial thickness of simple liquids*. Journal of Colloid and Interface Science, 2009. **337**(1): p. 307-310.
158. Deacon, G.B. and R.J. Phillips, *Relationships between the carbon-oxygen stretching frequencies of carboxylato complexes and the type of carboxylate coordination*. Coordination Chemistry Reviews, 1980. **33**(3): p. 227-250.
159. Knözinger, H. and P. Ratnasamy, *Catalytic aluminas: surface models and characterization of surface sites*. Catal. Rev. Sci. Eng., 1978. **17**(1): p. 31-70.
160. Nagashima, K. and F.D. Blum, *Proton Adsorption onto Alumina: Extension of Multisite Complexation (MUSIC) Theory*. Journal of Colloid and Interface Science, 1999. **217**(1): p. 28-36.
161. Klebanov, A.V., et al., *Electrosurface Properties of Hydr(oxides) and Oxide Nanostructures in 1 : 1 Electrolyte Solutions: 1. Adsorption*

- Characteristics of Boehmite, Goethite, and Silicon Dioxide*. Colloid Journal, 2001. **63**(5): p. 562-567.
162. Lefèvre, G., et al., *Hydration of  $\gamma$ -Alumina in Water and Its Effects on Surface Reactivity*. Langmuir, 2002. **18**(20): p. 7530-7537.
163. Brühne, S., et al., *Atomic Structure Analysis of Nanocrystalline Boehmite  $AlO(OH)$* . Crystal Growth & Design, 2008. **8**(2): p. 489-493.
164. Vig, J.R., *Ultraviolet-ozone cleaning of semiconductor surfaces*, in *Handbook of semiconductor wafer cleaning technology*, W. Kern, Editor 1993, Noyes Publications New Jersey. p. 233-273.
165. Song, W., et al., *Angle dependent X-ray photoemission study on UV-ozone treatments of indium tin oxide*. Applied surface science, 2001. **177**(3): p. 158-164.
166. Kim, S.Y., et al., *Effect of ultraviolet-ozone treatment of indium-tin-oxide on electrical properties of organic light emitting diodes*. Journal of Applied physics, 2004. **95**(5): p. 2560-2563.
167. Manfredi, J., *Chapter 28. Ozone Applications in Biotech and Pharmaceuticals*. Second Edition ed. Filtration and Purification in the Biopharmaceutical Industry 2007: CRC Press.
168. Ye, T., et al., *Photoreactivity of Alkylsiloxane Self-Assembled Monolayers on Silicon Oxide Surfaces*. Langmuir, 2001. **17**(15): p. 4497-4500.
169. Criegee, R., *Mechanism of Ozonolysis*. Angewandte Chemie International Edition in English, 1975. **14**(11): p. 745-752.
170. Awada, H., et al., *Correlation between Superhydrophobicity and the Power Spectral Density of Randomly Rough Surfaces*. Langmuir, 2010. **26**(23): p. 17798-17803.
171. Wenzel, R.N., *RESISTANCE OF SOLID SURFACES TO WETTING BY WATER*. Industrial & Engineering Chemistry, 1936. **28**(8): p. 988-994.
172. Wenzel, R.N., *Surface Roughness and Contact Angle*. The Journal of Physical and Colloid Chemistry, 1949. **53**(9): p. 1466-1467.

173. Stuart, B.H., *Infrared spectroscopy: fundamentals and applications* 2004: Wiley. com.
174. Casal, H.L. and H.H. Mantsch, *Polymorphic phase behaviour of phospholipid membranes studied by infrared spectroscopy*. *Biochimica et Biophysica Acta (BBA) - Reviews on Biomembranes*, 1984. **779**(4): p. 381-401.
175. Spangenberg, T., et al., *AFM in-situ characterization of supported phospholipid layers formed by solution spreading*. *physica status solidi (a)*, 2004. **201**(5): p. 857-860.